2006-03

# The impact of synoptic-scale flow on sea breeze front propagation and intensity at Eglin Air Force Base

Weaver, James C.

Monterey California. Naval Postgraduate School


# NAVAL POSTGRADUATE SCHOOL

**MONTEREY, CALIFORNIA**

# THESIS

**THE IMPACT OF SYNOPTIC-SCALE FLOW ON SEA BREEZE FRONT PROPAGATION AND INTENSITY AT EGLIN AIR FORCE BASE**

by

James C. Weaver

March 2006

| | |
|---|---|
| Thesis Advisor: | Wendell A. Nuss |
| Second Reader: | Haflidi H. Jonsson |

THIS PAGE INTENTIONALLY LEFT BLANK

| REPORT DOCUMENTATION PAGE | | | Form Approved OMB No. 0704-0188 |
|---|---|---|---|
| Public reporting burden for this collection of information is estimated to average 1 hour per response, including the time for reviewing instruction, searching existing data sources, gathering and maintaining the data needed, and completing and reviewing the collection of information. Send comments regarding this burden estimate or any other aspect of this collection of information, including suggestions for reducing this burden, to Washington headquarters Services, Directorate for Information Operations and Reports, 1215 Jefferson Davis Highway, Suite 1204, Arlington, VA 22202-4302, and to the Office of Management and Budget, Paperwork Reduction Project (0704-0188) Washington DC 20503. | | | |
| **1. AGENCY USE ONLY** ***(Leave blank)*** | **2. REPORT DATE** March 2006 | **3. REPORT TYPE AND DATES COVERED** Master's Thesis | |
| **4. TITLE AND SUBTITLE**: Title (Mix case letters) The Impact of Synoptic-Scale Flow on Sea Breeze Front Propagation and Intensity at Eglin Air Force Base | | | **5. FUNDING NUMBERS** |
| **6. AUTHOR(S)** James C. Weaver | | | |
| **7. PERFORMING ORGANIZATION NAME(S) AND ADDRESS(ES)** Naval Postgraduate School Monterey, CA 93943-5000 | | | **8. PERFORMING ORGANIZATION REPORT NUMBER** |
| **9. SPONSORING /MONITORING AGENCY NAME(S) AND ADDRESS(ES)** N/A | | | **10. SPONSORING/MONITORING AGENCY REPORT NUMBER** |
| **11. SUPPLEMENTARY NOTES** The views expressed in this thesis are those of the author and do not reflect the official policy or position of the Department of Defense or the U.S. Government. | | | |
| **12a. DISTRIBUTION / AVAILABILITY STATEMENT** Approved for public release; distribution is unlimited | | | **12b. DISTRIBUTION CODE** |


**13. ABSTRACT (maximum 200 words)**

This study investigates the impact of the synoptic-scale flow on the propagation and intensity of the sea breeze front at Eglin Air Force Base. The 925 mb wind direction and speed from the 12 UTC Tallahassee sounding was used to categorize 509 summer days as having an offshore, onshore, or coast parallel synoptic-scale flow regimes. Days with similar synoptic-scale flows were then composited together to create hourly surface analyses for each regime. Sea breeze frontogenesis, location and intensity were analyzed on hourly plots of temperature, winds and frontogenesis.

Results indicate that the most intense sea breeze fronts formed under 3-5 $ms^{-1}$ offshore, 7-9 $ms^{-1}$ coast parallel easterly, and 3-5 $ms^{-1}$ coast parallel westerly synoptic-scale flow while the weakest fronts formed under 0-3 $ms^{-1}$ onshore and coast parallel westerly flow. The inland penetration of the sea breeze front was restricted under offshore flow but propagated through the Eglin Range Complex under onshore flow.

The intensity of the sea breeze front was found to be a balance between convergence (frontogenetic) and turbulent mixing (frontolytic). Under onshore flow the sea breeze front formed late in the afternoon when convergence at the front was maximized and turbulent mixing decreased. Under offshore flow, the strongest sea breeze fronts formed early in the afternoon due to strong convergence between offshore and onshore winds and weak turbulent mixing.


| **14. SUBJECT TERMS** Sea Breeze, Sea breeze Front, Synoptic-scale Flow, Coastline Curvature, Eglin Air Force Base | | | **15. NUMBER OF PAGES** 129 |
|---|---|---|---|
| | | | **16. PRICE CODE** |
| **17. SECURITY CLASSIFICATION OF REPORT** Unclassified | **18. SECURITY CLASSIFICATION OF THIS PAGE** Unclassified | **19. SECURITY CLASSIFICATION OF ABSTRACT** Unclassified | **20. LIMITATION OF ABSTRACT** UL |

NSN 7540-01-280-5500 Standard Form 298 (Rev. 2-89)
Prescribed by ANSI Std. 239-18

THIS PAGE INTENTIONALLY LEFT BLANK

**Approved for public release; distribution is unlimited.**

**THE IMPACT OF SYNOPTIC-SCALE FLOW ON SEA BREEZE FRONT PROPAGATION AND INTENSITY AT EGLIN AIR FORCE BASE**

James C. Weaver
Captain, United States Air Force
B.S., North Carolina State University, 1996

Submitted in partial fulfillment of the
requirements for the degree of

**MASTER OF SCIENCE IN METEOROLOGY**

from the

**NAVAL POSTGRADUATE SCHOOL**
**March 2006**

Author: James C. Weaver

Approved by: Wendell A. Nuss
Thesis Advisor

Haflidi H. Jonsson
Second Reader

Philip A. Durkee
Chairman, Department of Meteorology

THIS PAGE INTENTIONALLY LEFT BLANK

# ABSTRACT

This study investigates the impact of the synoptic-scale flow on the propagation and intensity of the sea breeze front at Eglin Air Force Base. The period of study was May through September from 2001 to 2005. The 925 mb wind direction and speed from the 12 UTC Tallahassee sounding was used to categorize 509 days as having an offshore, onshore, or coast parallel synoptic-scale flow regimes. Days with similar synoptic-scale flows were then composited together to create hourly surface analyses for each regime. Sea breeze frontogenesis, location and intensity were analyzed on hourly plots of temperature, winds and frontogenesis.

Results indicate that the most intense sea breeze fronts formed under 3-5 $ms^{-1}$ offshore, 7-9 $ms^{-1}$ coast parallel easterly, and 3-5 $ms^{-1}$ coast parallel westerly synoptic-scale flow while the weakest fronts formed under 0-3 $ms^{-1}$ onshore and coast parallel westerly flow. The inland penetration of the sea breeze front was restricted under offshore synoptic-scale flow but propagated through the entire Eglin Range Complex under onshore flow.

The intensity of the sea breeze front was found to be a balance between convergence (frontogenetic) and turbulent mixing (frontolytic). Under onshore flow the sea breeze front formed late in the afternoon when convergence at the front was maximized and turbulent mixing decreased. Under offshore flow, the strongest sea breeze fronts formed early in the afternoon due to strong convergence between offshore and onshore winds and weak turbulent mixing.

THIS PAGE INTENTIONALLY LEFT BLANK

# TABLE OF CONTENTS

# LIST OF FIGURES

THIS PAGE INTENTIONALLY LEFT BLANK

# LIST OF TABLES

THIS PAGE INTENTIONALLY LEFT BLANK

# ACKNOWLEDGMENTS

I would like to thank my advisor, Professor Wendell A. Nuss, Department of Meteorology, Naval Postgraduate School, for his guidance and support during the development of this thesis. His meteorological expertise and programming ability were instrumental in the completion of this thesis. I would also like to thank Professor Haflidi H. Jonsson, CIRPAS, who served as my second reader. His insight and recommendations during the writing and revision process proved invaluable and significantly improved this thesis.

I would also like to thank Major Bryan Mackey, Director of Operations, 46th Weather Squadron, and the men and women of the 46th Weather Squadron for taking time from their busy schedules to discuss the problem of sea breeze forecasting at Eglin AFB. Their inputs and suggestions gave me critical insights into the nature of the problem that directly contributed to the completion of this thesis.

Last, but not least, I would like to thank my fellow students in the class of 2006. I would not have been able to complete this program without your help. I know the countless hours of group study paid off for everyone. I wish each of you the best of luck.

THIS PAGE INTENTIONALLY LEFT BLANK

# I. INTRODUCTION

## A. BACKGROUND

The Gulf Coast is one of the most convectively active regions in the nation (Stroupe et al. 2004). Eglin Air Force Base (AFB), located in the western Florida panhandle (Fig. 1), averages over 90 thunderstorm days per year. The majority of this thunderstorm activity occurs during the summer, with the installation averaging 68 thunderstorm days between May and September. Lightning associated with thunderstorms can cause injury to personnel and damage equipment. Thunderstorms also produce strong surface winds which results in low-level wind shear, heavy rain, hail, and can significantly reduce ceilings and visibility. Thunderstorms restrict all flight, maintenance, and ground operations at Eglin and are the primary summer forecasting problem for Air Force Weather meteorologists in this region.

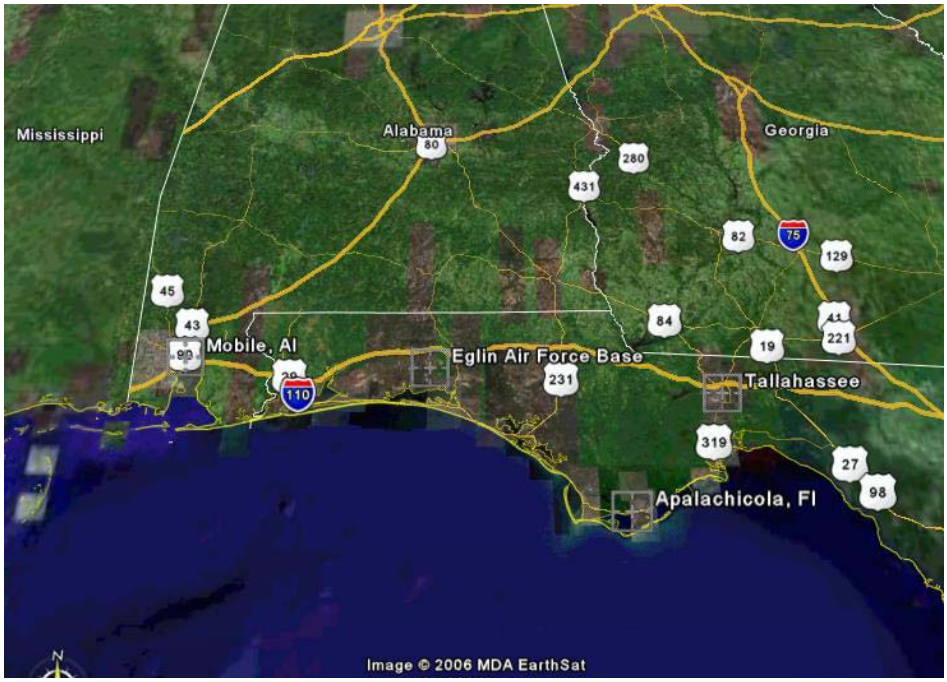


Figure 1. Eglin Air Force (AFB) is located in the western Florida Panhandle between Apalachicola, Fl and Mobile, Al.

The summer maximum in thunderstorm activity is primarily attributed to the daily sea breeze cycle. As far back as Byers and Rodebush (1948), summer thunderstorms in Florida have been linked to the afternoon sea breeze. To date, the majority of research

has focused on south Florida where the peninsular geography provides an excellent opportunity to investigate the relationship between the sea breeze and convective activity. During summer, when meteorological conditions are undisturbed by synoptic-scale weather systems, sea breezes form along the east and west coasts of the peninsula and propagate inland, often combining in central Florida and initiating thunderstorms. This daily cycle strongly modulates the location and timing of deep convection (Burpee and Lahiff 1984). The sea breeze front, located at the leading edge of the inland moving marine air, is a favored area for thunderstorm formation due to enhanced low-level convergence. Numerous investigators (Blanchard and Lopez 1985; Nichols et al. 1990; Boybeyi and Raman 1992; Zong and Tackle 1993; Wilson and Megenhardt 1996; Rao et al. 1999) identified such convergence lines associated with the sea breeze front as a primary mechanism in the formation and spatial distribution of warm season rainfall over the Florida Peninsula. While thunderstorm development along the sea breeze front is an almost daily occurrence, the timing and location of convection can vary dramatically from day to day. The onset of the sea breeze circulation and location of the sea breeze front similarly exhibit daily variability. This variability is primarily attributed to changes in the low-level synoptic-scale flow since surface forcing of the sea breeze varies little from day to day (Blanchard and Lopez 1985).

Numerical (Estoque 1962; Bechtold et al. 1991; Arritt 1993) and observational (Kingsmill 1995; Atkins and Wakimoto 1997; Gilliam et al. 2004) studies indicate that the synoptic-scale flow plays an important role in the daily evolution of the sea breeze. Whereas onshore synoptic-scale flow tends to create weaker sea breezes that form later in the day and propagate long distances inland, offshore flow creates stronger sea breezes that form earlier in the day and propagate only short distances inland. Coast-parallel flow creates sea breezes that are similar to the onshore and offshore cases. Thus, the interaction of synoptic-scale flow with the sea breeze circulation controls the location of sea breeze convergence zones that initiate thunderstorms.

Blanchard and Lopez (1985) created composite radar charts from south Florida and determined that changes in the synoptic-scale wind field correspond closely to changes in the observed radar data. Numerical modeling simulations conducted by Boybeyi and Raman (1992) suggested that the spatial and temporal variation of sea

breeze convergence zones and associated convective activity depend to a large extent on the direction and magnitude of the ambient wind over the Florida Peninsula. Under southeasterly synoptic flow, a strong convergence zone and significant rainfall occur primarily along the west coast of the peninsula. The onshore flow along the east coast creates a weak sea breeze while offshore flow along the west coast opposes the sea breeze, holding it at the coast and strengthening surface convergence. On the other hand, a southwesterly wind favors strong convergence and rainfall along the east coast, for similar reasons. Under light wind conditions, two lines of intense convergence and rainfall occur; one near each coast. Frank et al. (1967) found similar results and noted that days with relatively light winds were characterized by a line of deep convection located 20-40 km inland.

The role of coastline curvature and its modulating effects on the sea breeze has also been studied. Numerical simulations (Pielke 1974; Boybeyi and Raman 1992) suggest that convex coastlines exhibit strong sea breeze convergence while concave coastlines generate divergence. Thus, it seems likely that coastline irregularity strongly affects the location of precipitation (Baker et al. 2001).

The above studies provide firm evidence that sea breezes evolve differently in the presence of low-level synoptic-scale flow. Therefore, it should not be surprising that sea breezes forming along curved coastlines in the presence of synoptic-scale flow will not move inland at equal speeds, nor have equal intensity, because the flow relative to the coastline varies. Given the effects of synoptic flow over a complex coastline, is it possible to accurately forecast the location of the sea breeze front as it moves inland during the day? Surprisingly, given the amount of research, there has been little in the way of investigation into this aspect of the sea breeze. Most numerical simulations (Bechtold et al. 1991; Arritt 1993) are two-dimensional with the assumption of uniformity in the direction parallel to the coastline or model only offshore and onshore cases ignoring important coast-parallel flow regimes. While they provide important insight into the propagation speed of the sea breeze front in the presence of synoptic-scale flow, all evidence shows that the three-dimensional effects of complex coastlines can have a dramatic impact on the characteristics of the sea breeze. Observational studies by Gilliam et al. (2004) and Atkins and Wakimoto (1997) attempted to quantify the inland

propagation speed of sea breeze fronts along complex coastlines under specific synoptic-scale flow regimes. Their results will be discussed in depth in Chapter two.

While the majority of research has focused on the Florida Peninsula, several researchers have looked at the northern Gulf Coast and the role of the sea breeze in modulating summer convective activity. Satellite and lightning studies conducted for this region reinforce the importance of low-level synoptic flow in the formation and evolution of the sea breeze and associated convection. Stroupe et al. (2004) created a warm season lightning climatology and determined flash densities across the Gulf Coast are closely related to the prevailing low-level synoptic flow which controls the sea breeze. Furthermore, convex-shaped coastlines enhanced lightning development while concave coastlines diminished flash densities. Gould and Fuelberg (1996), using GOES-8 visible satellite images centered on Tallahassee, Fl to create a sea breeze satellite climatology, also discovered preferential areas for convective development over the Florida Panhandle under different synoptic-scale flow regimes.

## B. MOTIVATION

Eglin Range Complex, which includes Eglin Air Force Base and the Eglin Reservation, is one of the Air Force's largest bases and is home of the Air Armament Center, the primary weapons research and development center for the United States Air Force. The Eglin Range Complex consists of 724 square miles of varied multi-environmental land area with 45 test areas, 34 test systems/facilities, and 26 multipurpose systems/facilities for testing and evaluation of munitions and weapons systems (Fig. 2). The Eglin Range is the only Department of Defense range with both a water and land range for weapons testing. Both air-to-air and air-to-surface weapon tests exploit this varied topography that provides a land clutter background, a land/sea interface, and the water background of the Gulf of Mexico. The major test areas are Air-to-Ground Ranges, Gun Test Facilities, Electro-optical/Millimeter Wave Evaluation, Static Warhead Test Areas, and Kinetic Energy munitions Test Facility. Eglin AFB also is host to the 33d Fighter Wing and 53d Wing, the 20th Space Surveillance Squadron, the Navy School Explosive Ordnance Disposal, 919th Special Operations Wing (Hurlburt Field), the Army's 6th Ranger Training Battalion, Unmanned Aerial Vehicle Battlelab, and is the

future home of the Joint Strike Fighter. A total of over 120 aircraft, including F-16, F-4, A-10, F-111, T-38, F-15, UH-1 and the C-130, AC-130, RF-4 and HC-130 aircraft, operate from Eglin's runways.


Figure 2. The Eglin Range Complex

Eglin generated more than 500 sorties per month in 2005 (Mackey 2005, personal communications). When considering Eglin's large and varied mission, it's easy to understand that demand for the limited range space is high. Scheduling aircraft and range times is a complex task further complicated by the daily summer thunderstorms common to the region. Accurate forecasts of the timing and location of thunderstorms not only protects lives and resources, but enables planners to efficiently schedule valuable range space that costs over $20K per hour.

## C. CURRENT FORECAST TECHNIQUE

The 28th Operational Weather Squadron (OWS) at Shaw AFB is responsible for providing operational forecasts and resource protection for Eglin AFB. The 46th Weather Squadron (WS) located at Eglin AFB tailors these forecasts to create mission execution forecasts supporting air and ground operations. These forecast centers do not have a sea

breeze forecasting technique. However, they do have a technique for forecasting warm season thunderstorms initiated by the sea breeze front between June and September. The technique is called WINNDEX after Mr. Roger Wynn, who developed the technique in 1986. WINNDEX considers the following variables derived from the Tallahassee, FL sounding: 1) 2,000 ft wind direction to determine synoptic-scale low level flow that governs sea breeze front propagation speed; 2) dewpoint depression at 700, 600, and 500 mb to determine if sufficient moisture is available through the atmosphere to support deep convection; and 3) 12,000, 14,000, and 16,000 foot synoptic-scale wind direction to determine mid-level steering currents that govern thunderstorm movement. These factors produce values that, with the use of nomograms, provide the time period and likely location of thunderstorms, either Eglin AFB, the Eglin Range Complex, or both. While WINNDEX is a useful tool, a blanket forecast for thunderstorm development on the "Eglin Range Complex" is too general and highlights a weakness of the study. For example, thunderstorms forming along the coastline may allow use of other sections of the range, which measures 34 km from the southern to northern boundary and 81 km from east to west (Fig. 3). Currently, the nomagrams do not specify a *location* on the range complex for thunderstorm development.

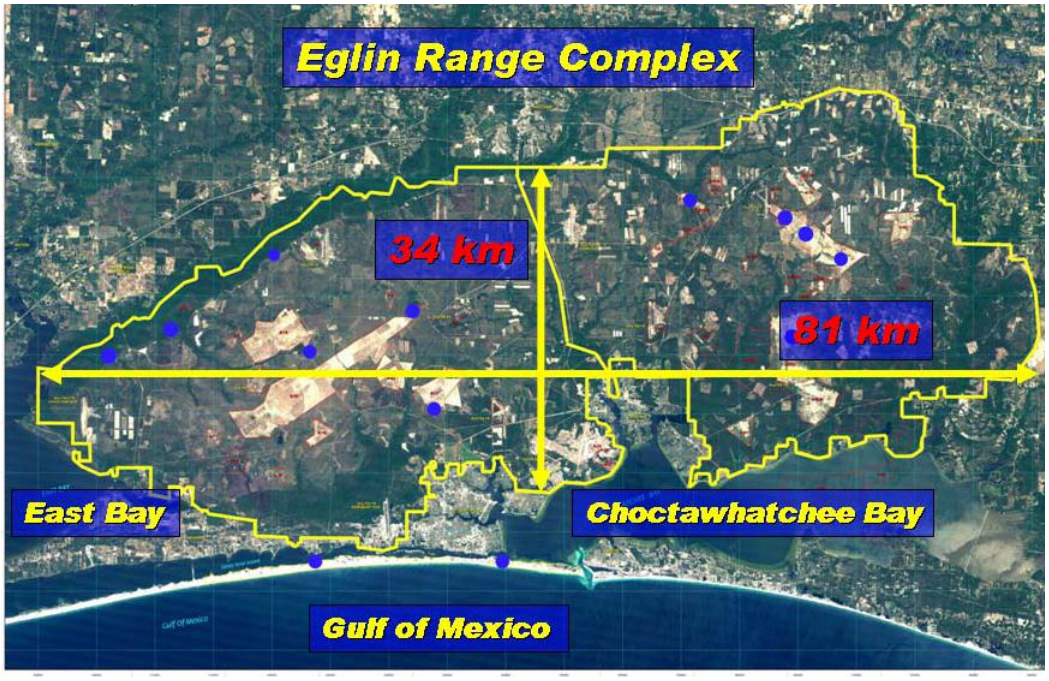


Figure 3. The Eglin Range Complex measures 34 km from north to south and 84 km from west to east.

## D. STATEMENT OF THE PROBLEM

During summer, the day-to-day problem facing forecasters is the timing and location of thunderstorms. Thunderstorm timing and location is a function of the onset of the sea breeze and location of the sea breeze front. The rate of inland penetration and intensity of the sea breeze front during any given day is largely a function of the low-level synoptic flow relative to the coastline. Therefore, an accurate forecast of the location of the sea breeze front is a critical step in accurately forecasting thunderstorm timing and location.

The purpose of this study is:

1. Examine the inland penetration of the sea breeze front along the Eglin coastline under specific synoptic-scale flow regimes using routinely available upper air and surface observations.
2. Examine the evolution of sea breeze front intensification under specific synoptic-scale flow regimes.
3. Compare the results with similar studies conducted along the North Carolina and Florida coastlines.
4. Create a nomogram of inland penetration distance of the sea breeze front with respect to time to be utilized by 46$^{th}$ WS and 28$^{th}$ OWS forecasters to increase the accuracy of summer thunderstorm forecasting.

This study will be restricted to the warm season, defined as May through September. The period of study is 2001 to 2005. The flow regime for each day of the study was categorized as offshore, onshore, coast-parallel, or calm based on the 925 mb wind direction and speed from the 12 UTC Tallahassee sounding. Surface weather observations were used to create composite charts of temperature, wind, pressure for each flow regime in order to study the hourly evolution of the sea breeze at Eglin.

THIS PAGE INTENTIONALLY LEFT BLANK

# II. BACKGROUND

## A. THE SEA BREEZE CIRCULATION

The sea breeze is a mesoscale, thermally-forced phenomenon that occurs at the land-sea boundary. The sea breeze arises from the development of a thermal gradient across the coastline as the land becomes warmer than the water. This situation primarily occurs during the warm season, i.e., from spring through autumn, when as a result of strong heating, the land becomes warmer than water. Synoptic-scale flow is weak during this period with clear skies, which allows maximum daytime solar heating and nighttime radiational cooling that result in a pronounced diurnal cycle in wind direction and speed along coastal regions.

Consider a flat coastline with no along-coast variation, no background flow, and a uniform temperature field across both land and water. After sunrise, the land will warm much faster than water due to its lower heat capacity and absence of mixing. In the presence of light synoptic-scale flow, a land-water temperature difference of approximately 3°C will initiate a sea breeze (Walsh 1974). Vertical heat fluxes warm air above the land surface and cause constant pressure surfaces aloft to bulge upward (Fig. 4). This leads to higher pressure and divergence aloft and low pressure at the surface.

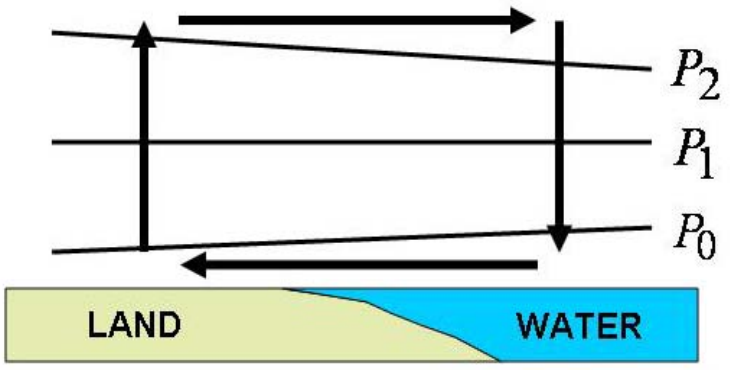


Figure 4. Schematic of the sea breeze circulation. Atmospheric warming cause constant pressure surfaces aloft to bulge upward while surface pressures fall over land. Wind accelerates onshore at the surface and return seaward aloft creating the sea breeze circulation.

In response to the thermally induced pressure gradients, winds accelerate offshore aloft and onshore at the surface. Surface winds are typically 5-10 $ms^{-1}$. Modeling (Arritt 1993; Bechtold et al. 1991) and observational (Kingsmill 1995; Laird et al. 1995) studies indicate the vertical extent of the sea breeze is between 1,500 to 3,000 feet. In this scenario, the temperature and pressure gradients occur only at, and perpendicular to, the coastline. Inland, there is no pressure gradient at the surface, so there is convergence over land and divergence over water. Air ascends in the convergent region at the coast and returns seaward aloft where it descends and diverges at the water surface, which completes the closed sea breeze circulation.

The magnitude of sea breeze winds is proportional to the temperature gradient. The direction of the wind associated with the sea breeze is directed inland perpendicular to the temperature and pressure gradients. Since the strongest thermal gradient is along the coast, the strongest sea breeze winds are in this region. The thermal gradient at the coast resembles a shallow cold front and is known as the sea breeze front. As the day progresses, the sea breeze front will penetrate inland. The distance inland that the sea breeze penetrates is limited by the heating of the cool air behind the front by the land, which acts to relax the temperature gradient. As the sun sets and heating ends, the land will cool more rapidly than the water, which at this time is starting to produce atmospheric heating. The temperature gradient reverses with radiational cooling over land causing surface pressures to rise and heating over water causing surface pressures to fall. Surface winds respond to the gradient reversal by accelerating toward the water, while winds aloft accelerate toward land to complete the closed circulation, which is the land breeze. This cycle will be repeated daily as long as synoptic conditions allow the land to heat and become warmer than the adjacent water.

Since the sea breeze cycle is thermally forced, it is constructive to look at a simple mathematical model to understand the impact of certain physical processes and their modifying effects on the circulation. The sea breeze can be modeled mathematically by integrating around the closed loop of the circulation. The following derivation is from Nuss (2005). The circulation C is defined as;

$$C = \int V \bullet dl \qquad (2.1)$$

where V is the velocity vector integrated around the total path length of the loop dl. Stokes Theorem is used to relate the circulation to the curl of the velocity integrated over the domain of the circulation;

$$C = \iint \nabla \times V dS \qquad (2.2)$$

The time rate of change of the circulation is given by differentiating equation (2.2) with respect to time, which results in the following relationship:

$$\frac{dC}{dt} = \frac{\iint \nabla \times V}{dt} dS \qquad (2.3)$$

This allows us to consider the circulation evolution by understanding the change in velocity within the domain. Using the concepts of circulation identified above, a simple mathematical model of the perturbation velocity field associated with the sea breeze can be developed. In perturbation theory, velocity is divided into two parts, a basic state portion which is constant with time, and a perturbation portion, which is the local deviation of velocity from its basic state. To simplify the model, the assumptions made in the idealized sea breeze situation described above are used along with the assumption that the sea breeze is shallow compared to the scale height of the atmosphere. In this situation, there are no pressure perturbations and buoyancy is due to potential temperature perturbations only.

Following the derivation by Hsu (1970), an equation to estimate the maximum wind in the sea breeze at time (t=0), the time of the maximum thermal gradient, is;

$$U_{\max} = \frac{kg\Delta\theta' Z}{\left(k^2 + \Omega^2\right)\theta_o L} \qquad (2.4)$$

$\Delta\theta'$ is the temperature perturbation associated with the sea breeze front, $k$ is a linear friction constant, $\Omega$ is the earth's rotational speed, $\theta_o$ is the initial background temperature, $Z$ represents the depth of the sea breeze circulation and $L$ is the length scale over which the thermal gradient occurs. Based on equation (2.4), several processes

can impact sea breeze intensity. First, a large thermal perturbation results in stronger sea breeze winds. As the perturbation increases, the sea breeze winds increase. Next, the depth over which the sea breeze circulation occurs impacts the strength of the circulation. Deep circulations are strong circulations while shallow circulations are weak ones. Finally, the length scale over which the thermal gradient occurs has an opposite effect on sea breeze intensity. Small length scales imply sharp thermal gradients that force strong sea breezes. As the length scale increases, sea breeze intensity decreases.

Modifying influences to the sea breeze are not restricted to the variables in this simple equation. Factors that alter the diurnal heating cycle, synoptic-scale flow, and coastline characteristics all act to modify the evolution of the sea breeze circulation (Nuss 2005). While the focus of this research is on the impact of the synoptic-scale flow, each factor is important and will be briefly discussed.

## B. MODIFYING EFFECTS

### 1. The Diurnal Heating Cycle

Since the sea breeze is a thermally forced phenomenon, any factor that modifies the diurnal heating cycle will affect the evolution of the sea breeze. Such factors include the time of year, land surface characteristics, cloud cover, static stability, and planetary boundary layer depth (Nuss 2005).

For a sea breeze to develop, land must be warmer than the adjacent water. Summer, with its long days and high sun angle, favors the sea breeze due to increased solar insolation and heating of land surfaces. Additionally, synoptic-scale weather systems are rare during summer. Therefore, the diurnal heating cycle forces the daily weather in coastal regions.

The physical properties of the underlying land surface also have a direct impact on the structure and diurnal evolution of the sea breeze. Variations in surface albedo, specific heat, and soil moisture content determine the rate and magnitude of heat and moisture fluxes that control the timing and magnitude of the land-water temperature gradient. A sandy, dry soil will heat much more rapidly than a moist, vegetative area

where incoming solar radiation is partitioned between heating and evaporation of moisture. The result is a larger diurnal temperature change and larger land-water temperature gradient. In addition, changes in the spatial distribution of land types can force local mesoscale circulations that can interact with the sea breeze to focus convergence and convection. Marshall et al (2004) determined, by comparing numerical models using pre-1900 land cover and 1997 land cover, that anthropogenic land cover changes in the Kissimmee River Basin of Florida increased surface temperatures and decreased rainfall in the region.

Cloud cover plays an important role in sea breeze modification by altering the surface heating pattern. This modification can be both positive and negative. Clouds present at the time of sea breeze generation will limit the amount of radiative heating and can delay the onset of the sea breeze. If land does not become warmer than water, the sea breeze will not form. A weak sea breeze will result if cloud cover persists through the entire heating cycle. Clouds also act to intensify the land-water thermal gradient. Cloudy skies over water coupled with clear skies over land results in an amplified temperature gradient and a strong sea breeze. Clouds also form in the region of convergence and vertical motion associated with the sea breeze front. The effect can be both frontogenetical and frontolytic. If cloud cover acts to reduce radiational heating of the cool marine while leaving regions ahead of the front clear, the temperature gradient is enhanced and the sea breeze front strengthens.

Static stability influences the strength of the sea breeze by controlling the depth over which the circulation develops. Strong static stability damps vertical motion which reduces the amount of mixing and results in a shallow boundary layer and weak sea breeze circulation. Conversely, weak static stability can enhance vertical motions and boundary layer mixing. The result is a deep boundary layer and a strong sea breeze circulation.

## 2. Synoptic-Scale Flow

Both observation and numerical research suggest that the sea breeze evolves differently under the influence of a prevailing background synoptic flow (Estoque 1962; Bechtold et al. 1991; Arritt 1993; Zong and Takle 1993; Atkins and Wakimoto 1997; Gilliam et al. 2004). The intensity and rate of inland penetration of the sea breeze are strongly modulated by the presence of a background flow.

### *a. Model Studies*

Estoque (1962) was one of the first investigators to examine the influence of synoptic-scale flow on the sea breeze. Using a numerical model, he considered offshore, onshore, coast-parallel with land on the left and coast-parallel with land on the right flow across a straight coastline. Results determined that a 5 $ms^{-1}$ offshore flow produced the strongest sea breeze circulation. Offshore flow acted to advect warm air over land towards the coastline, strengthening the temperature and pressure gradients. By 1100LT, the sea breeze was only evident by a weakening of the offshore flow at the coastline as the thermal perturbation strengthens. The delayed onset of the sea breeze has important implications. First, the sea breeze front is held at the coastline keeping cool marine air offshore. Radiational heating continued over land and the offshore flow advected the warm air towards the coast, generating a concentrated thermal gradient within 8 km of the coastline. As a result, the largest vertical motions at the sea breeze front were associated with offshore flow. Offshore flow also restricted the inland penetration of the sea breeze front. By 1700LT, the sea breeze front moved approximately 10 km inland of the coastline.

On the other hand, Estoque (1962) determined a 5 $ms^{-1}$ onshore flow produced the weakest sea breeze circulation. The advection of cool marine air inland inhibited heating and resulted in weaker gradients of temperature and pressure. Therefore, little vertical motion was associated with the sea breeze front under onshore conditions. Inland penetration of the sea breeze front under onshore flow is difficult to determine because the flow everywhere in the domain is onshore. However, the sea

breeze front could be detected by slightly stronger onshore flow across the weak temperature gradient. By 1100LT, the sea breeze front was located approximately 8 km inland and moved to a position 50 km from the coastline by 1700LT.

Estoque (1962) also examined a case with no synoptic-scale flow and found that the magnitude of the circulation and vertical motion was similar to the offshore case. There are several important differences. First, the onset of the sea breeze occurs earlier without opposing flow. Onshore flow is evident by 1100LT and the sea breeze front had penetrated close to 18 km inland. By 1700LT, the sea breeze front was located approximately 32 km inland. However, the magnitude of the circulation and vertical motion was similar to the offshore case. Check alignment all the way through

Bechtold et al. (1991) investigated the influence of synoptic-scale flow on sea breeze evolution with a two-dimensional non-linear model by varying the magnitude of the ambient flow. Bechtold et al. (1991) considered offshore flow of 5 and 10 $ms^{-1}$ along with a no-wind case. In agreement with Estoque (1962), Bechtold et al. (1991) determined an offshore flow between 5 and 6 $ms^{-1}$ produced the strongest sea breeze circulations and vertical motion. The temperature gradient associated with the sea breeze strengthened between 1200LT and 1500LT. Analysis suggested that lack of mixing between the two air masses was responsible for the strong thermal perturbation. The sea breeze front remained within 13 km of the coastline under a 5 $ms^{-1}$ offshore flow and did not show a significant move inland until 1800LT. Between 1800LT and 2100LT, the thermal gradient weakened due to turbulent mixing as the sea breeze front reached a distance of 31 km inland. Interestingly, increasing the magnitude of the offshore flow decreased the strength of the circulation and suppressed vertical motion. Results indicated an offshore flow of 10 $ms^{-1}$ suppressed formation of a thermal gradient at the coastline and transported the sea breeze circulation offshore. In the no-wind case, the sea breeze front was located close to the coastline with a well defined thermal gradient at 1200LT. The gradient weakened between 1500 and 1800LT as the sea breeze front penetrated almost 100 km inland. The sea breeze front pushed through the entire model domain by 2100LT.

Arritt (1993) conducted 31 numerical model simulations to investigate the characteristics of the sea breeze under various synoptic-scale flows by varying the magnitude of the flow from calm to 15 $ms^{-1}$ offshore. His results compare favorably to Estoque (1962) and Bechtold et al. (1991). First, increased opposing flow from 0 to 5 $ms^{-1}$ resulted in increased sea breeze intensity and stronger upward vertical motion. In addition, increased opposing flow delayed the onset of the sea breeze and slowed its inland penetration. Figure 5 details the inland penetration of the sea breeze as a function of time for various opposing flows. For example, the onset of the sea breeze was delayed

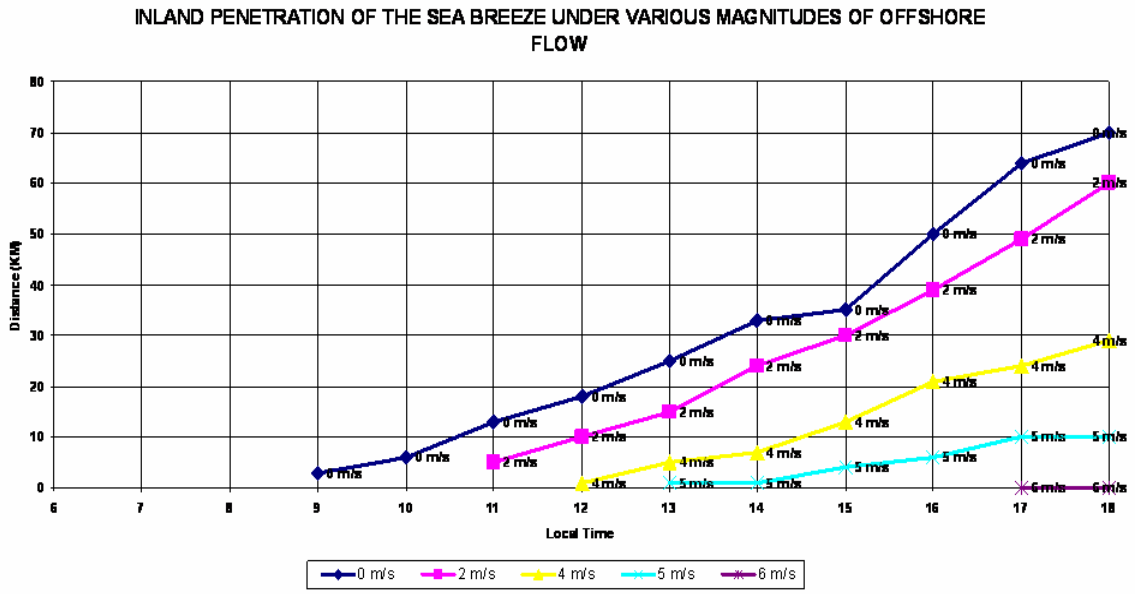


Figure 5. Inland penetration of the sea breeze as a function of geostrophic offshore flow and local time. The distance value of 0 represents the coastline. Geostrophic flow values of 0 or calm (blue), 2 $ms^{-1}$ (pink), 4 $ms^{-1}$ (yellow), 5 $ms^{-1}$ (turquoise), and 6 $ms^{-1}$ (purple). Distances are measured in km. (From Ref. Arritt, 1993).

until 1300L and the sea breeze front moved approximately 10 km inland in the presence of 5 $ms^{-1}$ offshore flow. Opposing flow of 6 $ms^{-1}$ produced the strongest sea breeze winds and upward vertical motion while restricting the inland penetration of the sea breeze front to the coastline. The largest thermal gradient was also associated with the 6 $ms^{-1}$ offshore flow. Offshore flow greater than 6 $ms^{-1}$ resulted in a well defined sea breeze circulation located entirely offshore in agreement with results obtained by

Bechtold et al. (1991). Arritt (1993) further demonstrated that convergent frontogenesis is the main source term for sea breeze frontogenesis and the effect of convergent frontogenesis is maximized for 3-6 $ms^{-1}$ offshore flow. Convergence between the offshore flow and onshore sea breeze winds concentrates the thermal gradient at the coastline resulting in sea breeze front intensification.

Arritt (1993) indicated the presence of onshore flow of more than 3 $ms^{-1}$ suppressed the thermal perturbation associated with the sea breeze. Inland penetration distances of the sea breeze front where not calculated since the flow everywhere is onshore and the front is ill defined. Vertical motions associated with the sea breeze front are much weaker under onshore flow than offshore flow; however, that weak vertical motion is maximized late in the period (1800LT) for onshore flow up to $3 ms^{-1}$. In addition, convergent frontogenesis is suppressed resulting in a weak thermal perturbation of the large scale flow. A similar study by Zhong and Tackle (1993) indicated the sea breeze was suppressed for onshore flow exceeding 5 $ms^{-1}$ and Cetola (1997) found that an onshore flow of 4 $ms^{-1}$ along the Cape Canaveral coast was enough to suppress the sea breeze.

Model simulations conducted by Gilliam et al. (2004) determined the inland propagation distance of 70 km at 1700LT for a sea breeze forming under onshore flow of 2 $ms^{-1}$ along the coastline of North Carolina. In their simulation, the sea breeze forms earlier in the day and propagates inland steadily with slight acceleration after 1800LT. Sea breeze strength, as determined through vertical velocity, indicated a weak sea breeze through early afternoon with strengthening between 1800-2000LT. The sea breeze front propagated 80-100 km inland by that time.

While impacts to the sea breeze under onshore and offshore flow are well documented, coast-parallel cases have received less attention. Synoptic-scale flow parallel to the coastline represents an intermediate sea breeze evolution relative to the onshore and offshore cases. Synoptic-scale flow with land on the right develops when the large scale pressure pattern has high pressure over land and low pressure over water. Surface friction tends to produce a weak offshore wind component, so a sea breeze that develops in this situation has characteristics of the offshore flow case (Zhong and Tackle

1993; Nuss 2005). Sea breezes that develop under synoptic-scale winds that blow with land on the left have characteristics of the onshore case because surface friction produces an onshore component (Zhong and Tackle 1993; Nuss 2005).

Numerically, Estoque (1962) found that when the synoptic-scale wind blows with land on the right the offshore component helped strengthen the temperature and pressure gradient at the coast similar to the offshore flow case, but with a slightly weaker magnitude. Under 5 $ms^{-1}$ coast-parallel flow, a compact, 6 km thermal gradient was evident at 1100LT stretching to 18 km by 1700LT. This compact temperature gradient results in strong vertical motions by 1700LT. The modeled sea breeze front penetrated approximately 5 km onshore by 1100LT and moved inland only 18 km by 1700LT. Conversely, the sea breeze that developed under 5 $ms^{-1}$ coast-parallel flow with land on the left was slightly stronger that the sea breeze that formed under direct onshore flow. By 1100LT, the sea breeze front was approximately 2 km inland and a thermal gradient stronger than a true onshore case formed. By 1700LT, the sea breeze front was approximately 30 km inland with calculated upward vertical motion evident slightly stronger than the onshore case.

Most numerical modeling simulations discussed above only consider two-dimensional effects when modeling the sea breeze and ignore important three-dimensional effects such as coastline curvature, land inhomogeneity, and coast-parallel flow. Given these limitations, they do provide useful insight into the behavior of the sea breeze under various background flows. All results agree that a 5 $ms^{-1}$ offshore flow produces the strongest sea breeze while onshore synoptic-scale flow less than 3 $ms^{-1}$ produces the weakest sea breeze. Sea breezes forming under offshore flow start and are most intense during late morning. Opposing flow delays the onset of the sea breeze and restricts its inland penetration. As a result, the strongest thermal perturbations form at the coast as cool marine air remains offshore and does not mix with warm air over land. Sea breezes move inland slowly under light offshore flow and are most intense during the early afternoon, after which they weaken and accelerate inland. Sea breezes forming under onshore flow begin earlier in the day and strengthen slightly during the late afternoon.

Convergence is the dominant term in sea breeze frontogenesis and is maximized under offshore flow as it meets with onshore sea breeze winds at the coast. Strong convergence results in the strongest upward vertical motion at the sea breeze front. Convergence is suppressed when the flow is onshore as winds everywhere are directed onshore. Increasing the magnitude of both offshore and onshore flow suppressed sea breeze formation. Offshore flow of 6 $ms^{-1}$ transports the sea breeze circulation offshore. However, results differ on the magnitude of onshore flow required to suppress the sea breeze. Values ranging from 3-5 $ms^{-1}$ have been documented. Nevertheless, there is agreement that stronger onshore flow suppresses sea breeze development.

### *b. Observational Studies*

Atkins and Wakimoto (1997) used dual-doppler techniques to investigate the characteristics of the sea breeze along the Florida coast near the Kennedy Space Center. The sea breeze front is often delineated by a "thin line" of enhanced reflectivity values in the optically clear boundary layer (Atkins and Wakimoto, 1997). The thin line is attributed to the density gradient and insects caught in the turbulent mixing at the leading edge of cool marine air. Based on research by Atkins et al. (1995), who determined that the sea breeze thin line and kinematic sea breeze frontal boundary are collocated, they were able to track the sea breeze under different flow regimes. The evolution of the sea breeze was summarized in three stages: morning, afternoon, and late afternoon. Under offshore flow, a thin line of reflectivity values approximately 16 DBZ associated with the sea breeze front formed at the coastline. Reflectivity values increased through the day as the front slowly moved inland. This front movement was attributed to increasing convergence along the front due to strengthening sea breeze flow. By late afternoon, reflectivity values along the front were at their maximum while the width of the thin line shrank, indicating increased frontogenesis. This observation of a stronger sea breeze front that propagates slowly inland reaching maximum strength in the afternoon agrees with numerical model results. Sea breeze fronts forming under offshore flow exhibited larger vertical velocity at the leading edge of the circulation, indicating stronger gradients of temperature and pressure along the front, also in agreement with

numerical results. Reflectivity values normally increased from morning to afternoon as sea breeze frontogenesis increased, thereby making this an effective method to monitor the daily evolution of the sea breeze front. However, the intensity of the sea breeze front is a function of the synoptic-scale flow, so the intensity of the thin line will vary.

Atkins and Wakimoto (1997) found no easily identifiable thin line along the Cape Canaveral coast under onshore flow conditions. Results indicate a frontal zone formed between the sea breeze and ambient airmass but convergence and frontogenesis were small because the ambient and sea breeze winds are in the same direction. Furthermore, no identifiable cloud line was evident on visible imagery. The sea breeze frontal zone became evident in visible imagery late in the day as cumulus clouds developed. Radar did not detect a thin line but did indicate convective cells co-located with cumulus cells on visible satellite imagery. The sea breeze frontal zone penetrated approximately 40-60 km inland by late afternoon, farther inland than offshore or coast-parallel flow and in agreement with Gilliam et al. (2004), Arritt (1993), and Estoque (1962). Observations indicate that gradients of temperature and moisture are small with the sea breeze frontal zone on onshore flow days. The only indication of sea breeze passage was a strengthening of the onshore flow. Under coast-parallel flow with land on the right over Cape Canaveral, convergence at the sea breeze front was smaller than with offshore cases. Atkins and Wakimoto (1997) were not able to detect a thin line with radar until late afternoon during which time convergence along the front increased. Reflectivity values however, where smaller than true offshore cases. Furthermore, the sea breeze front penetrated further inland than true offshore flow cases.

### 3. Coastline Characteristics

Coastline characteristics such as curvature and topography act to alter the convergence patterns of the sea breeze. As discussed above, thermal gradients that force the sea breeze form parallel to the coastline and the resultant sea breeze flow is directed onshore perpendicular to the gradient. Therefore, coastlines that exhibit curvature act to create convergent or divergent sea breezes. Convex coastlines such as points or headlands produce sea breezes that converge over land. Convergence of sea breeze fronts act to initiate convection and strongly determines the location and timing of precipitation

(Baker et al. 2001). Sea breezes along concave coastlines, such as bays, become divergent and diminish the chance for convergence and frontal lifting. Numerical simulations conducted by Boybeyi and Raman (1992) show enhanced convergence associated with the convex coastlines of the Florida peninsula. The magnitude of the curvature is also a factor. Small bays or headlands may simply weaken the thermal gradient along the coast instead of changing the direction, resulting in intensity changes of the sea breeze without altering the patterns of convergence along the coastline (Nuss 2005). An example of convergent and divergent regions along the Florida coastline is illustrated in Fig. 6.

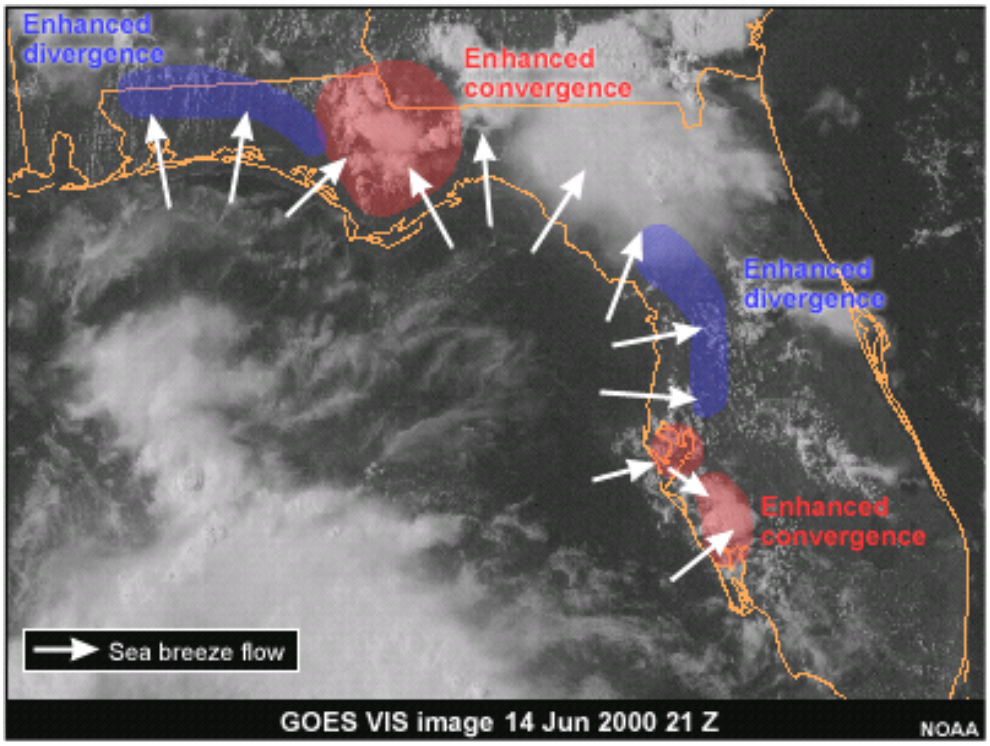


Figure 6. Convergent and divergent sea breeze flow along the curved coastline of Florida. Red areas indicate headlands that enhance convergence due to sea breeze front interaction. Blue areas indicate divergent regions. (From Ref. COMET, http://meted.ucar.edu/mesoprim/seabreez/print.htm, 2003)

In addition to curvature, inland water bodies force their own mesoscale circulations that interact with the sea breeze to alter convergence patterns. Numerous studies have documented the complex interaction of the sea breeze front with river breezes along the Cape Canaveral coastline (Laird et al. 1995; Zhong and Tackle 1993).

While river breezes are weaker than the sea breeze, they have a strong influence on where convection develops as the sea breeze front propagates inland. Convergence lines associated with the river breezes remained stationary around the river until disrupted by the sea breeze. The intersection point of these two features is a good predictor of initial and subsequent convective development (Laird et al. 1995; Zhong and Tackle 1993). Doppler radar (Laird et al. 1995) and high resolution satellite imagery (Atkins and Wakimoto 1997) have been used to detect breezes forced by inland water bodies.

Armed with this knowledge, it should not be surprising that sea breeze fronts forming along curved coastlines in the presence of synoptic-scale flow will not move inland at equal speeds, nor have equal intensity, because the flow relative to the coastline varies. An idealized example of flow along a concave coastline is given in Fig. 7, where the grey arrow represents the synoptic-scale flow. In the center of the bay the flow is offshore, but it is coast-parallel with land on the right on the west side of the bay and coast-parallel with land on the left on the east side of the bay. Therefore, an intense sea breeze front is expected close to the coast in the center of the bay along with a moderately intense sea breeze front that moves a short distance inland on the west side of the bay, and a weak sea breeze front that propagates a good distance inland on the east side of the bay. From this example, it is obvious that changing the synoptic-scale flow can have dramatic effect on how the sea breeze evolves along a curved coastline.

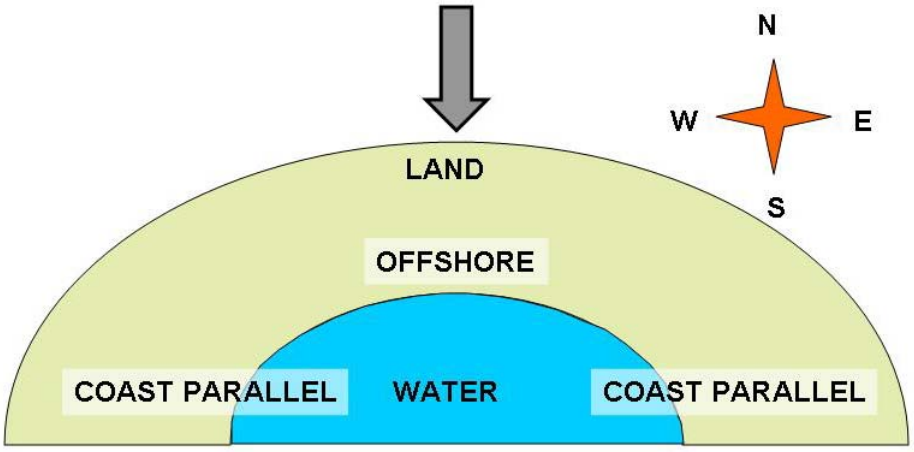


Figure 7. Example of synoptic-scale flow along a concave coastline. The grey arrow represents the direction of the synoptic-scale flow. Under northerly winds, the flow is offshore, but it is coast-parallel with land on the right on the west side of the bay and coast-parallel with land on the left on the east side of the bay.

In a study of sea breezes along the North Carolina coast, Gilliam et al (2003) observed the sea breeze front to be weaker and propagate further inland when flow was coast-parallel compared to portions of the coast where the relative flow was offshore. The sea breeze front only became detectable by late afternoon. Numerical solutions indicated that a sea breeze forming under 2 $ms^{-1}$ southerly coast-parallel flow would move approximately 40 km inland by 1700LT while northerly offshore coast relative flow limited the inland penetration of the sea breeze to 30 km.

Since inland bays and water bodies force their own breezes, the direction and magnitude of the synoptic-scale flow has the same modifying effects as on the sea breeze. Eglin has a complex coastline that includes two inland bays with thin barrier islands between ocean and bays that complicates sea breeze behavior. The geography and climatology of the region around Eglin AFB will be described in the next section.

## C. EGLIN AFB GEOGRAPHY AND SUMMER CLIMATOLOGY

### 1. Area Geography

The Eglin Range Complex sits at the apex of a large coastal bay bounded by Apalachicola, Fl to the east and Mobile, Al to the west (Chap 1, Fig. 1). The Eglin Range Complex covers approximately 720 square miles, and reaches its highest point at 250 feet on the northwest corner. The range is approximately 36 km wide and measures 85 km from east to west. It is bordered along the north by rivers and on the east by creeks. The southern boundary runs along Choctawhatchee Bay and the Gulf of Mexico. The western boundary reaches East Bay. The majority of the terrain is either flat or made up of gentle rolling hills covered with woods of scrub oak and pine trees. This terrain is cut by many shallow creeks with steep-walled valleys and is dotted with numerous ponds and tiny lakes. Large marshes to the northwest and southwest surround the Yellow River and East Bay. The northern boundary of the range is approximately 36 km from the Gulf of Mexico and

The Florida Panhandle's topography inclines northward from the Gulf of Mexico, and reaches its highest elevation of 345 feet just north of Eglin Range Complex. The coastal bays are large, shallow bodies of water fed directly with fresh water inflow. The Choctawhatchee and Pensacola Bays average depth is 4.5 m. This, combined with the regular inflow of fresh water, causes water temperature fluctuations much greater than those of the Gulf of Mexico, both diurnally and seasonally, and results in significant local weather effects. The Choctawhatchee Bay is just east of Pensacola Bay on the western end of the Florida Panhandle. The bay is separated from the Gulf of Mexico along most of its length, but connects through the Pensacola and East passes entering through the south at Destin Pass. Pensacola Bay is in the Western Florida panhandle near the Florida-Alabama border. The Pensacola Bay system is the fourth largest in Florida, one third of which is in Florida, and two thirds of which are in Alabama. The bay is separated from the Gulf of Mexico by a combination of a peninsula, the Santa Rosa Sound, and Santa Rosa Island. Water exchange with the Gulf takes place between Santa Rosa Island and Perdido Key.


Figure 8. The Eglin Range Complex covers approximately 720 square miles. It is bordered along the north by rivers and on the east by creeks. The southern boundary runs along Choctawhatchee Bay and the Gulf of Mexico while the western boundary reaches Pensacola's East Bay.

As mentioned above, the synoptic-scale flow relative to the coastline plays a significant role in modifying the sea breeze. Inspection of Figures 1 and 8 reveals that the coastline along this region is concave. The coastline curves southeastward at the eastern extent of the range and bends slightly southwestward at the western extent of the range (Fig. 8). At the eastern section of the range, the coastline is oriented 120° - 290°, so a southeasterly or northwesterly wind would be coast-parallel. At the western extent of the range, the coastline is oriented 255° - 75°, so a west-southwesterly and east-northeasterly synoptic-scale wind would be coast-parallel. Based on the coastline curvature, the sea breeze at Eglin should display significant along-coast variability in strength and inland penetration speed based on the direction of the synoptic-scale flow.

## 2. Eglin Climatology

Several criteria have been given for sea breeze initiation. First, the land must be warmer than the water. Research indicates that a temperature difference of as little as 1°C can initiate a sea breeze. The stronger the temperature difference, the stronger the sea breeze. We can use this information to determine when the sea breeze becomes active at Eglin AFB. Figure 9 compares Eglin AFB (KVPS) and Duke Field (KEGI) average monthly high temperatures to average monthly sea surface temperatures recorded at Buoy 42039. Buoy 42039 is located in the Gulf of Mexico approximately 115 nautical miles south of Eglin AFB. By April, Eglin AFB average high temperatures are approximately 2° C warmer than the sea surface temperature. The maximum land water temperature difference is 3° C in June and decreases by October when Gulf of Mexico temperatures become warmer than land. Therefore, we would expect the sea breeze activity starting in April, reaching maximum intensity in June, then ending by October.

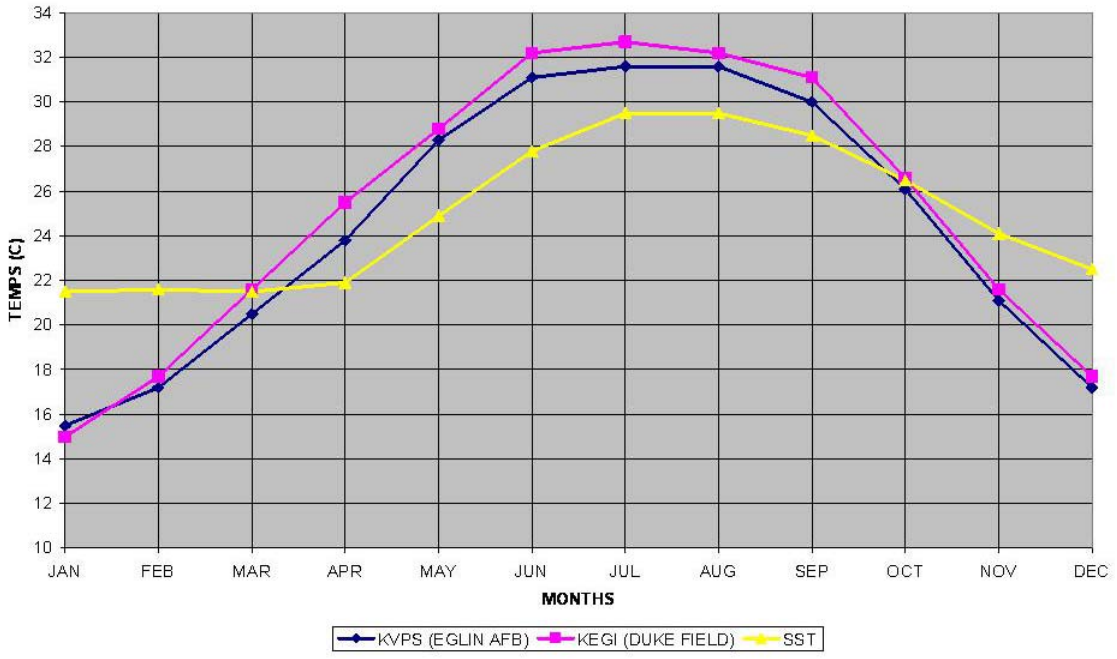


Figure 9. Comparison of average monthly high temperatures (°C) between Eglin AFB (blue) and Duke Field (pink) average to the monthly sea surface temperatures (°C ) recorded at Buoy 42039 (yellow), located in the Gulf of Mexico approximately 115 nautical miles south of Eglin AFB

Figure 10 contains plots of wind direction for the months of April to October as a function of local time. K. Borne et al (1998) used the occurrence of a distinct reversal in the surface wind direction within 24 hours, not attributed to a synoptic scale circulation, as the principal criterion to recognize the sea breeze along the Swedish coast. The figure shows that the winds are primarily northerly for all months between midnight and 0500L. As the sun rises and surface heating commences, the winds respond by turning east-southeasterly. This is considered to be an influence of the Choctawhatchee Bay and the initiation of the sea breeze. Average monthly temperatures for the bay are similar to Buoy 42039, but detailed daily records are not available. Since the depth of the bay is shallow, significant diurnal temperature changes are likely and it is possible that bay temperatures can be significantly cooler by mid morning, thereby initiating the southeasterly wind. By 1500-1700L, winds in all months are southwesterly, which is onshore. As the sun sets and land cools, winds return to a northerly direction and complete the 24 hour wind reversal.

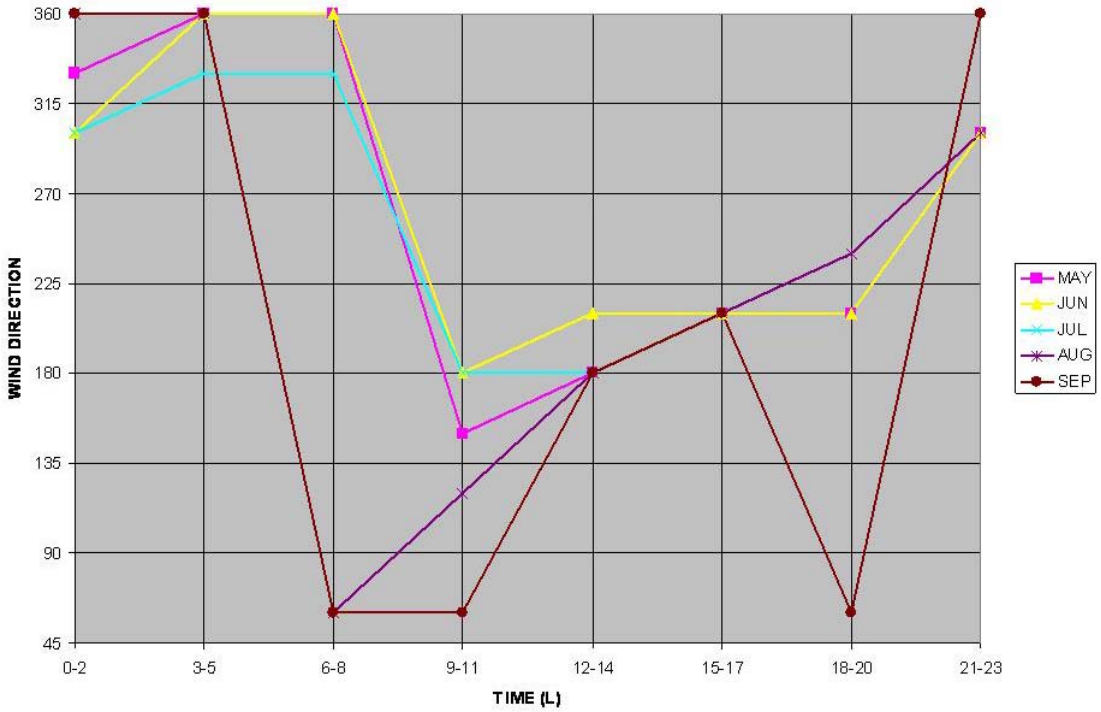


Figure 10. Wind direction as a function of local time (CDT) at Eglin AFB for the months of May (pink), June (yellow), July (turquoise), August (purple), and September (red).

The impact of the synoptic-scale flow along the complex coastline of Eglin on sea breeze evolution is investigated in subsequent chapters. Chapter III outlines the data used in this study as well as the analysis methods employed. Results are discussed in Chapter IV.

# III. DATA AND METHODOLOGY

765 days from May through September, 2001 to 2005, were considered for this study. Days with similar low-level winds were grouped together in order to investigate the impact of the synoptic-scale flow on the sea breeze at Eglin. The methods used to gather the data and procedures used to group days by flow regime are described in the following sections.

## A. DATA

### 1. Radiosonde Data

Radiosonde data from 2001 to 2005 were available for download on the University of Wyoming website (http://weather.uwyo.edu/upperair/sounding.html). Tallahassee, Fl (KTLH) was chosen as the site that best describes the low-level flow in the Eglin region. Tallahassee is 217 km east of Eglin AFB and is the closest routinely available radiosonde observation. The 12 UTC sounding for each day of the study was downloaded and saved as a text file. The 925 mb wind direction, speed, month, day, and year from each sounding was entered into a spreadsheet. 12 UTC soundings were available for 737 of the 765 days considered for this study (Table 1).

| 12 UTC KTLH SOUNDINGS | | | | | | |
|---|---|---|---|---|---|---|
| | MAY | JUNE | JULY | AUGUST | SEPTEMBER | TOTALS |
| 2001 | 30 | 29 | 29 | 27 | 23 | 138 |
| 2002 | 31 | 30 | 31 | 31 | 29 | 152 |
| 2003 | 30 | 29 | 31 | 31 | 30 | 151 |
| 2004 | 29 | 27 | 31 | 30 | 30 | 147 |
| 2005 | 30 | 30 | 30 | 30 | 29 | 149 |
| TOTALS | 150 | 145 | 152 | 149 | 141 | 737 |

Table 1. Available 12 UTC KTLH upper air soundings by month and year.

## 2. Surface Observations

Observations from 19 sites located in and around the Eglin Range Complex (Fig. 11) were collected for each day of the study. Each type of observation is discussed in the following sections.

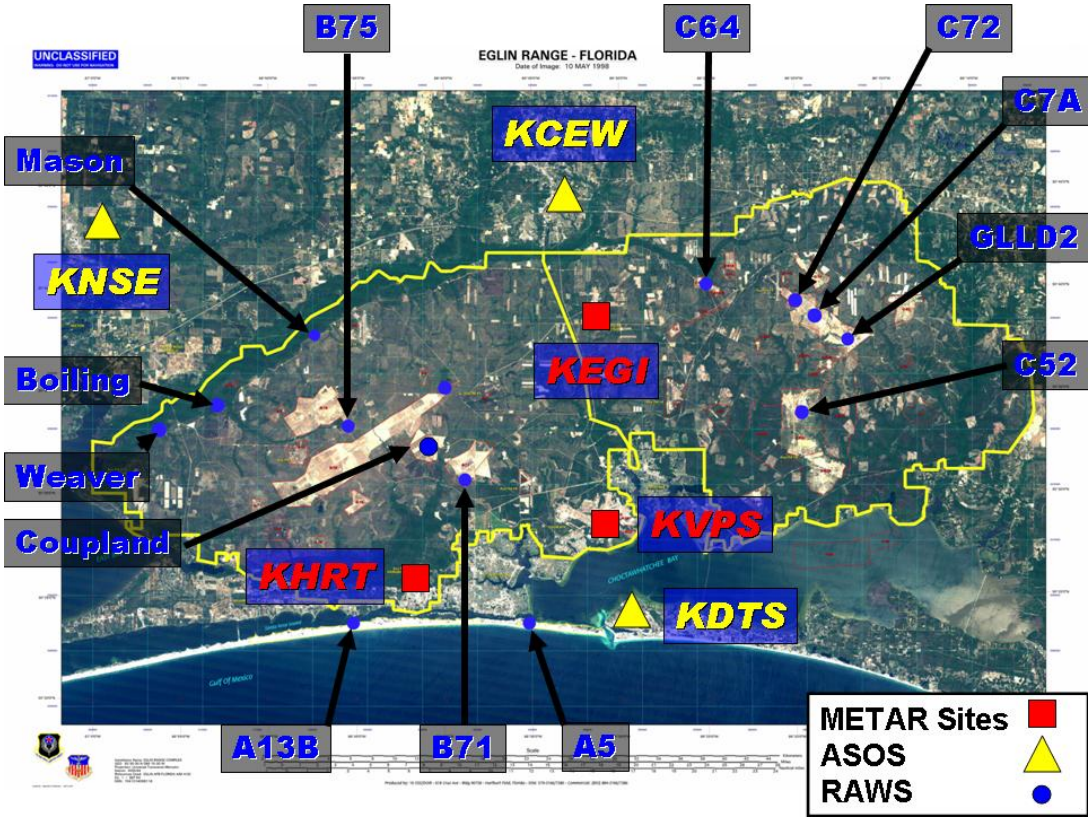


Figure 11. Locations of automated and manned surface weather observations used in this study. Red squares indicate locations of METAR sites, yellow triangles indicate locations of ASOS sites, and blue circles indicate locations of RAWS sites.

### *a. Remote Automated Weather Sensor (RAWS) Sites*

The RAWS system is a fixed meteorological weather system employed by the 46$^{th}$ Training Wing to support flying and ground missions on the Eglin Range Complex (Fig. 12). 13 sensors were available for the study period. The Model 555 Data Acquisition System, a self-contained microprocessor-based environmental data collection system, records temperature (°F), wind speed (knots), direction (knots), wind gusts (knots), relative humidity (%), and barometric pressure (Ins Hg) at two minute intervals.

The data is transmitted via a Very High Frequency (VHF) radio link from the remote system to the 46th WS where it is recorded on a computer.

Figure 12. Picture of the RAWS at site C-72.

RAWS data was obtained from the 45th WS in the form of tab delimited text files. Incomplete or corrupt observations were removed from the data set. Table 2 details the RAWS system locations, elevations, and data availability.

| REMOTE AUTOMATED WEATHER SENSORS (RAWS) | | | | |
|---|---|---|---|---|
| **SENSOR** | **LAT (D.M.S)** | **LONG (D.M.S)** | **ELEV (FT MSL)** | **DATA AVAILABILITY** |
| A-5 | 30.23.43N | 86.35.47W | 10 | 2001, 2002, 2003, 2004, 2005 |
| A-13B | 30.23.39N | 86.45.59W | 10 | Sep 2004, 2005 |
| B-71 | 30.31.04N | 86.38.25W | 149 | 2001, 2002, MAY-JUN 2003, 2004, 2005 |
| B-75 | 30.33.13N | 86.45.36W | 201 | 2001, 2002, 2003, 2004, 2005 |
| C-52N | 30.34.49N | 86.19.41W | 183 | 2001, 2002, 2003, 2004, 2005 |
| C-72 | 30.39.44N | 86.20.47W | 258 | 2001, 2002, 2003, 2004, 2005 |
| BOILING | 30.34.43N | 86.53.59W | 25 | 2001, 2002, 2003, 2004, 2005 |
| MASON | 30.38.31N | 86.47.12W | 25 | 2001, 2002, 2003, 2004, 2005 |
| WEAVER | 30.33.11N | 86.56.18W | 25 | 2001, 2002, 2003, 2004, 2005 |
| COUPLAND | 30.31.28N | 86.39.10W | 253 | 2001, 2002, 2003 |
| C7A | 30.38.13N | 86.19.56W | 210 | 2003, 2004, 2005 |
| GLLD2 | 30.37.52N | 86.17.21W | 206 | 2003, 2004, 2005 |
| C64 | 30.40.15N | 86.25.08W | 198 | JUNE 2003, 2004, 2005 |

Table 2. RAWS Sensor Data

Sensors Boiling, Mason, and Weaver are used to support Army Ranger training along the Yellow River (Ref Figure 11 for location). The region is heavily forested and the sensors are located in small clearings surrounded by trees. As a result, weaker wind speeds are reordered at these sites because the trees block the wind sensors. This also resulted in many observations of calm winds. However, wind direction compared favorably to surrounding observations. Given the need for observations from this region of the study domain, data from the three RAWS sites were not excluded, but impacted the analysis. Impacts are discussed in the next chapter.

### *b. METAR Sites*

Air Force Weather personnel record and disseminate surface weather observations from Eglin AFB, Duke Field, and Hulbert Field. Weather observations are coded and disseminated in Aviation Routine Weather Reports, or METAR code. The Air Force Combat Climatology Center (AFCCC) provided hourly METAR observations in the form of comma delimited text files. Wind direction, speed (knots), gust (knots), temperature (C), dew point (C), and pressure (Ins Hg) were used in this study. Visual quality control was conducted and corrupt or missing data was removed from the data set.

Observations are recorded and disseminated daily without breaks in service at both Eglin AFB and Hulbert Field. However, Duke Field is a limited duty station and observations are recorded and disseminated Monday through Friday between 14 UTC and 4 UTC. Table 3 details the location and data availability of the three METAR sites.

| METAR SITES | | | | | |
|---|---|---|---|---|---|
| STATION | ICAO | LAT (D.M.S) | LONG (D.M.S) | ELEV (FT MSL) | DATA AVAILABILITY |
| EGLIN AFB, FL | KVPS | 30.28N | 86.31W | 95 | MAY-SEP 2001-2005 |
| DUKE FIELD, FL | KECI | 30.39N | 86.31E | 197 | MAY-SEP 2001-2005 |
| HULBERT FIELD, FL | KHRT | 30.25N | 86.4W | 36 | MAY-SEP 2001-2005 |

Table 3. METAR Sites.

### *c. Automated Surface Observing System (ASOS) Sites*

ASOS sites are located at regional airfields and are not augmented by human observers. Sensors measure and record wind direction, speed (knots), gust (knots), temperature (C), dew point (C), and pressure (Ins Hg), format the observation in METAR code, and disseminate the observation. Hourly surface observations from three ASOS sites were obtained from AFCCC in comma delimited text files. The same quality control measures were conducted with ASOS data as with RAWS and METAR files. Table 4 details the location and data availability of the ASOS sites.

| ASOS SITES | | | | | |
|---|---|---|---|---|---|
| STATION | ICAO | LAT (D.M.S) | LONG (D.M.S) | ELEV (FT MSL) | DATA AVAILABILITY |
| CRESTVIEW, FL | KCEW | 30.46N | 86.31W | 220 | MAY-SEP 2001-2005 |
| DESTIN, FL | KDTS | 30.24N | 86.28W | 23 | MAY-SEP 2001-2005 |
| WHITING FIELD, FL | KNSE | 30.43N | 87.1W | 200 | MAY-SEP 2001-2005 |

Table 4. ASOS Sites

### 3. GOES Satellite Data

GOES-12 IR satellite imagery was available from the National Climatic Data Center Historical GOES Browser Server (http://cdo.ncdc.noaa.gov/GOESBrowser) and Unisys Satellite Imagery Achieve (http://weather.unisys.com/archive/sat_ir/) websites. Between the two sources, imagery was available for each day of the study.

### 4. KEVX WSR-88D Radar Data

Base Reflectivity products from the Eglin WSR-88D (KEVX) were obtained from the National Climatic Data Center (NCDC) web site (http://www.ncdc.noaa.gov/oa/radar/radarresources.html) and are used to present case studies of sea breeze events. The KEVX NEXRAD site is located 60 km east of Eglin AFB and provides excellent coverage of the Eglin Range Complex. Data was obtained using the NCDC NEXRAD Inventory Search Tool and displayed using the NCDC Java NEXRAD Viewer.

### 5. NCEP/NCAR Surface Reanalysis

In order to composite days with similar synoptic-scale flows, surface observations had to be fit to a horizontal grid. NCEP/NCAR reanalysis variables of air temperature, mean sea level pressure, zonal and meridional wind components were used by an interpolation scheme to combine the observations with the surface reanalysis fields to produce an objective analysis on a 2 km grid. The variables used are Class A variables and are considered the most reliable class of variables because they are strongly influenced by observed data (Kalnay et al. 1996). Reanalysis variables were available at a horizontal resolution of 2.5°, temporally every six hours at 00, 06, 12, and 18 UTC, and in standard GRIB format from the NPS Department of Meteorology. The interpolation method is covered in a later section.

## B. METHOD OF ANALYSIS

Numerical and observational studies have demonstrated that three factors largely determine the development, evolution, and inland penetration of the sea breeze. These

factors are adequate differential heating between land and water, coastline shape and low-level synoptic flow. The analysis methodology was developed to ensure that each factor is addressed and a complete set of sea breeze days was compiled.

### 1. Removal of Disturbed Days

The first step in this study was to compile a set of days that were not influenced by tropical or synoptic-scale weather disturbances. Cloud cover associated with these types of disturbances, especially significant cloud cover at sunrise, limits the amount of differential heating between land and water and disrupts the normal summertime convective regime, resulting in a weak or non-existent sea breeze. In order to filter these days from the study, a subjective classification scheme was used to designate each day as "disturbed" or "undisturbed" based on the 12 UTC GOES-12 IR image. A similar classification scheme was employed by Burpee (1979) in a study of south Florida convection and by Biggar (1992) in his study of sea breeze enhanced thunderstorms along the Florida Panhandle. If the IR image indicated cloud cover over the Eglin area, the day was tentatively classified as "disturbed". The final determination was made based on the 12 UTC KVPS observation. If more than 50% cloud cover was reported, the day was classified as "disturbed" and eliminated from the study. Of the 737 days considered, a total of 228 days were classified as "disturbed" and eliminated, leaving 509 "undisturbed" days with the potential for developing a strong sea breeze.

### 2. Synoptic-Scale Flow Regimes

In order to examine the influence of the synoptic-scale flow on the sea breeze, a classification scheme was required to determine if the flow was offshore, onshore, or coast-parallel for the 509 "undisturbed" days of the study. The objective was to create flow regimes so that the wind within each would be approximately parallel or perpendicular to the coastline. This determination was based on the coastal geometry of the Eglin region (Fig. 13). Even though the coastline is concave, its orientation is basically west to east. Therefore, the flow regime was classified as Coast-Parallel Westerly (coast parallel with land on the left) if low-level winds were between 256-289° and Coast Parallel Easterly (coast parallel with land on the right) if the low-level winds

were between 075-119°. Flow from 290-074° was classified as Offshore and flow between 120-255° was classified as Onshore. An additional flow regime of Calm was established if the wind speed was less than 3 $ms^{-1}$, regardless of flow direction, in order to study the sea breeze under light synoptic-scale flow.

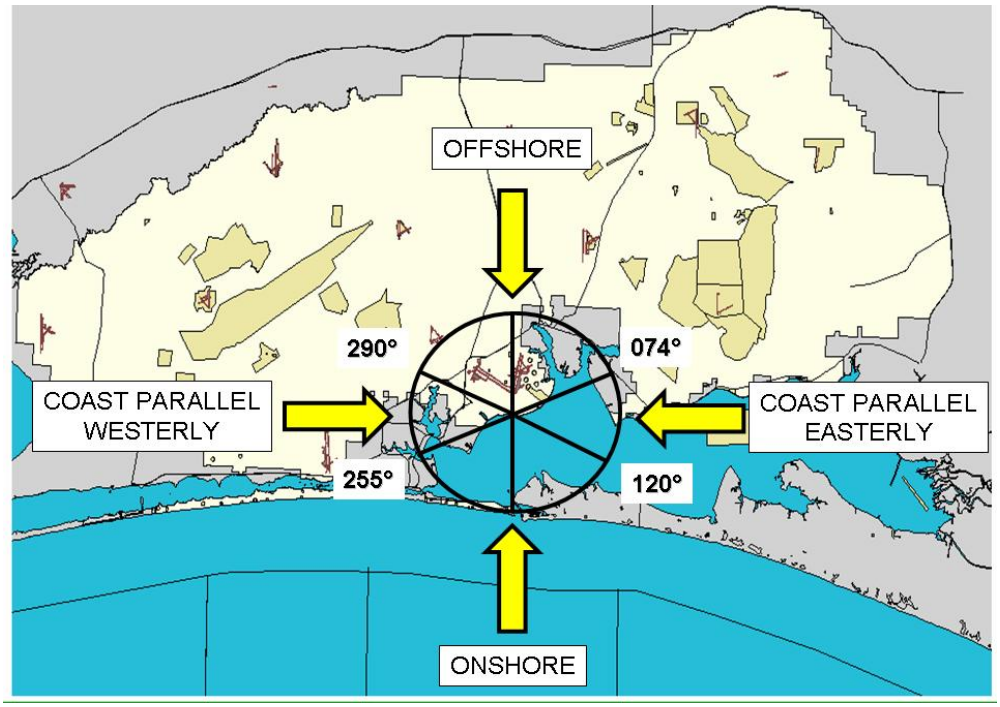


Figure 13. Quadrants for classifying the synoptic-scale flow over Eglin AFB, Fl. The flow regime was classified as Coast-Parallel Westerly (coast parallel with land on the left) if low-level winds were between 256-289° and Coast Parallel Easterly (coast parallel with land on the right) if the low-level winds were between 075-119°. Flow from 290-074° was classified as Offshore while flow between 120-255° was classified as Onshore.

A distinction is made between light, moderate, and strong flow since increasing the strength of the synoptic-scale winds has a dramatic effect on the development, evolution, and movement of the sea breeze front. Opposing synoptic flow inhibits the inland penetration of the sea breeze but also enhances the convergence and upward vertical motion along the sea breeze front. Conversely, onshore synoptic flow aids in the inland penetration of the sea breeze but limits the development of convergence along the sea breeze front. Therefore, offshore flow was divided into 3-5, 5-7, 7-9, and > 9 $ms^{-1}$

bins and onshore flow was divided into 0-3, 3-5, and greater than 5 $ms^{-1}$ bins. Since coast parallel flows are hybrids of the offshore and onshore regimes, Coast Parallel Westerly uses the onshore speed bins and Coast Parallel Easterly uses the offshore speed bins.

## 3. Categorizing Days According to Flow Regime

This study follows previous Florida studies (Lopez and Holle 1987; Biggar 1992; Gould and Fuelberg 1996; Stroupe et al. 2004) by grouping days that have similar synoptic-scale flows. Each of the 538 days was designated as Offshore, Onshore, Coast Parallel Westerly, or Coast Parallel Easterly based on the 925 mb wind direction taken from the corresponding day's 12 UTC KTLH sounding. The 925 mb flow was assumed to be representative of the synoptic-scale flow over the Eglin region. Previous studies (Lopez and Holle 1987; Cetola 1997; Stroupe et al. 2004) used similar methods to determine flow regimes for the Florida Panhandle. 12 UTC is the morning sounding for the Eglin region, 0700L CDT, and therefore represents the low-level flow regime the sea breeze developed under as daytime heating commenced. In addition, this level is considered the gradient level and located above the nightly radiation inversion, under which wind direction and speed are influenced by mesoscale processes and not representative of the synoptic-scale flow. Once the flow regime was determined, the 925 mb wind speed was used to place that day in the appropriate speed bin associated with the flow regime. The date, wind direction, and wind speed in knots and $ms^{-1}$ were entered into a spreadsheet. Of the 509 "undisturbed" days, 122 were classified as Offshore, 210 were classified as Onshore, 53 were classified as Coast Parallel Westerly, and 77 were classified as Coast Parallel Easterly. Table 5 lists the total number of days that fell into each flow regime and speed bin. Reference Appendix A through E for complete lists of days included in each flow regime.

| 2001-2005 SYNOPTIC SCALE REGIME TOTALS | | | | | | | | |
|---|---|---|---|---|---|---|---|---|
| FLOW REGIME | OFFSHORE | | | | ONSHORE | | | CALM |
| SPEED BIN | 3-5 m/s | 5-7 m/s | 7-9 m/s | >9 m/s | 0-3 m/s | 3-5 m/s | >5 m/s | < 3 m/s |
| # of Days | 52 | 34 | 17 | 19 | 38 | 80 | 92 | 107 |
| Avg Direction (°) | 345 | 333 | 355 | 38 | 185 | 189 | 192 | 199 |
| Avg Speed (Kts) | 7.54 | 11.09 | 15.12 | 24.00 | 3.87 | 7.56 | 13.32 | 3.54 |
| Avg Speed (m/s) | 3.88 | 5.71 | 7.78 | 12.60 | 1.99 | 3.89 | 6.85 | 1.82 |
| | | | | | | | | |
| FLOW REGIME | CP EASTERLY | | | | CP WESTERLY | | | |
| SPEED BIN | 3-5 m/s | 5-7 m/s | 7-9 m/s | >9 m/s | 0-3 m/s | 3-5 m/s | >5 m/s | TOTAL DAYS |
| # of Days | 7 | 20 | 26 | 14 | 12 | 13 | 28 | 509 |
| Avg Direction (°) | 99 | 91 | 94 | 91 | 270 | 271 | 270 | |
| Avg Speed (Kts) | 7.71 | 10.65 | 15.08 | 23.94 | 3.42 | 7.15 | 13.75 | |
| Avg Speed (m/s) | 3.97 | 5.48 | 7.76 | 12.32 | 1.76 | 3.68 | 7.08 | |

Table 5. 2001-2005 synoptic-scale flow regime totals.

## 4. Multiquadric Interpolation

Hourly analyses of the 509 days were produced using the surface observations obtained from the study area to allow compositing of like regimes. To accomplish this task, a multiquadric interpolation scheme developed by Nuss and Titley (1994) was employed to fit the scattered surface observations to an analysis grid. The interpolation scheme, called 3DMQ, used two dimensional interpolation to combine the scattered observations with a first guess field into a surface analysis on a 2 km grid covering the area. NCEP/NCAR reanalysis fields were used as the first guess field. The benefit in using the multiquadric interpolation scheme is that by fitting the observations to a regular grid, computational diagnostics can be performed on the meteorological fields. Nuss and Titley (1994) demonstrated that multiquadric interpolation, which uses hyperboloid radial basis functions, is superior to several other interpolation schemes to fit scattered data to uniform grids while retaining small scale features resolved by the observations. Furthermore, Nuss and Titley (1994) demonstrated the superior accuracy of multiquadric interpolation over Cressman and Barnes interpolation schemes with meteorological observations distributed across a land-sea boundary.

Following Nuss and Titley (1994), the interpolation equation using radial basis functions is

$$H(X) = \sum_{i=1}^{N} \alpha_i Q(X - X_i) \qquad (3.1)$$

where $H(X)$ is a spatially varying field such as temperature or pressure and $Q(X - X_i)$ is a radial basis function where $Q(X - X_i)$ represents the vector between an observation point $X_i$ and any other point in the domain. The coefficients $\alpha_i$ are weighting functions that are specified. The multiquadric method uses hyperboloid functions as the basis functions in the form

$$Q(X - X_i) = -\left( \frac{\|X - X_i\|^2}{c^2} + 1.0 \right)^{\frac{1}{2}} \quad (3.2)$$

where $c$ is an arbitrary, and typically, small constant called the multiquadric parameter. Here $X$ represents the position vector in two dimensions.

The problem in applying this technique to meteorological observations is that errors and incomplete sampling of small scale features may result in unrealistic analyses. Observation error can be addressed using a smoothing parameter $\lambda$ that filters unresolved scales from the analysis. The observation error can be varied for different observation sources with the result that the analysis will fit more closely to some observations than others. In this study, less error was assigned to the actual observations than to the reanalysis fields.

The multiquadric parameter becomes important when spacing between observations becomes very small. For small values of $c$, very tight gradients are easily represented. For large values of $c$, the interpolation cannot easily represent tight gradients or fit closely spaced observations. However, observation spacing with this data set is not a factor, so $c$ is small and can easily represent the gradients.

A shell script called run3dmq organized the input fields for 3DMQ. 3DMQ required an observation time and two first guess times that straddle the observation time. NCEP/NCAR reanalysis fields were available at six hour intervals (00, 06, 12, 18 UTC) and at 2.5° resolution; therefore, 3DMQ linearly interpolated the meteorological variables in time to provide the first guess field on the 2 km grid. For example, an analysis using observations from 16 UTC on 5 June would be fit between first guess analyses at 12 UTC and 18 UTC from 5 June. Wind direction, speed (knots), temperature (C), dew point (C)

or relative humidity (%), and pressure (In Hg) were extracted from the observation text files. 3DMQ was run for 00 through 23 UTC for each of the 509 days of the study. Each run of 3DMQ produced output files for temperature, U wind component, V wind component, moisture, geopotential height and sea level pressure. A hardcopy of surface winds, temperature and available observations was generated for each run of 3DMQ for quality control purposes (Fig. 14). If missing or bad observations were detected, the observation was removed and 3DMQ was re-run for that hour.

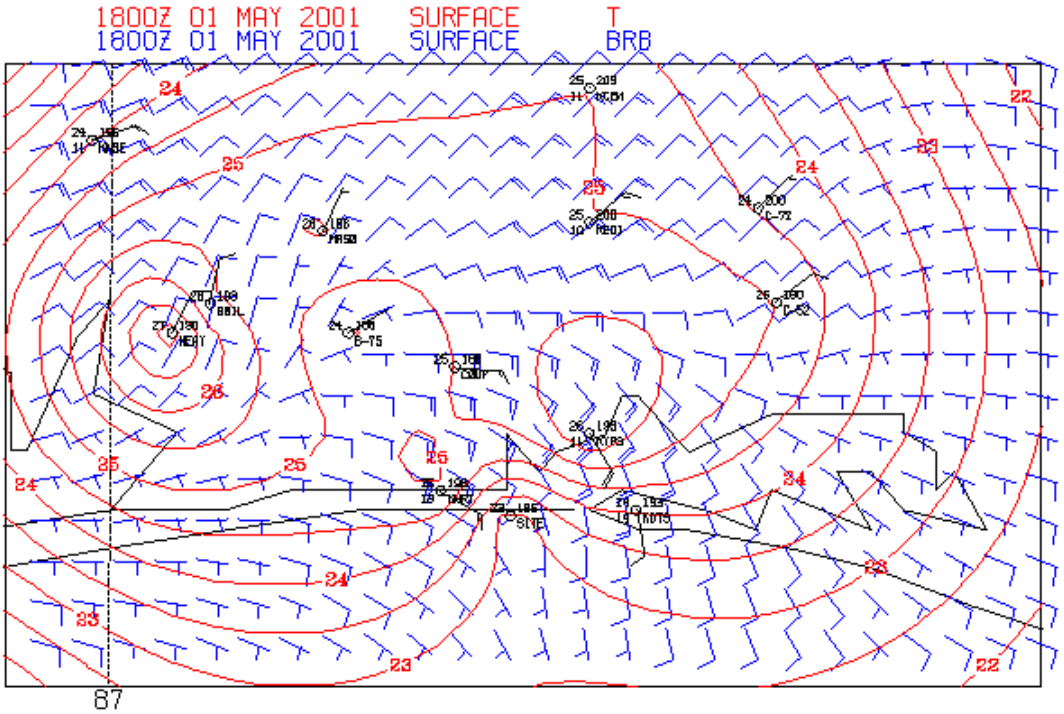


Figure 14. Output from the multiquadric interpolation scheme 3DMQ over the study domain. Surface isotherms in °C are colored red, winds in knots are blue and station plots of available observations are black. Gridded fields are available at 2 km resolution.

There are several properties of the multiquadric interpolation scheme that must be highlighted. The first issue that arises is the lack of observations at the boundaries of the domain, especially the southern and eastern boundaries. An important property of the multiquadric technique is that it smoothly analyzes the scales represented by the observations in one region while not producing undesired results elsewhere (Nuss and Titley 1994). In our case, the boundaries of the domain are data-sparse while the center

of the domain is more data-dense. The multiquadric interpolation scheme retains the large-scale features at the boundaries of the domain without sacrificing resolution of the small-scale features at the center of the domain. The lack of observations at the boundaries causes the analyses to default to the 2.5° resolution first guess field. The result is a distinct circular shape to the isotherm analysis seen in Figure 15. It is unlikely any conclusions can be drawn from analysis or computations generated at the edges of the study domain due to the lack of resolution. Secondly, the RAWS sites discussed in section 2.B.1 influence the objective analysis by decreasing the wind field at each grid point along the Yellow River. The placement of the RAWS in a forested region resulted in wind speeds that are weaker than surrounding stations. The effect of the interpolation scheme is to resolve this feature and decrease the magnitude of the first guess velocity field in this region. Therefore, wind speed along the Yellow River is consistently weaker.

### 5. Compositing

Once surface analyses were completed for each of the 509 days, they were composited by flow regime via a program called AVERAGE. AVERAGE is a FORTRAN program developed by Professor Wendell Nuss that takes a list of gridded data and computes the mean of the specified field at each grid point. The result is a composite field over the study domain which can then be displayed. Composite surface analyses were generated for each of the flow regimes to investigate the hourly evolution of the sea breeze under the various synoptic-scale flow regimes. Results from the composites are discussed in the next chapter.

### 6. VISUAL

The VISUAL program is a FORTRAN program developed by Prof. Wendell Nuss to display a wide variety of meteorological datasets. The program is based on NCAR Graphics and XGKS graphical software for plotting. The gridded analyses generated from 3DMQ were manipulated and displayed using VISUAL to diagnose characteristics of the sea breeze.

### 7. Sea Breeze Front Intensity

A common diagnostic equation used to determine frontal strength is Frontogenesis. Frontogenesis (frontoloysis) is defined as the rate of increase (decrease) of the magnitude of the temperature gradient with time (Carlson 1991, p. 351). Following Carlson (1991, p. 353), the Frontogenesis equation is

$$\frac{d}{dt}\left(-\frac{\partial\theta}{\partial y}\right)=-\left(\frac{\partial u}{\partial y}\right)\left(\frac{\partial\theta}{\partial x}\right)+\left(\frac{\partial v}{\partial y}\right)\left(\frac{\partial\theta}{\partial y}\right)+\left(\frac{\partial\omega}{\partial y}\right)\left(\frac{\partial\theta}{\partial p}\right)-\frac{\partial}{\partial y}\left(\frac{\partial\theta}{\partial t}\right) \quad (3.1)$$

where the time rate of change of the one-dimensional temperature gradient, $-\left(\frac{\partial\theta}{\partial y}\right)$, is considered a measure of frontal strength. The y-direction is taken to be across the front towards cold air. Equation (3.1) relates certain physical processes, which act to strengthen or weaken the thermal gradient, to the evolution of the potential temperature gradient over time.

The first term on the right hand side of equation 3.1 describes the effect of horizontal shear in rotating along-front thermal gradients $\frac{\partial\theta}{\partial x}$ into cross-front thermal gradients. The continued effect of the shear wind field is to push the isotherms together with time (Fig. 15).

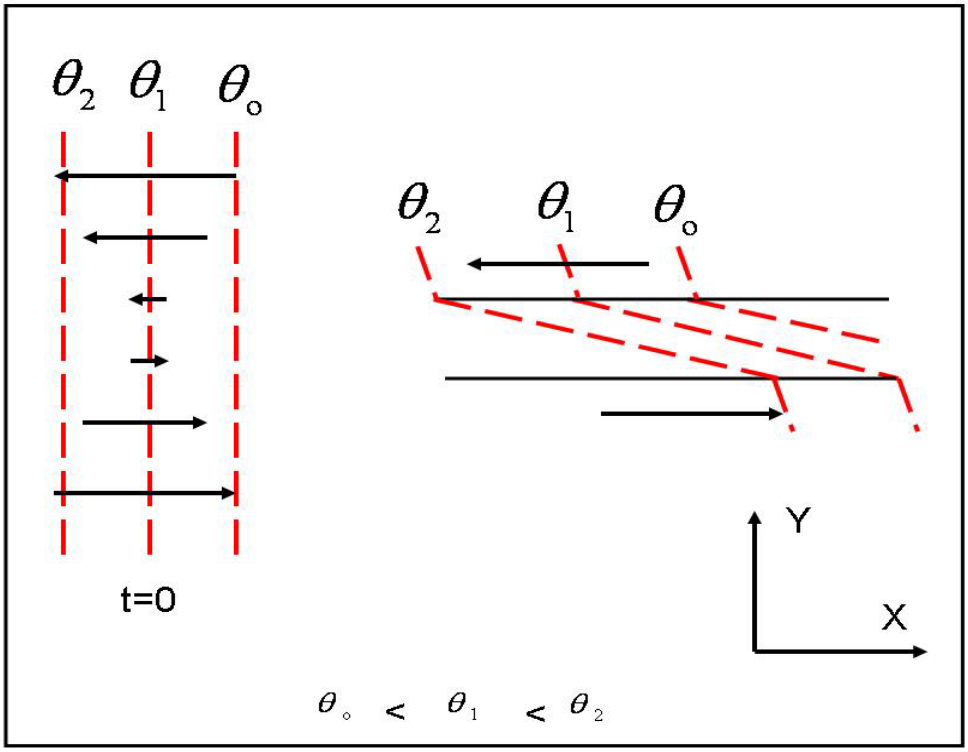


Figure 15. Schematic temperature deformation for pure shear. Broken red lines represent isotherms. Arrows represent the direction and magnitude of the initial wind deformation (t=0). (From Ref. Carlson 1991).

The second term contains the effects of confluence or convergence in the cross-front wind components $\frac{\partial v}{\partial y}$ in concentrating a thermal gradient. In confluent deformation, the flow pattern acts to compress the thermal gradient with time, as shown in Fig. 16. Arritt (1993) determined that convergence is the dominate term in sea breeze frontogenesis. When the synoptic scale flow is directed offshore, the temperature gradient is enhanced by convergence between the offshore flow and sea breeze winds. Conversely, when the synoptic-scale flow is directed onshore, convergence is suppressed and the thermal gradient is not intensified.

Frontogenesis is important because the process that acts to alter the intensity of thermal gradients in fronts results in important vertical circulations that can organize clouds and precipitation. Changes in the intensity of the sea breeze front, as measured by frontogenesis, can indicate likely areas and times of strong vertical motions that create

clouds and precipitation. The third and fourth term, the tilting and diabatic terms, represent important physical process but are not evaluated in this thesis.

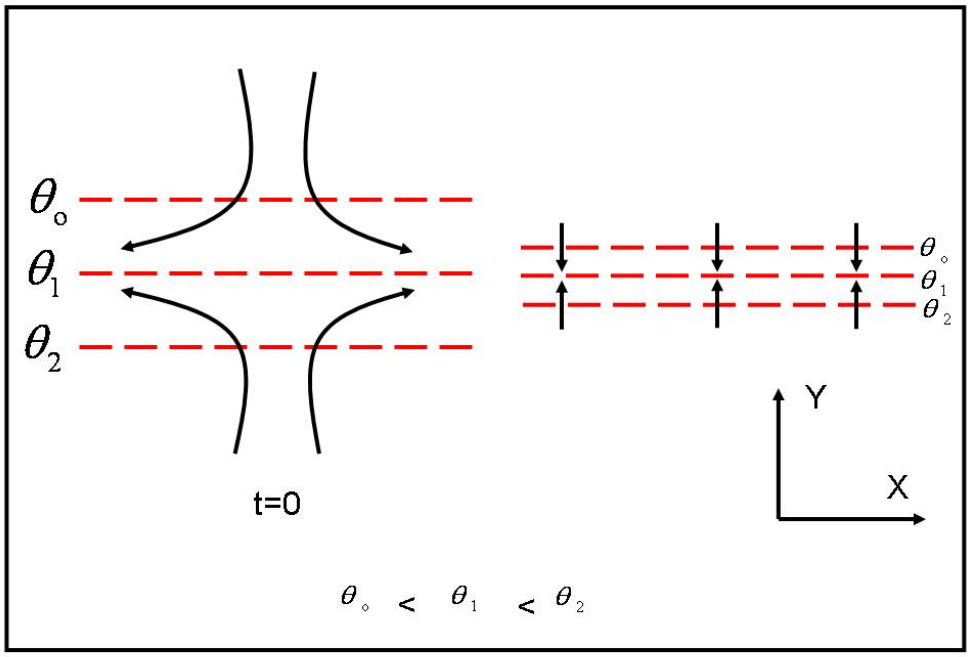


Figure 16. Schematic deformation pattern for pure confluence. The broken red lines represent isotherms and arrows the magnitude and direction of the wind. The initial wind and temperature distribution is at t=0. (From Ref. Carlson 1991).

The strength of the sea breeze front is a balance between the frontogeneic effect of convergence and the frontolytic effect of turbulent mixing. As the cool sea breeze air mass moves inland, it converges with warm air that has been heated over land. The convergence of onshore sea breeze winds with opposing flow over land acts to tighten the thermal gradient between the two airmasses which leads to the formation of the sea breeze front. On the other hand, as the cool sea breeze air penetrates inland, it is heated by the land and warms through turbulent mixing. This process acts to reduce the temperature contrast between the two air masses, which is frontolytic.

Results from the composites of offshore, onshore, and coast parallel synoptic-scale flow regimes are presented in the next chapter.

# IV. RESULTS

This chapter presents the results of the composite surface charts generated for the calm, offshore, onshore and coast parallel flow regimes. Hourly composite surface analyses where generated starting at 06 UTC (0100 CDT) through 05 UTC (2400 CDT) for each synoptic-scale flow regime to determine the impact of the synoptic scale flow on the inland penetration and intensity of the sea breeze at Eglin.

Through the use of frontogenesis and temperature analysis, the impact of the synoptic scale flow on the inland penetration and intensity of the sea breeze front at Eglin is investigated. A case study is presented for each synoptic-scale flow regime using surface analyses and WSR-88D reflectivity products to gain insight into the characteristics of the sea breeze prior to presenting the results of the composites. The case studies provide a representative example of what the composite generalizations are based on and illustrate some of the data limitations. WSR-88D reflectivity products are not impacted by these limitations and provide observed data that can be used to help interpret the composites.

## A. COMPOSITES

### 1. Calm

The Calm regime is presented first because an understanding of sea breeze evolution free of synoptic-scale influences provides a good baseline from which to infer the impact of the other synoptic-scale flows on sea breeze evolution. Estoque (1962) noted that the magnitude of the circulation and vertical motion associated with the sea breeze in a no-wind case were similar to the offshore case, but had several important differences. Firstly, the onset of the sea breeze occurred earlier without opposing flow. Secondly, the sea breeze front penetrated farther inland than the offshore flow case.

A case study is presented to highlight the characteristics of the sea breeze under calm synoptic wind conditions at Eglin, followed by the Calm composites.

### *a. 7 May 2005 Case Study*

The synoptic-scale winds from the 7 May 2005 12 UTC Tallahassee sounding was from the northeast at 0.5 $ms^{-1}$. The sea breeze began at 15 UTC (UTC=CDT + 5h), approximately three hours after sunrise. A weak 2 to 3 °C temperature gradient had developed between RAWS sites 20 km inland and the coast. Isotherms were aligned parallel to the coastline of the Gulf of Mexico and turned northeastward at Eglin AFB following the coastline of Choctawhatchee Bay. Due to the orientation of the isotherms along the coast, the sea breeze winds were southeasterly along the coast of Choctawhatchee Bay and southerly along the Gulf of Mexico coastline. Flow was light, approximately 2.5 $ms^{-1}$, in response to the weak thermal gradient.

By 18 UTC, the sea breeze had penetrated 20 km inland from the Gulf of Mexico and the Choctawhatchee Bay (Fig 17). The tightest temperature gradient is seen along the coastline and the leading edge of the sea breeze is only evident as a wind shift line. However, cool sea breeze air has surged north from the Gulf of Mexico and Choctawhatchee Bay to RAWS sites Coupland and B-75.

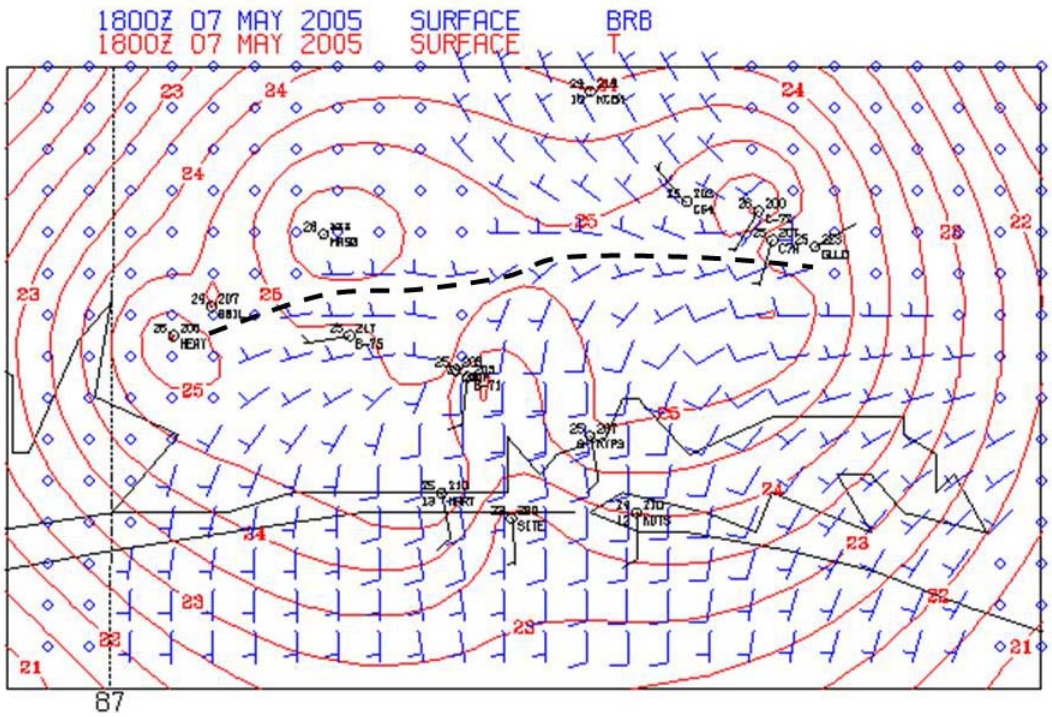


Figure 17. Surface analysis at 18 UTC for 07 May 2005, a Calm flow day. Isotherms (°C) are in red contoured every half degree and winds (full barb 5 $ms^{-1}$, half-barb 2.5 $ms^{-1}$) are plotted at 2 km grid points. Available station observations are plotted in black with temperature (°C top left), sea level pressure (mb top right), winds (full barb 5 $ms^{-1}$, half-barb 2.5 $ms^{-1}$), dewpoint (°C bottom left), and station identification (bottom right). The heavy dashed line represents the location of the wind shift associated with the leading edge of the sea breeze.

A weak thin line is detectable in the 18 UTC KEVX base reflectivity product (Fig. 18) and corresponds to the leading edge of the onshore flow from the 18 UTC surface analyses (Fig. 17). The reflectivity is weak in the thin line because the thermal gradient associated with the sea breeze front is weak, even though wind convergence is evident in the surface analyses.

By 21 UTC, the sea breeze front had penetrated 28 km inland and was located near Crestview (KCEW). The thin line had increased in intensity as it moved north, indicating the sea breeze front strengthened over the past three hours. The 21 UTC surface analyses shows southwesterly sea breeze winds of 10 $ms^{-1}$ along the coastline extending as far north as the center of the Eglin Range Complex. The thermal gradient also intensified as cool marine air was advected inland. A 3 °C temperature gradient had

developed between the sea breeze front and the coastline, which explains the increasing strength of the thin line seen on radar.

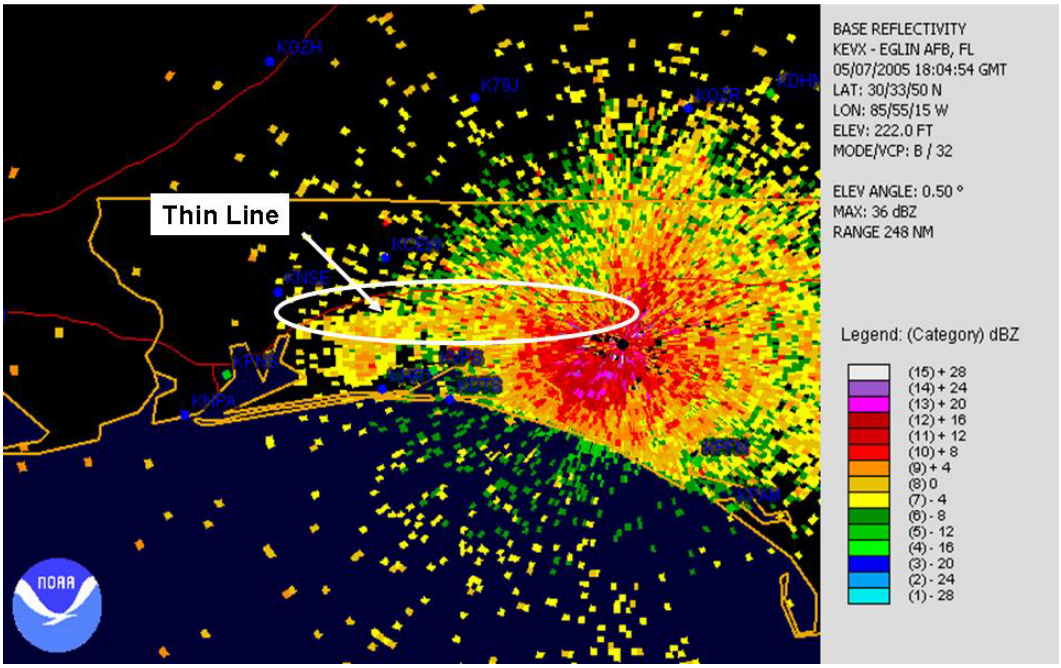


Figure 18. 18 UTC 07 May 2005 KEVX base reflectivity product illustrating the thin line associated with the sea breeze front. The white arrow indicates the direction of the synoptic-scale flow. Station identifiers are in blue and the reflectivity scale is shown on the right hand side of the image. (From Ref. National Climatic Data Center, http://www.ncdc.noaa.gov/oa/radar/radardata.html, February 2006).

By 23 UTC, the sea breeze is located north of Crestview (KCEW). There is very little temperature gradient across the Eglin Range any more as the cool marine air covers the entire area. Winds are southwesterly across the range complex at 5-8 $ms^{-1}$. The thin line on radar and continues to strengthen as the front moves north. Atkins and Wakimoto (1997) suggested that sea breeze fronts often strengthen in the late afternoon due to increased convergence at the sea breeze front as sea breeze flow increases, and due to decreased mixing at the front by boundary layer convection, which decreases by late afternoon. This seems to be happening here. This sea breeze front did not initiate convection as it moved through the Eglin Range.

### *b. Calm Composite*

107 days were categorized as Calm. The average magnitude of the synoptic scale flow is 1.8 $ms^{-1}$. Under calm conditions, the sea breeze begins between 15 and 16 UTC. The strongest thermal gradient occurs along the coastline and the along-coast temperature contours are aligned parallel to the coastline along the Gulf of Mexico; however, the contours bend northeastward and follow the northern coastline of the Choctawhatchee Bay. This indicates that the temperature perturbation created by the bay is large enough to alter the direction of the along-coast temperature contours. As a result, sea breeze onset often begins with winds from the southeast at Eglin AFB. Southeast flow is perpendicular to the along-coast isotherms along this section of coastline. The sea breeze front is weak at this time. There is little opposing flow north of the sea breeze front; therefore convergence along the front is minimal.

By 19 UTC, the sea breeze front is located 25 km from the Gulf of Mexico, 15 km from the Choctawhatchee Bay, and is oriented east to west across the range as indicated by the blue line in Figure 19. A weak temperature gradient has formed along the leading edge of the sea breeze and frontogenesis values of < 20 $K$ $Day^{-1}$ 100 $km^{-1}$ are located along this thermal band. The thermal gradient formed as air behind the front warmed by less than 0.2 °C between 16 and 19 UTC while air temperatures north of the sea breeze front warmed by 1.2 °C over the same three hour period. Thus a 0.8 °C temperature gradient evolved over a 10 km distance. According to equation 2.4, the strength of the sea breeze is proportional to the temperature perturbation across the sea breeze front and inversely proportional to the length scale of the temperature gradient. Under Calm synoptic-scale flow, differential heating increased the temperature perturbation while reducing the length scale of the temperature gradient, thereby increasing the strength of the sea breeze front. By 20 UTC the sea breeze front is north of Crestview and out of the Eglin Range Complex.

Frontogenesis values of 400 $K$ $Day^{-1}$ 100 $km^{-1}$ located to the northeast of East Bay are a result of wind data obtained from the RAWS sensors discussed in Chapter Three (Fig. 19). Analyses of the wind data from the RAWS sensors consistently led to frontogenesis values inconsistent with other observations. It was concluded these data

were of insufficient quality to be used in this study. While it is likely a temperature gradient associated with the sea breeze front exists in this region, the effect of stronger sea breeze flow moving into the region of consistently weak or calm winds acts to increase the convergence in the region, resulting in large frontogenesis values. In addition, reflectivity values associated with the thin line observed in the case study (Fig. 18) do not support the intense sea breeze front implied by the 400 $K$ Day$^{-1}$ 100 km$^{-1}$ frontogenesis values. Therefore, results from this region will not be included in this or the following composites analyses

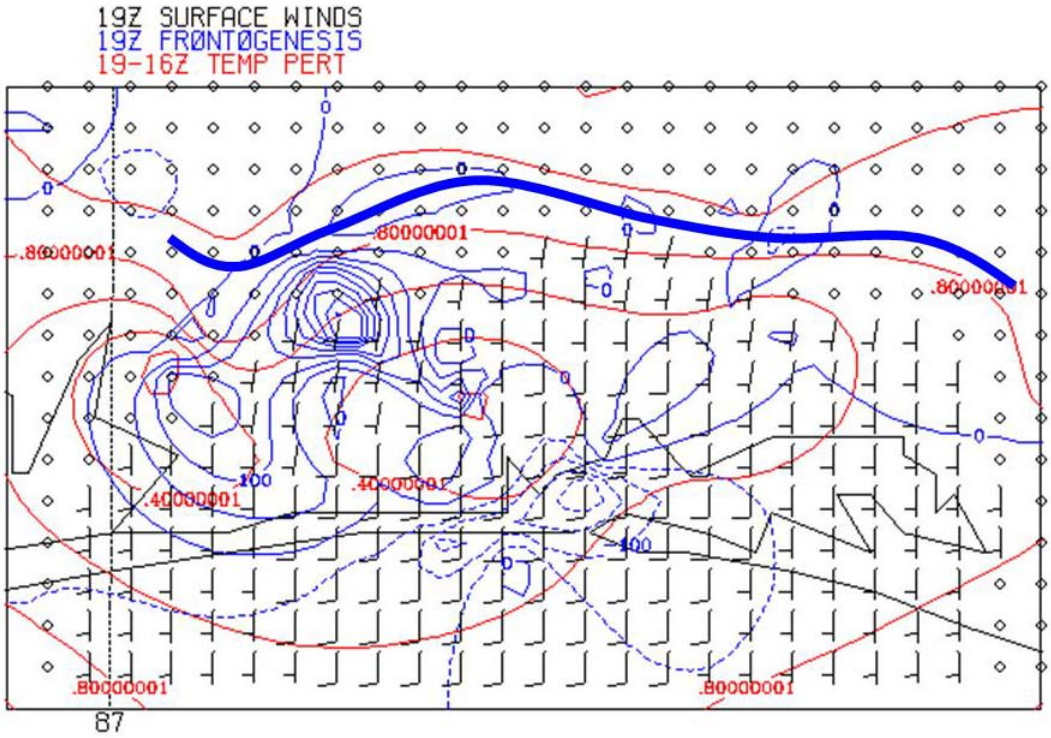


Figure 19. Computed 3-hourly air temperature change (19-16 UTC in °C) contoured every 0.2 °C in red, 19 UTC frontogenesis plotted in blue contours every 50 $K$ Day$^{-1}$ 100 km$^{-1}$ and 19 UTC surface wind barbs (full barb 5 $ms^{-1}$, half-barb 2.5 $ms^{-1}$) for the Calm synoptic-scale flow regime. The heavy blue line indicates the location of the sea breeze front at the leading edge of the temperature gradient.

A graphical illustration of the inland penetration and intensity of the sea breeze front is presented in Figure 20. Based on the along-coast isotherm analyses as in Figure 19, inland penetration distances of the sea breeze front are measured from the Choctawhatchee Bay instead of the Gulf of Mexico in the eastern half of study domain. The sea breeze began by 1530 UTC and by 16 UTC, the sea breeze front was located 10 km inland from the Gulf of Mexico and 5 km inland from the Choctawhatchee Bay. The sea breeze could only be detected by a wind shift line as it moved to a position 20 km from the Gulf of Mexico and 15 km from Choctawhatchee Bay by 19 UTC. The sea breeze front intensified by 20 UTC as onshore flow strengthened to 10 $ms^{-1}$ and convergence increased. Increased convergence, coupled with differential heating, decreased the length scale of the temperature gradient associated with the sea breeze front. By 21 UTC, the sea breeze front had moved north of the Eglin Range Complex.

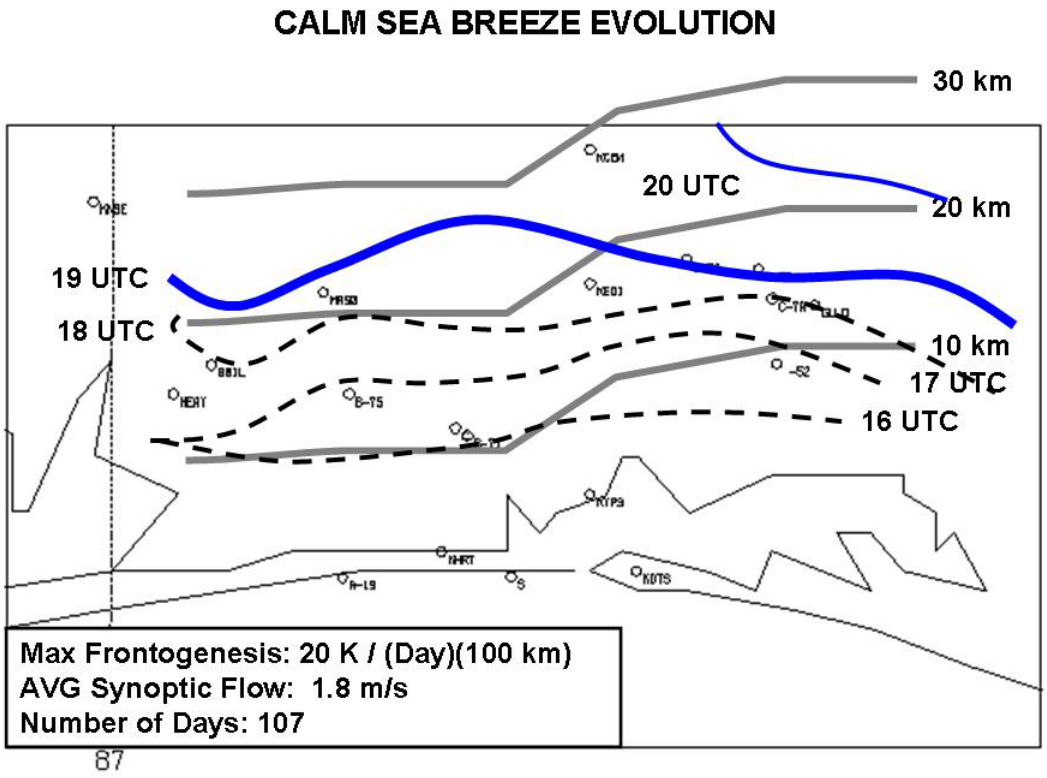


Figure 20. Illustration of the position and intensity of the sea breeze front for Calm synoptic-scale flow in the Eglin Range Complex. Blue lines indicate positions of the sea breeze front and the bold blue line indicates the most intense sea breeze at that hour. Grey lines indicate the distance inland (km) from the Gulf of Mexico and Choctawhatchee Bay.

### 2. Offshore Synoptic-Scale Flow

Studies indicate that offshore synoptic-scale flow produces the most intense sea breezes. It delays the onset of the sea breeze at the coast, which results in increased heating of land surfaces while the marine air over water remains cool. The convergence of the offshore flow over land and the onshore sea breeze winds enhances the thermal gradient and produces strong sea breeze fronts. Evidence suggests that these fronts are most intense during the late morning and early afternoon. Sea breeze fronts forming under offshore flow remain near the coastline until afternoon, at which time the front starts moving inland and decreases in intensity.

#### *a. 23 June 2005 Case Study*

Figure 21 presents the surface analysis at 12 UTC 23 June 2005, an offshore flow day. The 12 UTC KTLH sounding indicated the low-level synoptic-scale flow was from the northeast (55°) at 3.1 $ms^{-1}$. The surface analysis shows that winds were from the northwest to north at 2.5 $ms^{-1}$ across the Eglin Range and coastal areas. Temperatures inland are 21 °C while coastal stations report temperatures near 25 °C, creating a 4 °C temperature gradient over 20 km, with the land cooler than the water. The isotherms are roughly parallel to the Choctawhatchee Bay and bend southwestward towards Hulbert Field. The base reflectivity product from the KEVX WSR-88D (not shown) shows a thin line along the coast to the east of Destin, but a thin line is not evident along the Choctawhatchee Bay and Gulf of Mexico coastline.

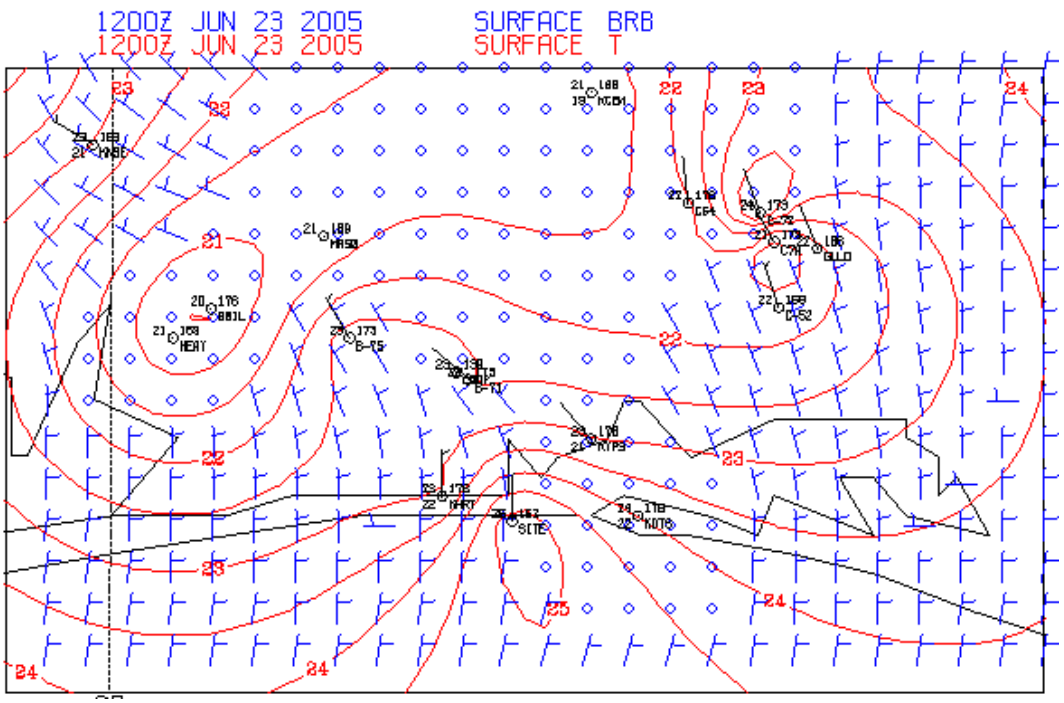


Figure 21. Surface analysis at 12 UTC for 23 June 2005, an offshore flow day. Isotherms (°C) are in red contoured every half degree and winds (full barb 5 $ms^{-1}$, half-barb 2.5 $ms^{-1}$) are plotted at 2 km grid points. Available station observations are plotted in black with temperature (°C top left), sea level pressure (mb top right), winds (full barb 5 $ms^{-1}$, half-barb 2.5 $ms^{-1}$), dewpoint (°C bottom left), and station identification (bottom right).

The sea breeze begins at 1630 UTC, and by 18 UTC (Fig. 22) the sea breeze front is located 10 km inland from the Gulf of Mexico, close to the coast of the Choctawhatchee Bay. Southerly flow behind the front is 5 $ms^{-1}$ while northeast winds north of the sea breeze front have increased to 5-8 $ms^{-1}$. A 1.5 °C temperature gradient has developed between the sea breeze front and the coastline, a distance of 10 km. Of note: Cool sea breeze air surged north to RAWS sites B-75 and Coupland and the isotherms marking the leading edge of the sea breeze front show distinct along–front undulations. The undulations along the front are a result of the northeast synoptic-scale flow. While this is considered light offshore flow, the complex nature of the coastline in this region creates along-coast variations in the flow regime. The coastline near Eglin AFB (KVPS) is oriented northeast to southwest, which is parallel to the synoptic-scale flow and enabled the sea breeze to penetrate further inland to the RAWS sites. East of

Eglin the synoptic-scale flow is more offshore and west of Hulbert Field (KHRT) the flow is parallel to the coast. As a result, the sea breeze front stays close to the coast of the Choctawhatchee Bay and is able to penetrate further inland from the Gulf of Mexico.

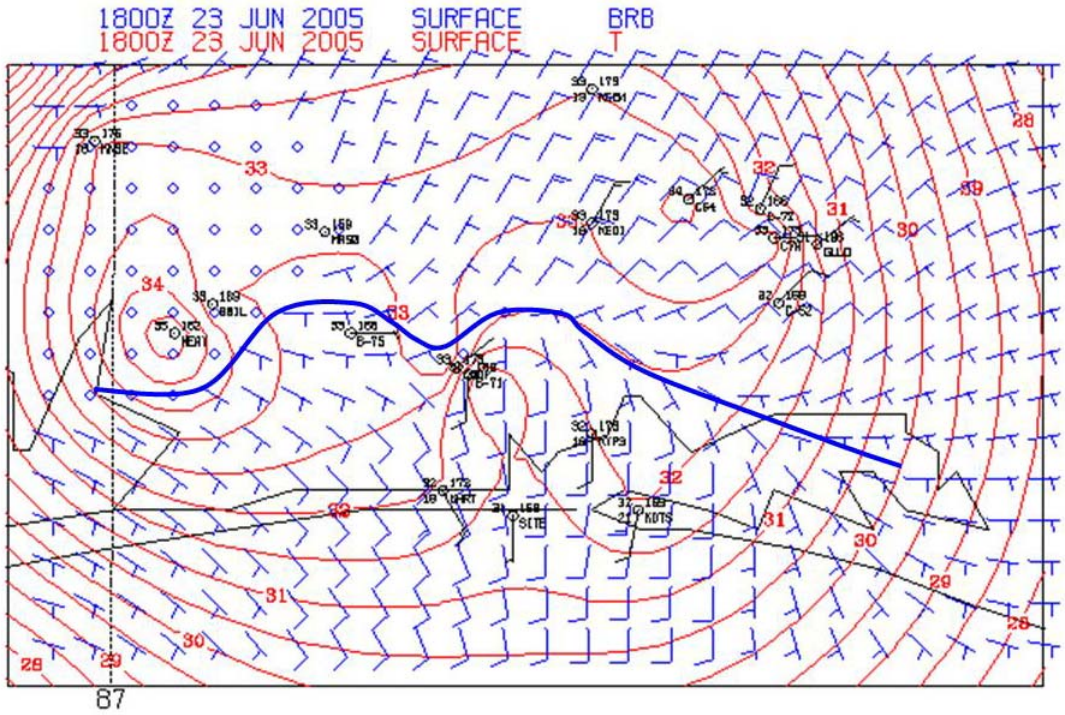


Figure 22. Surface analysis at 18 UTC for 23 June 2005. The sea breeze front has penetrated 10 km inland from the Gulf of Mexico. The heavy blue line indicates the position of the sea breeze front.

The corresponding 18 UTC radar image (Fig. 23) indicates a well defined thin line associated with the sea breeze front. The thin line exhibits the same along-front variations indicated by the isotherm analysis in Figure 22. However, it is apparent that the thin line has taken the shape of the coastline. The sea breeze front is located 10 km inland from East Bay and extends northeastward to a point north of Eglin AFB. From this point, the thin line is held close to the coast of Choctawhatchee Bay. A thin line also formed on the south side of Choctawhatchee Bay to the east of Destin (KDTS). The synoptic-scale flow is offshore along this section of coastline and holds the sea breeze and associated thin line at the coast. Reflectivity values along the thin line approach 20 dBZ in this region while reflectivity values of 10 to 15 dBZ are associated with the

thin line on the Eglin Range Complex, indicating a stronger sea breeze front in the presence of the offshore flow.

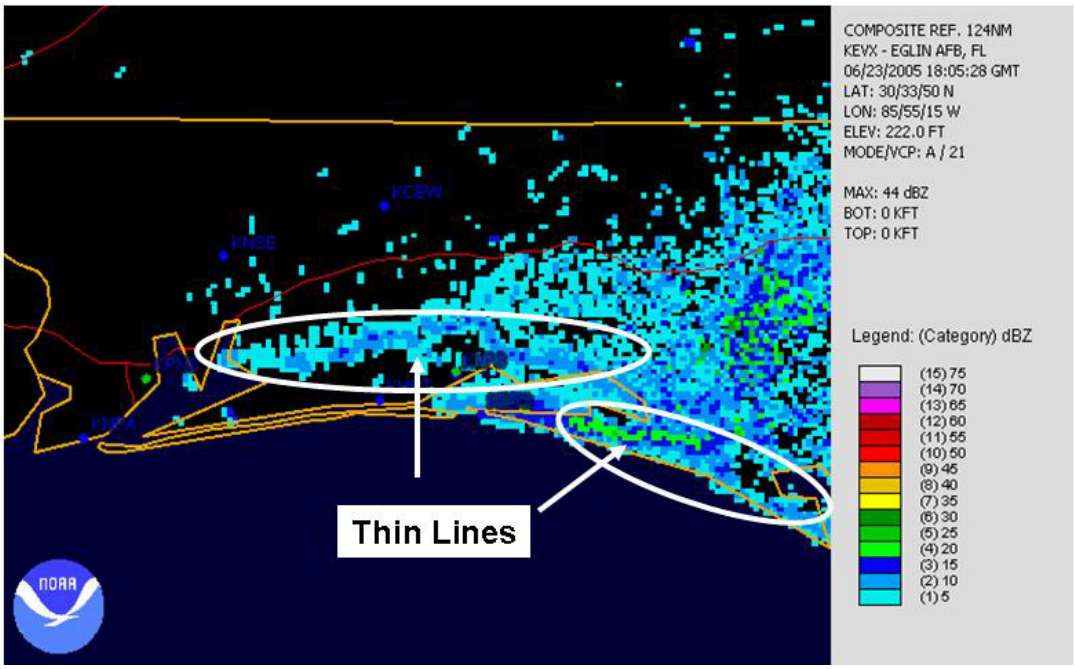


Figure 23. 18 UTC 23 June 2005 KEVX base reflectivity product illustrating the thin line associated with the sea breeze front. The front moved 10 km inland between KVPS and the East Bay where the synoptic-scale flow is coast parallel. The front is held at the coastline of the Choctawhatchee Bay where the flow is offshore. An intense thin is located west of Destin where the synoptic-scale flow is offshore (From Ref. National Climatic Data Center, http://www.ncdc.noaa.gov/oa/radar/radardata.html, February 2006).

By 21 UTC, the sea breeze has penetrated 25 km inland from the Gulf of Mexico. It bends southeastward to a position 10 km north of the Choctawhatchee Bay. Reflectivity values of 20 to 25 dBZ are associated with the thin line located north of Choctawhatchee Bay, indicating the sea breeze front is strongest in the region where the synoptic-scale flow is offshore. Reflectivity values along the thin line further west are between 10 and 15 dBZ and indicate a less intense front where the synoptic-scale flow is coast-parallel. By 23 UTC, the sea breeze front has penetrated through the entire Eglin Range Complex.

### *b. Offshore Composites*

The sea breeze for the offshore regime begins 1630 UTC under 3-5 $ms^{-1}$ offshore flow, one hour later than the Calm regime. The sea breeze is first evident as a weakening in the offshore flow along the coastline. By 18 UTC, the sea breeze front is located 10 km inland from the Gulf of Mexico and 5 km inland from the Choctawhatchee Bay. The front is oriented northeast to southwest, which is the orientation of the coastline from the eastern tip of Choctawhatchee Bay westward to East Bay. Sea breeze flow is from the southeast at 2.5 $ms^{-1}$.

The sea breeze front reaches its maximum intensity between 18 and 19 UTC 20 km from the Gulf of Mexico and 15 km from the Choctawhatchee Bay (Fig. 24). Regions north of the sea breeze front experience three hour temperature perturbations of over 2 °C while coastal regions behind the sea breeze front experience three hour perturbations of 0.8 °C. The result is a concentrated temperature perturbation gradient over a 20 km distance. Frontogenesis values of 325 $K$ Day$^{-1}$ 100 km$^{-1}$ are located along the perturbation gradient. Strong frontogenesis occur in this area as sea breeze winds along the coast, now at 10 $ms^{-1}$, converges with weaker onshore flow at the leading edge of the front. This speed convergence acts to concentrate the isotherms and intensify the sea breeze front. The same frontogenetical forcing occurred under the Calm regime, but the temperature perturbations and wind convergence are larger under offshore flow. A frontogenesis maximum also occurs 10 km north of Eglin AFB where the coastline of the Choctawhatchee Bay bends northeastward. The bend in the coastline at Eglin AFB creates a convergent region by altering the along-coast isotherms. Since sea breeze winds accelerate onshore perpendicular to the along-coast isotherms, flow west of the bend moves northward while flow along the bend moves northwestward, converging north of Eglin AFB.

By 20 UTC, the sea breeze front orients to a northwest to southeast position 30 km from the Gulf of Mexico and 12 km from the Choctawhatchee Bay. Between 20 and 21 UTC, onshore flow turned southwesterly and the sea breeze front accelerated through the Eglin Range Complex with decreasing intensity.

A graphical illustration of the position of the sea breeze front under 3-5 $ms^{-1}$ offshore flow is presented in Figure 26A. The position of the sea breeze front in this and subsequent figures was determined by analysis of temperature, winds and frontogenesis in the composites. Initially, the sea breeze front is oriented northeast to southwest and remains within 12 km of the coastline between 16 and 18 UTC. By 19 UTC, the sea breeze front is oriented east to west and reaches its maximum intensity as differential heating creates a strong thermal gradient that speed convergence concentrates approximately 15 to 20 km inland from the Gulf of Mexico and Choctawhatchee Bay. Sea breeze winds are southerly at 5 $ms^{-1}$ while the sea breeze front is oriented east to west. Sea breeze winds become southwesterly by 20 UTC, after which the sea breeze front orients northwest to southeast and accelerates inland while decreasing in intensity. Arritt (1993) found that the sea breeze began between 1100 and 1200L in the presence of 3 $ms^{-1}$ offshore flow. Gilliam et al (2004) indicated that the sea breeze along North Carolina remained within 10 km of the coast under 2 $ms^{-1}$ offshore flow until 1300L, was 20 km inland by 1700L, and 30 km by 1800L. The 3-5 5 $ms^{-1}$ composite agrees well with these previous studies.

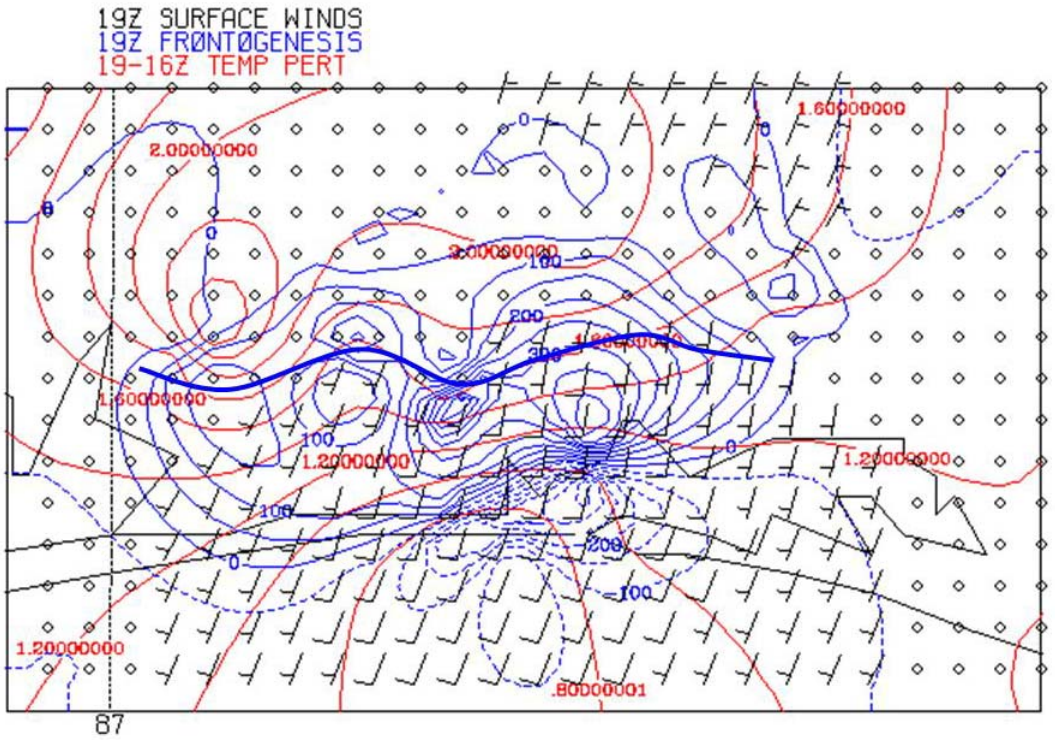


Figure 24. Computed 3-hour air temperature change (19-16 UTC in °C) contoured every 0.2 °C in red, frontogenesis plotted in blue contours every 50 $K$ Day$^{-1}$ 100 km$^{-1}$ at 19 UTC and surface wind barbs (full barb 5 $ms^{-1}$, half-barb 2.5 $ms^{-1}$) at 19 UTC for the Offshore 3-5 $ms^{-1}$ regime. The blue line represents the location of the sea breeze front as analyzed from temperature, winds, and frontogenesis.

Increasing the magnitude of the offshore flow to 5-7 $ms^{-1}$ produced the expected effects on the sea breeze. First, onset of the sea breeze was delayed by approximately 1 hour when compared to the 3-5 $ms^{-1}$ regime. Secondly, the sea breeze front penetrated only 12 to 15 km inland from the Gulf of Mexico and Choctawhatchee Bay by 21 UTC, after which air temperatures cool over the Eglin Range complex and the sea breeze weakens in place (Fig. 26B). The sea breeze front reached maximum intensity at 16 UTC with frontogenesis values of 150 $K$ Day$^{-1}$ 100 km$^{-1}$, and maintained this intensity through 20 UTC.

Past studies (Estoque 1962; Bechtold et al. 1991; Arritt 1993; Gilliam et al. 2004) indicated that the strongest sea breeze formed under 5-6 $ms^{-1}$ offshore flow. In this study, the 5-7 $ms^{-1}$ regime produced the weakest sea breeze front while 3-5 $ms^{-1}$ opposing flow produced the strongest front. A comparison in temperatures at the time of maximum frontal intensity between the two regimes indicates that 5-7 $ms^{-1}$ offshore flow suppressed the temperature perturbation across the Eglin Range (Fig. 25). Temperatures were 0.5 to 0.8 °C cooler in the 5-7 $ms^{-1}$ regime when compared to the 3-5 $ms^{-1}$ regime. In addition, onshore winds in the 5-7 $ms^{-1}$ regime were 4 $ms^{-1}$ weaker across the temperature gradient than the 3-5 $ms^{-1}$ regime. Therefore, increasing the magnitude of the offshore synoptic scale flow suppressed the temperature perturbation across the sea breeze front. The weaker perturbation resulted in weaker onshore flow that failed to concentrate the temperature gradient across the sea breeze front. According to equation 2.4, a smaller temperature perturbation over a longer length scale results in a weaker sea breeze.

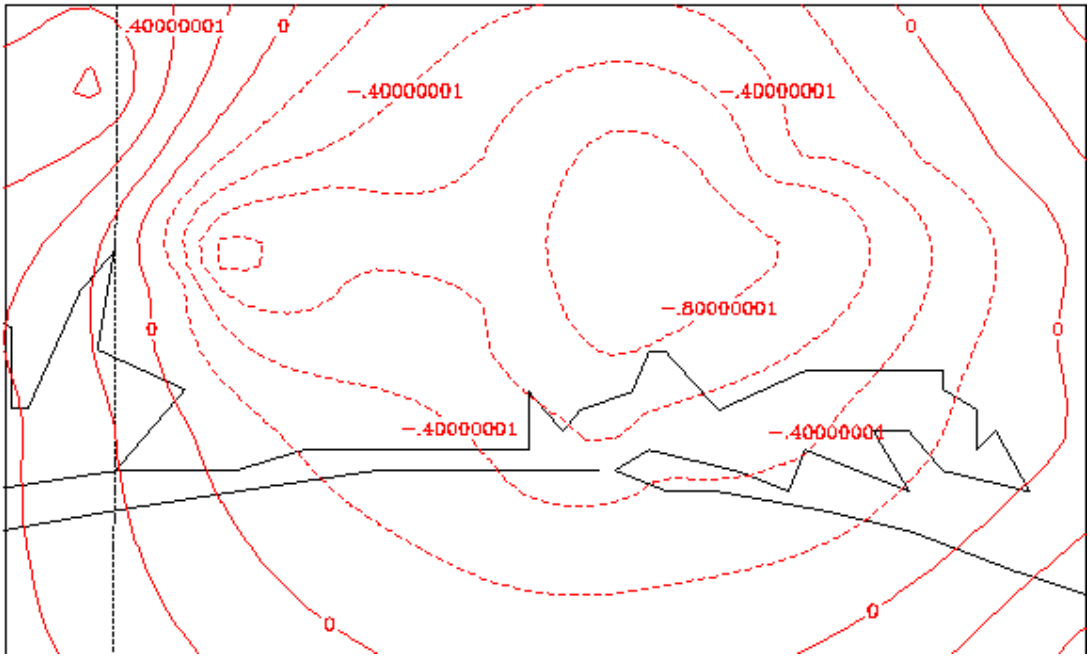


Figure 25. Air temperature difference (°C contoured every .2) between the 3-5 $ms^{-1}$ offshore flow regime at 19 UTC and the 5-7 $ms^{-1}$ offshore flow regime at 20 UTC. Negative values indicate the air temperature from the 3-5 $ms^{-1}$ regime are warmer than the 5-7 $ms^{-1}$ regime.

Under 7-9 $ms^{-1}$ offshore flow, onset of the sea breeze is delayed until 18 UTC, 2 hours after the 3-5 $ms^{-1}$ regime. As expected, increasing the magnitude of the offshore synoptic-scale flow restricted the inland penetration of the sea breeze front. Under this flow regime, the sea breeze front penetrated to the coastline of the Choctawhatchee Bay and 10 km inland from the Gulf of Mexico by 21 UTC (Fig 26C). The sea breeze front is strongest between 19 and 20 UTC with frontogenesis values of 225 $K$ Day$^{-1}$ 100 km$^{-1}$ located along the coastline. Maximum frontogenesis occurred when air temperatures cooled behind the sea breeze front by 1 °C while warming by 1.2 °C north of the front. In this regime, stronger offshore flow is present at the sea breeze front, which acts to increase convergence with the onshore sea breeze flow and intensify the thermal gradient. The increased convergence results in a stronger sea breeze front when compared to the 5-7 $ms^{-1}$ regime.

Offshore synoptic-scale flow greater than 9 $ms^{-1}$ suppressed the development of the sea breeze along Eglin's coastline. Numerically, Arritt (1993) found a sea breeze circulation for opposing flow of 9 $ms^{-1}$; however, the circulation is located entirely offshore. A determination cannot be made about the presence of a sea breeze offshore in this study due to lack of observations off the Eglin coastline.

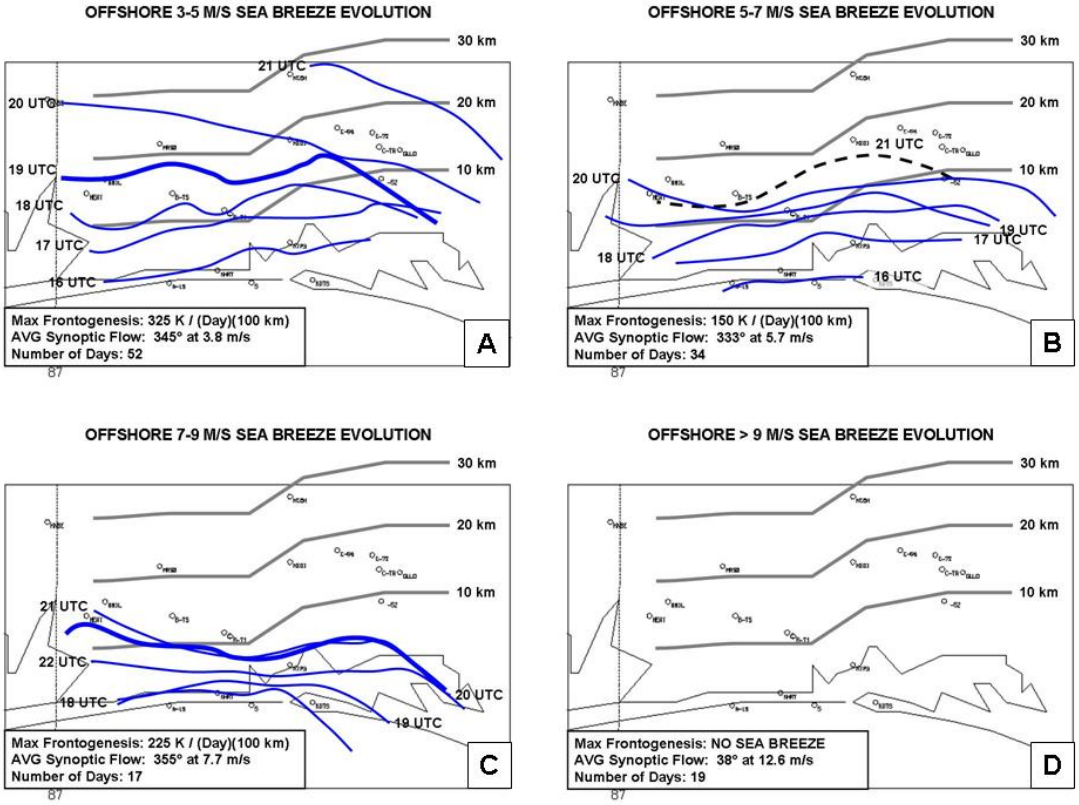


Figure 26. Illustration of the position and intensity of the sea breeze front for Offshore synoptic-scale flow of (A) 3-5 $ms^{-1}$, (B) 5-7 $ms^{-1}$, (C) 7-9 $ms^{-1}$ and (D) >9 $ms^{-1}$ in the Eglin Range Complex.

### 3. Onshore Synoptic-Scale Flow

Previous numerical and observational studies agree that the presence of onshore synoptic-scale flow of 3 $ms^{-1}$ or less produces the weakest sea breeze. The advection of cool marine air inland inhibits heating and results in weaker gradients of temperature and pressure. Inland penetration of the sea breeze front under onshore flow is difficult to determine because the flow everywhere in the domain is onshore. However, the sea breeze front can be detected by slightly stronger onshore flow across the weak temperature gradient associated with the sea breeze front. Convergent frontogenesis is suppressed under onshore flow resulting in a weak thermal perturbation of the large scale flow. Therefore, little vertical motion is associated with the sea breeze front under onshore conditions. In addition, the sea breeze can travel large distances inland under onshore flow, and usually intensifies late in the period (1800L). Increasing the

magnitude of the onshore flow suppresses sea breeze development; however, there is not a consensus in the literature on the magnitude of the flow required to suppress the sea breeze.

Composites were constructed for onshore flow of 0-3, 3-5, and greater than 5 $ms^{-1}$ and are presented after examining a case study of an onshore flow event.

### *a. 20 June 2001 Case Study*

The 12 UTC Tallahassee sounding indicated that the low level synoptic flow over the Florida Panhandle on 20 Jun 2001 was from 195° at 2 $ms^{-1}$. Surface observations prior to the onset of the sea breeze indicated a light offshore wind developed overnight over the Eglin Range Complex. The sea breeze began at 1430 UTC and by 15 UTC the sea breeze had penetrated 12 km inland from the Choctawhatchee Bay (Fig 27). However, no sea breeze is evident along the coast west of Hulbert Field. There is little thermal gradient at the leading edge of the sea breeze, only a convergence zone located between 5 $ms^{-1}$ southerly flow and 2.5 $ms^{-1}$ southeasterly flow. A thin line is not present on the corresponding 15 UTC KEVX base reflectivity product, which supports the observation that a sea breeze front has not formed.

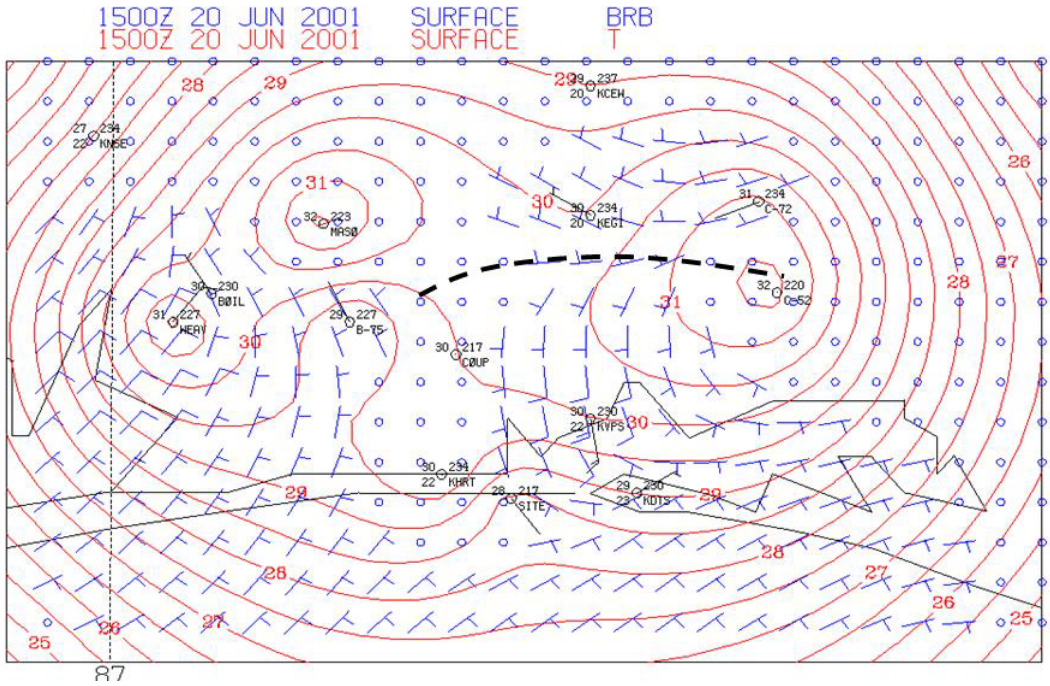


Figure 27. Surface analysis at 15 UTC for 20 June 2001. The sea breeze front has penetrated 12 km inland from the Choctawhatchee Bay but flow remains offshore along the coastline west of Hulbert Field. Dashed black line indicates the wind shift associated with the leading edge of the sea breeze

By 18 UTC, a weak thermal gradient is located 20 km inland indicating formation of the sea breeze front. There is 2 °C temperature gradient between the coast and the sea breeze front, and winds along the coast are southerly at 10 $ms^{-1}$. The 1830 UTC KEVX reflectivity product indicated thunderstorms formed along the sea breeze front (Fig 28). A thin line associated with the sea breeze front was not detected on radar prior to thunderstorm initiation. The thunderstorms continue to move north with the sea breeze front and are located over 30 km inland by 20 UTC.

Under onshore flow, the sea breeze began between 14 and 15 UTC. The sea breeze front was not detected until 18 UTC. Prior to that, a wind shift and strengthening of the onshore flow was the only indication the sea breeze was moving inland. By 18 UTC, a weak thermal gradient formed 20 km inland and was the first indication of a sea breeze front. Thunderstorms formed along the sea breeze front by 1830 UTC. A thin line associated with the sea breeze was not detected before thunderstorm initiation.

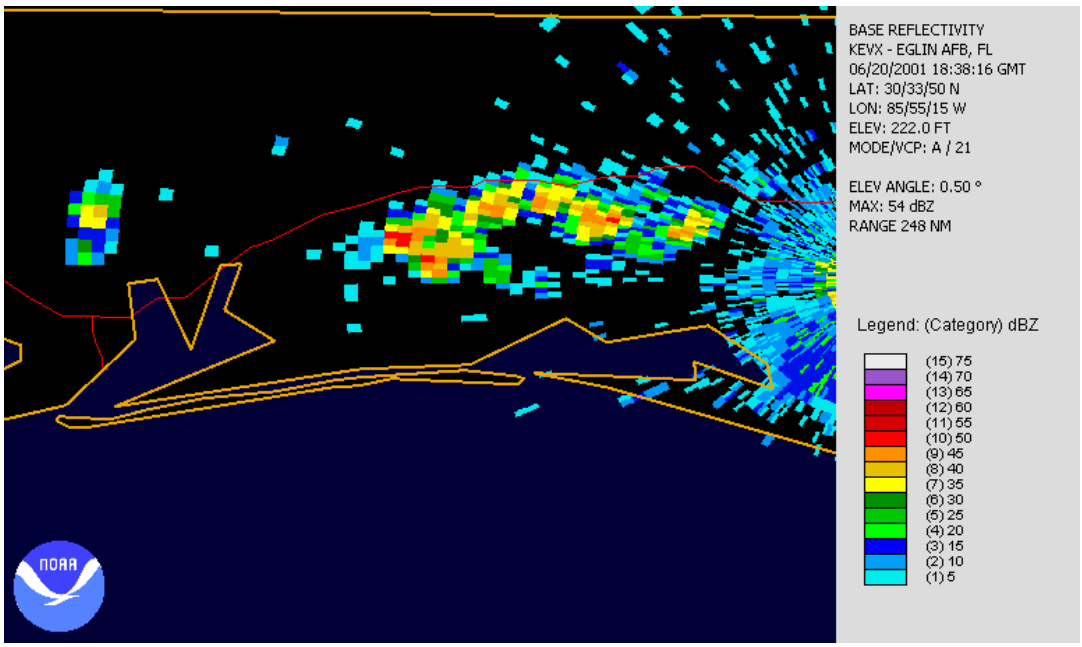


Figure 28. 1830 UTC base reflectivity product from 20 June 2001. Thunderstorms formed along the sea breeze front 20 km inland. (From Ref. National Climatic Data Center, http://www.ncdc.noaa.gov/oa/radar/radardata.html, February 2006).

### *a. Onshore Composites*

Analyses of the 0-3 $ms^{-1}$ onshore flow composite indicates the average start time of the sea breeze is 15 UTC. There is no concentrated thermal gradient evident indicating a sea breeze front until 18 UTC. By 19 UTC, the sea breeze front is located 20 km inland in a region where temperature perturbation contours start to concentrate (Fig. 29). Frontogenesis values of 40 to 60 $K$ $Day^{-1}$ 100 $km^{-1}$ along the contours indicate the sea breeze front is undergoing weak intensification. The weakness of the sea breeze front can be understood using equation 2.4, which states that the strength of the sea breeze is proportional to the temperature perturbation across the sea breeze front and inversely proportional to the length scale of the temperature gradient. At 19 UTC, there is a .4 °C temperature perturbation that occurs over a length scale of 10 km. By comparison, the strongest sea breeze front formed under light offshore flow where the temperature perturbation was 1.5 °C over 10 km. When the synoptic scale flow is onshore, cool marine air advects farther inland earlier in the day, suppressing the temperature perturbation which results in a weak sea breeze front. Between 19 and 20 UTC, the sea breeze front moved to a point 30 km inland and started to weaken.

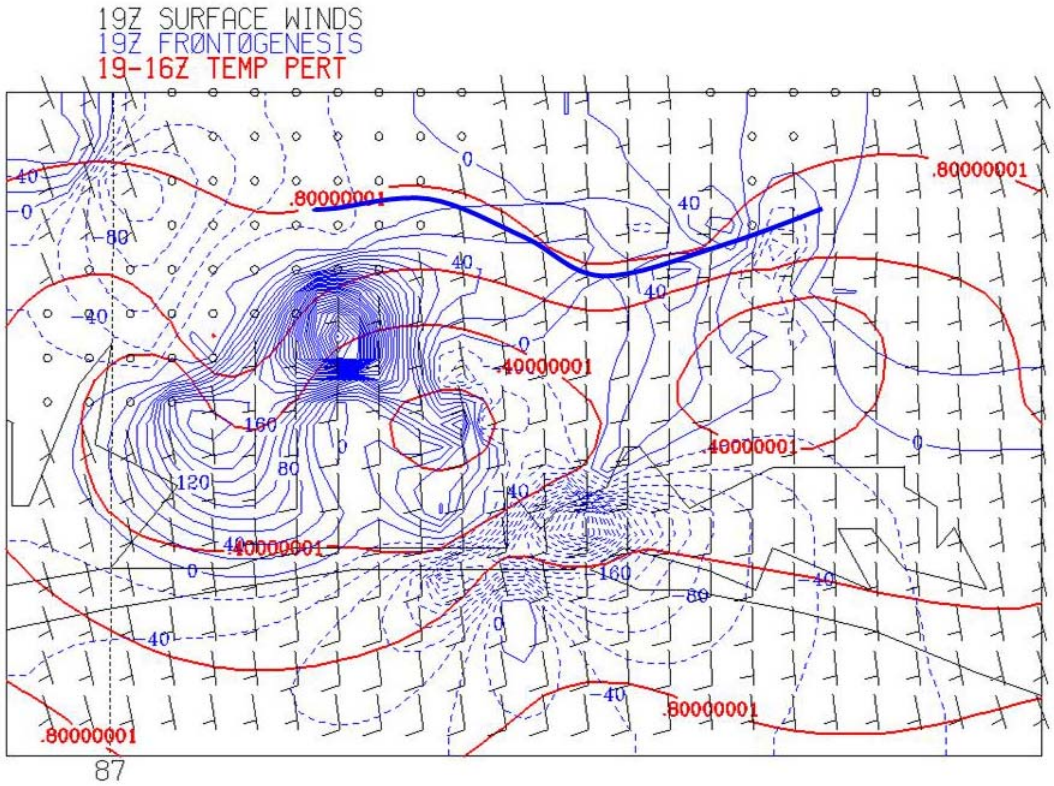


Figure 29. Computed 3-hourly air temperature change (19-16 UTC in °C) contoured every 0.2 °C in red, 19 UTC frontogenesis plotted in blue contours every 20 $K$ Day$^{-1}$ 100 km$^{-1}$ and surface wind barbs (full barb 5 $ms^{-1}$, half-barb 2.5 $ms^{-1}$) at 19 UTC for the Onshore 0-3 $ms^{-1}$ regime. The blue line indicates the position of the sea breeze front based on analysis of temperature, wind and frontogenesis.

Increasing the magnitude of the onshore synoptic scale flow produced a similar sea breeze evolution. Under 3-5 $ms^{-1}$ onshore flow, the sea breeze begins between 14 and 15 UTC. By 16 UTC, light southeasterly flow extends 20 km inland. As with the 0-3 $ms^{-1}$ regime, there is no identifiable sea breeze front, only a weak convergence zone at the leading edge of 5 $ms^{-1}$ southerly winds. By 18 UTC, a weak thermal gradient formed in the convergent region where air temperatures north of the convergence zone warm faster than regions south of the convergent zone. The sea breeze front forms between 15 and 18 km inland and reaches maximum intensity at 19 UTC, 22 km from the Gulf of Mexico and 15 km from the Choctawhatchee Bay. Frontogenesis

values of 100 $K$ Day$^{-1}$ 100 km$^{-1}$ located 15 km north of the Choctawhatchee Bay indicate sea breeze front intensification. This front is stronger than the sea breeze front that formed under 0-3 $ms^{-1}$ flow. Comparing three hour temperature perturbations between 16 and 19 UTC for both regimes revealed that while temperatures warm by 0.8°C north of the sea breeze front for both regimes, there is no temperature change south of the front in the 3-5 $ms^{-1}$ regime while temperatures warm slightly under 0-3 $ms^{-1}$ flow. The differential heating results in a weak increase in the thermal gradient under 3-5 $ms^{-1}$ onshore flow leading to a stronger sea breeze front.

Onshore flow greater than 5 $ms^{-1}$ suppressed the development of a sea breeze front. Onshore winds were evident along the coast at 12 UTC and were onshore through the entire Eglin Range Complex by 14 UTC. At 17 UTC, a weak convergence line formed 20 km inland between stronger 5 $ms^{-1}$ sea breeze flow advancing northward and 2.5 $ms^{-1}$ southeasterly flow. A weak thermal gradient formed 30 km inland in the convergent region by 18 UTC, but by 19 UTC this gradient was not evident as temperatures cooled across the Eglin Range. This might have been the initiation of a sea breeze front, but since it propagated out of the study domain, there is no way to tell if a sea breeze front formed.

A graphical illustration of the sea breeze propagation and intensity is presented in Figure 30 for the onshore regime. The sea breeze began at 15 UTC under 0-3 $ms^{-1}$ flow and at 12 UTC under 5 $ms^{-1}$ onshore flow. A sea breeze front formed at 19 UTC for both 0-3 and 3-5 $ms^{-1}$ onshore flow regimes 20 km inland. The fronts formed in a convergence zone at the leading edge of 5 $ms^{-1}$ southerly flow when differential heating across the convergence zone enhanced the temperature gradient. The strongest sea breeze front formed at 19 UTC under 3-5 $ms^{-1}$ onshore flow. Synoptic-scale flow greater than 5 $ms^{-1}$ suppressed sea breeze front development on the Eglin Range Complex; however, a weak thermal gradient developed at 18 UTC close to 30 km inland and could have been the initiation of a sea breeze front. Finally, the sea breeze fronts that formed under onshore flow propagated through the Eglin Range Complex the fastest. These findings are consistent with studies by Atkins and Wakimoto (1997) and Gilliam et

al. (2004) who found that the sea breeze front formed late in the day for onshore synoptic-scale flow as convergence increased along the front and turbulent mixing of the airmasses decreased. However, the sea breeze fronts were much weaker than fronts forming in the presence of offshore flow because the temperature perturbations are smaller and the length scales of the thermal gradients are larger.

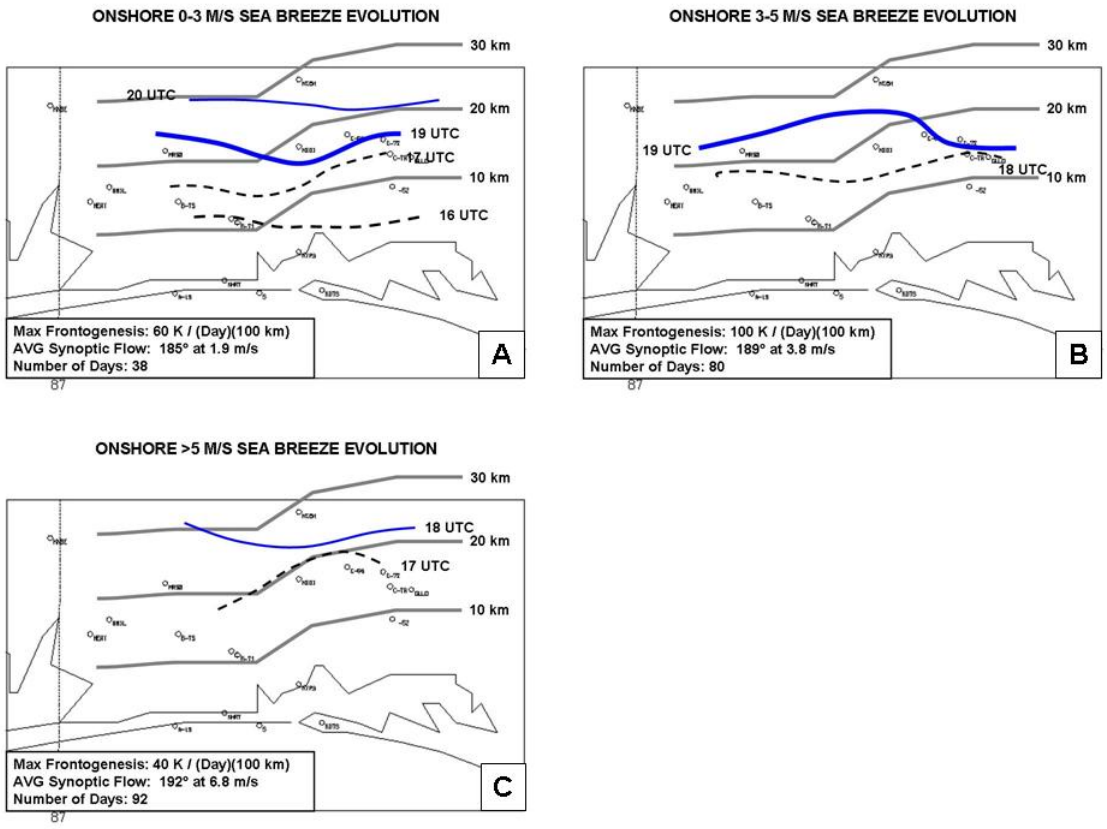


Figure 30. Illustration of the position and intensity of the sea breeze front for Onshore synoptic-scale flow of (A) 0-3 $ms^{-1}$, (B) 3-5 $ms^{-1}$, and (C) > 5 $ms^{-1}$ in the Eglin Range Complex.

### 4. Coast Parallel Easterly Synoptic-Scale Flow

Synoptic-scale flow with land on the right develops when the large scale pressure pattern has high pressure over land and low pressure over water. Surface friction tends to produce a weak offshore wind component, so a sea breeze that develops in this situation has characteristics of the offshore flow case (Zhong and Tackle 1993; Nuss 2005). Sea breezes forming under coast parallel offshore flow start earlier, however, are not as intense as sea breezes forming under offshore synoptic-scale flow.

### *a. 20 September 2005 Case Study*

Figure 31 presents the surface analysis at 12 UTC 20 September 2005, which was a coast parallel easterly flow day. The 12 UTC KTLH sounding indicated the low-level synoptic-scale flow over the region was east-northeast (075°) at 6.2 $ms^{-1}$. Inland stations reported temperatures of 22 °C while coastal temperatures are 26 °C. This is a 4 °C temperature difference over approximately 20 km. The surface data shows light north to northeasterly flow across much of the Eglin Range Complex and coastal stations.

By 18 UTC, the leading edge of the thermal gradient had advanced inland from the coastline, indicating the onset of the sea breeze. The sea breeze front penetrated 10 km inland from the Gulf of Mexico and 8 km from Choctawhatchee Bay (Fig. 32). A 4 °C temperature difference between inland and coastal stations is still evident; however, the isotherms have concentrated along the coastline indicating a tightening thermal gradient and intensifying sea breeze front. Surface winds increased from the south at 5-10 $ms^{-1}$ along and approximately 10 km inland from the Gulf of Mexico and Choctawhatchee Bay, then back to the east-southeast at the eastern section the Eglin Range. Offshore flow is evident over the northern section of the range.

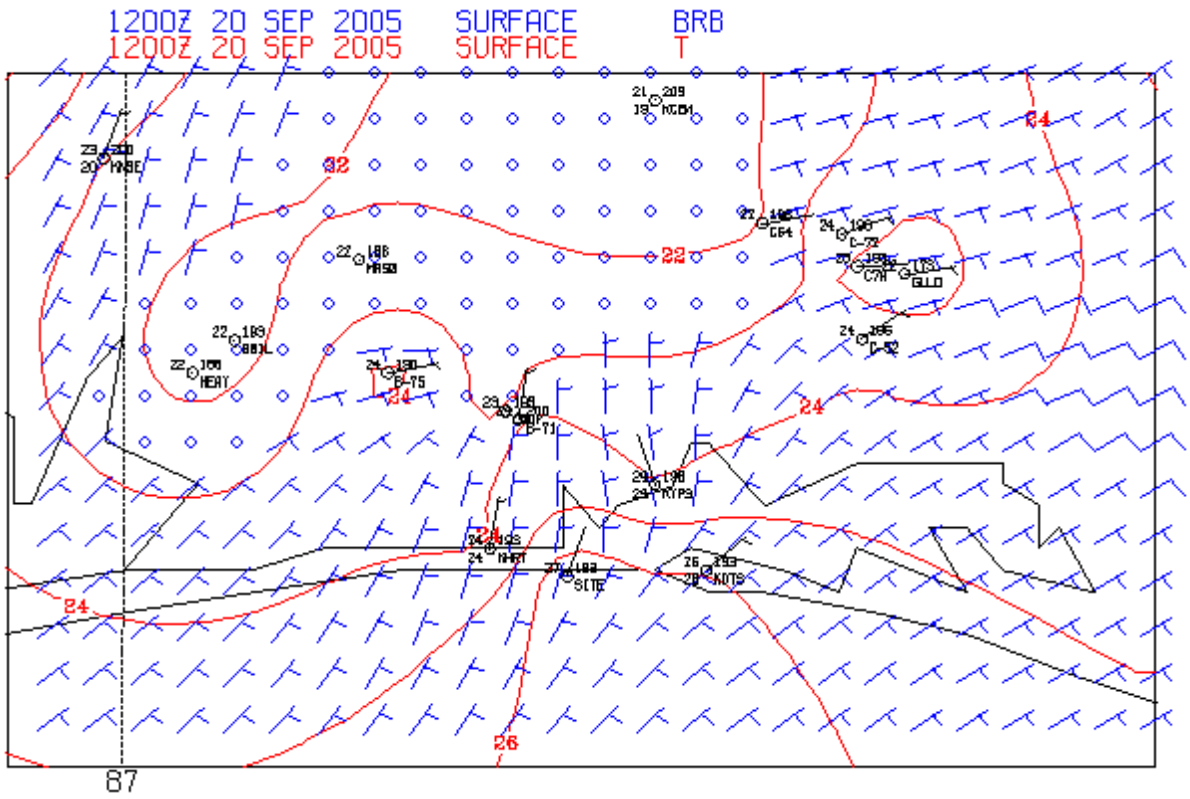


Figure 31. Surface analysis at 12 UTC for 20 September 2005, a coast parallel offshore flow day. Isotherms (°C) are in red contoured every half degree and winds (full barb 5 $ms^{-1}$, half-barb 2.5 $ms^{-1}$) are plotted at 2 km grid points. Available station observations are plotted in black with temperature (°C top left), sea level pressure (mb top right), winds (full barb 5 $ms^{-1}$, half-barb 2.5 $ms^{-1}$), dewpoint (°C bottom left), and station identification (bottom right).

The KEVX base reflectivity product from 18 UTC indicates a well defined thin line associated with the sea breeze stretching from East Bay to Eglin AFB, then bending southeastward towards Choctawhatchee Bay (Fig 33). Reflectivity values between 15 and 20 dBZ are associated with the thin line. The location of thin line corresponds with the leading edge of the temperature gradient and wind convergence indicated in the 18 UTC surface analyses. The east-northeast synoptic-scale flow has restricted the inland penetration of the sea breeze front along the eastern section of the Choctawhatchee Bay where the flow is offshore. The sea breeze moved inland farther over the western half of the domain where the flow is coast parallel.

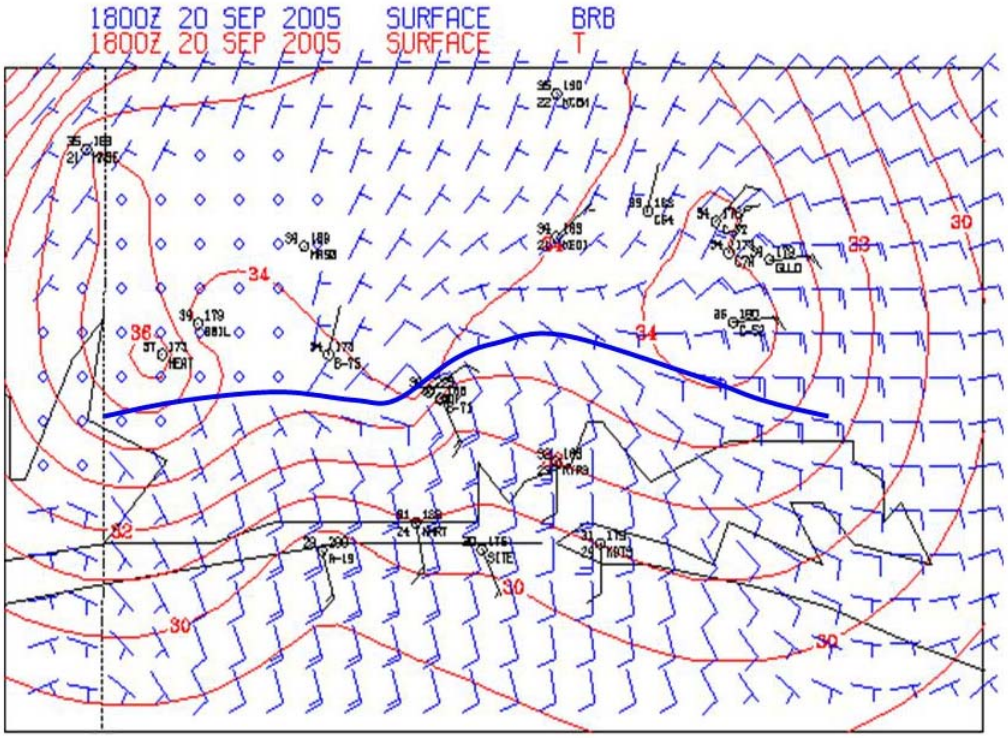


Figure 32. Surface analysis at 18 UTC for 20 September 2005. The sea breeze front penetrated 10 km inland and intensified as indicated by the intensifying thermal gradient at the coast.

By 21 UTC, the front moved inland to a position along the Yellow River in the west, but has remained quasi-stationary near Eglin AFB and the Choctawhatchee Bay. Northeasterly flow over the interior of the Eglin Range allowed temperatures to warm to 35 °C while stations along the coast under onshore flow have remained near 31 °C. Differential heating tightened the temperature gradient between the coastline and the leading edge of the sea breeze front 12 km inland while convergence between northeasterly flow and southerly sea breeze flow concentrate the thermal gradient. The corresponding base reflectivity product indicates the thin line has strengthened as well, with reflectivity values increasing to 20 to 25 dBZ (Fig. 34). The thin line is located 20 km inland from the Gulf of Mexico and 10 km inland from the Choctawhatchee Bay.

By 23 UTC, the sea breeze front has weakened and the thin line is not detectable on radar over land; however, a strong thin line was located in the Gulf of Mexico south of KDTS. To account for this movement, the 00 UTC sounding from

Tallahassee was checked to see if the low-level flow over the region changed since 12 UTC. The 925 mb flow backed to the northeast and increased to 9.8 $ms^{-1}$ since 12 UTC. This suggests that the strong offshore flow suppressed the sea breeze over land and advected the sea breeze front over the Gulf of Mexico.

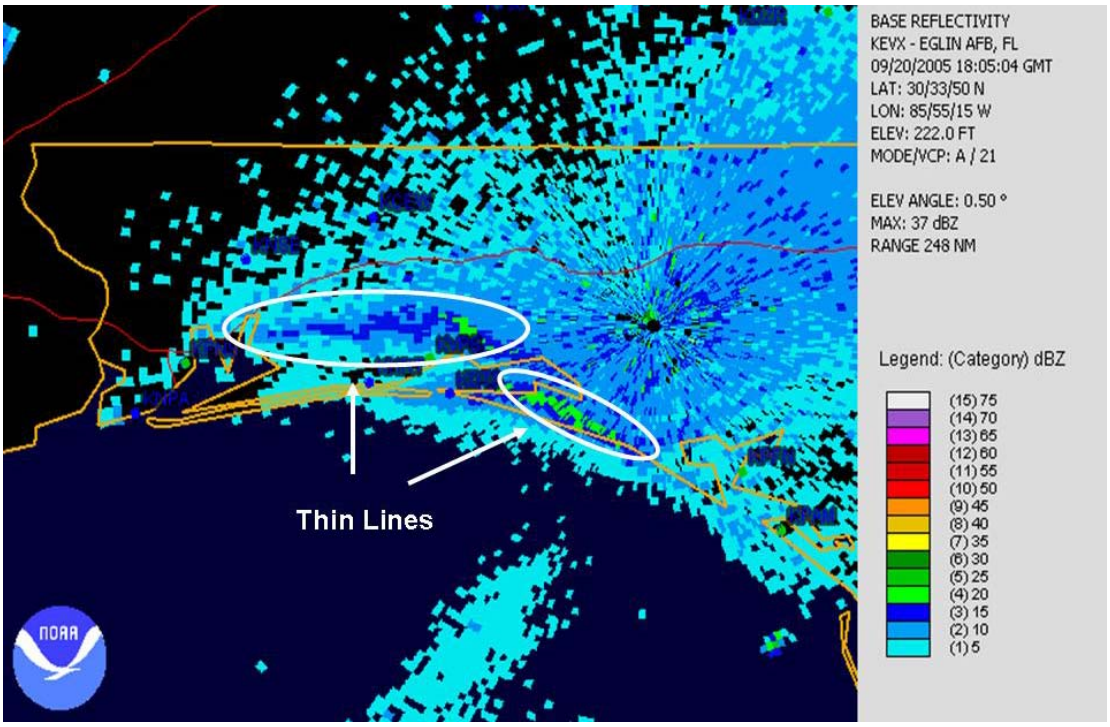


Figure 33. 18 UTC 20 September 2005 KEVX base reflectivity product illustrating the thin line associated with the sea breeze front. Reflectivity values between 15 and 20 dBZ are indicated along the front. (From Ref. National Climatic Data Center, http://www.ncdc.noaa.gov/oa/radar/radardata.html, February 2006).

Under coast parallel easterly flow, the sea breeze started at 15 UTC and moved approximately 20 km inland where the flow was parallel to the coast and 10 km from the coastline where the synoptic-scale flow retained an offshore component. The sea breeze front intensified between 15 and 21 UTC and maximum reflectivity values were detected at 21 UTC. The sea breeze front reached its furthest point inland at 21 UTC, after which the sea breeze weakened as the temperature gradient relaxed and the synoptic-scale flow increased.

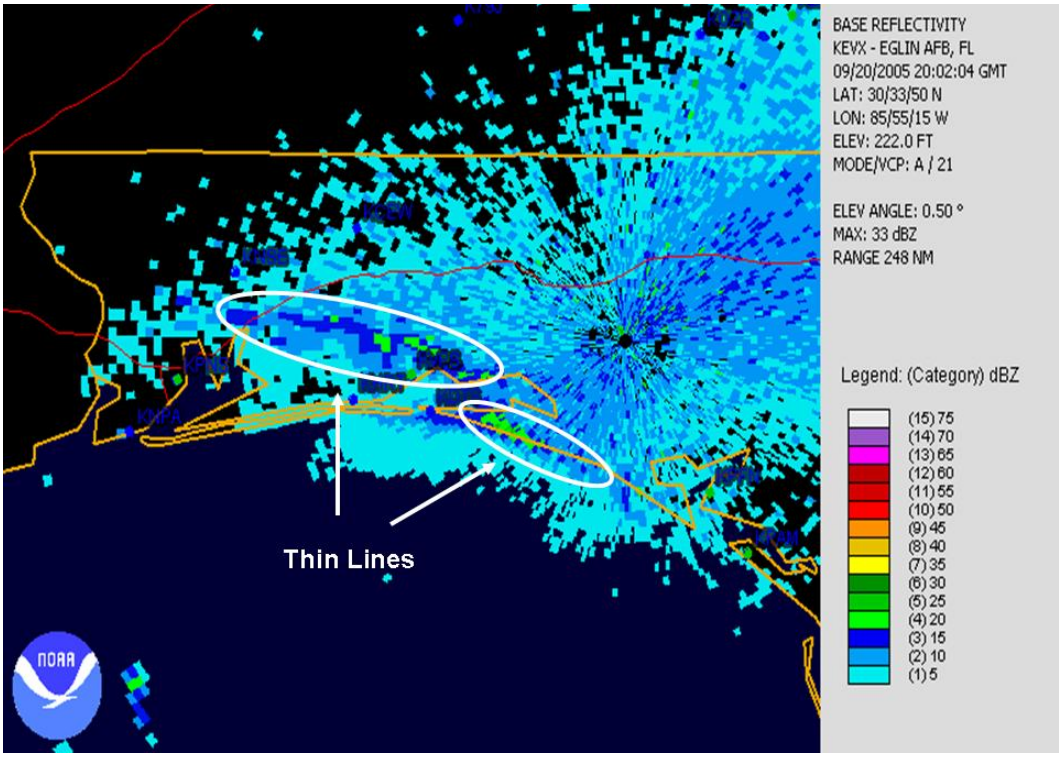


Figure 34. 20 UTC 20 September 2005 KEVX base reflectivity product illustrating the thin line associated with the sea breeze front. The front moved 20 km inland between KHRT and the East Bay where the synoptic-scale flow is coast parallel. The front is held at the coastline of the Choctawhatchee Bay and crosses the bay to KDTS where the flow is offshore. (From Ref. National Climatic Data Center, http://www.ncdc.noaa.gov/oa/radar/radardata.html, February 2006).

### *b. Coast Parallel Easterly Composites*

Composite analysis indicates the sea breeze began between 14 and 15 UTC for the 3-5 $ms^{-1}$ regime. The sea breeze front is ill defined at this time, but is located 12 km inland from the Choctawhatchee Bay. By 18 UTC, the sea breeze front becomes better defined. Winds north of Duke Field are easterly while southerly onshore flow has penetrated 20 km inland. The three hour temperature change between 15 and 18 UTC indicates air temperatures in the easterly flow increase 2 °C while air temperatures in the onshore flow increase 1 °C (Fig. 35). A concentrated thermal gradient develops 20 km inland near East Bay, bulges northward to a position 25 km inland in the center of the domain and drops southeasterly towards the Choctawhatchee Bay. Frontogenesis values of 150 $K$ Day$^{-1}$ 100 km$^{-1}$ along the thermal band indicate intensification of the sea breeze front as convergence between easterly flow and southerly onshore flow

concentrates the thermal gradient. Sea breeze winds respond to the intensifying thermal gradient by increasing to 10 $ms^{-1}$ along the coastline of Choctawhatchee Bay and the Gulf of Mexico.

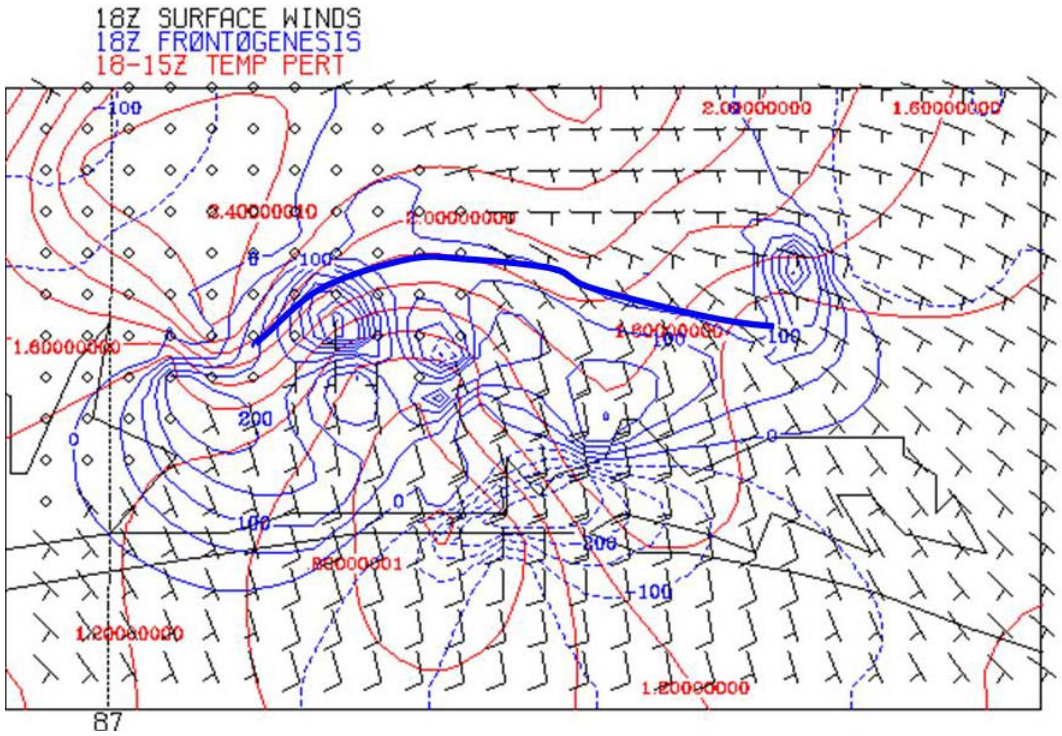


Figure 35. Computed 3-hourly air temperature change (18-15 UTC in °C) contoured every 0.2 °C in red and Frontogenesis plotted in blue contours every 50 $K$ Day$^{-1}$ 100 km$^{-1}$ and wind barbs (full barb 5 $ms^{-1}$, half-barb 2.5 $ms^{-1}$) for Coast Parallel Easterly 3-5 $ms^{-1}$ regime. Solid blue line indicates the position of the sea breeze front based on analyses of temperature, winds and frontogenesis.

By 20 UTC, temperatures over the western section of the domain have cooled by 1 to 1.5 °C indicating the sea breeze front has moved through this region. The front moved 30 km north of the Gulf of Mexico and 20 km north of the Choctawhatchee Bay, oriented northwest to southeast. Frontogenesis values of 125 $K$ Day$^{-1}$ 100 km$^{-1}$ along the thermal gradient indicated the sea breeze front weakened over the preceding two hours. By 23 UTC, the sea breeze front moved through the entire domain.

Under the 5-7 $ms^{-1}$ regime, onshore flow begins along the coast by 17 UTC between Choctawhatchee Bay and East Bay, 2.5 hours later than the 3-5 $ms^{-1}$ regime. Similar to the 3-5 $ms^{-1}$ composite, the sea breeze front is ill-defined until 18 UTC, at which point air temperatures inland warm more than 1.5 °C compared to temperatures along the coast (Fig. 36). Frontogenesis increases with values of 125 $K$ Day$^{-1}$ 100 km$^{-1}$ located along the temperature gradient 10 km inland from the Choctawhatchee Bay and Gulf of Mexico. The sea breeze front is oriented northeast to southwest, conforming to the coastline shape. The sea breeze front weakens by 19 UTC and is located 10 km from the Choctawhatchee Bay and 18 km from the Gulf of Mexico. This is the maximum distance inland the sea breeze front penetrates under 5-7 $ms^{-1}$ Coast Parallel Easterly synoptic-scale flow. Northeasterly winds strengthened across the entire Eglin Range Complex by 21 UTC and the sea breeze front weakened in place.

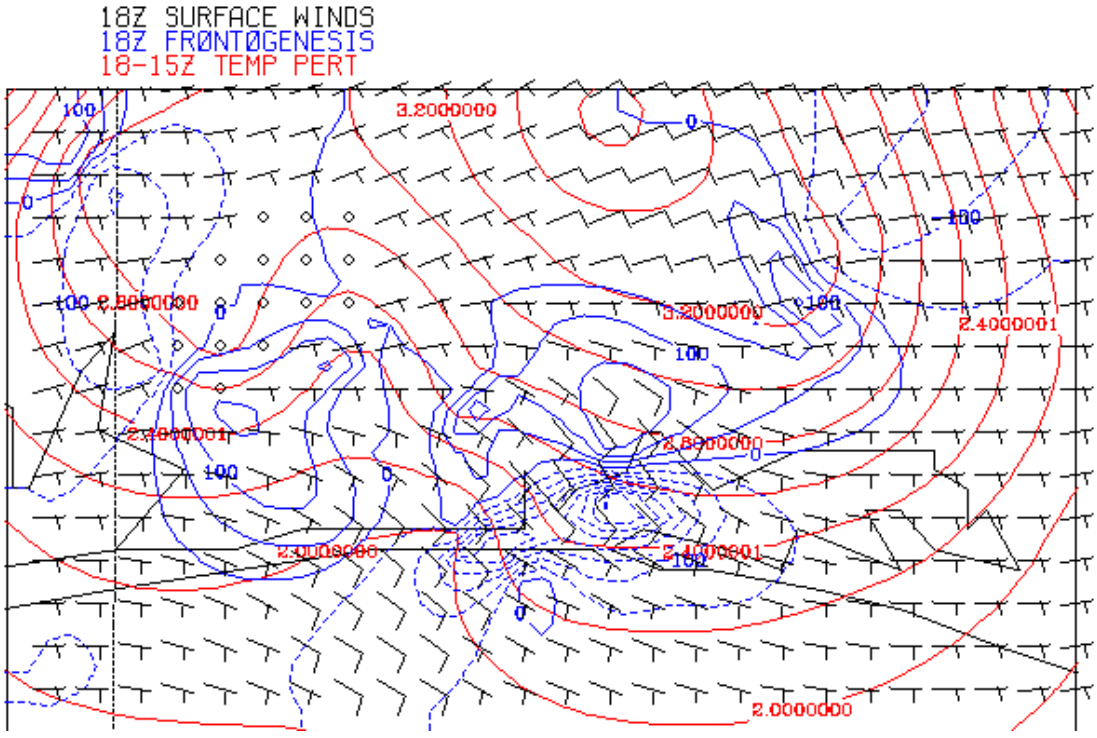


Figure 36. Computed 3-hourly air temperature change (18-15 UTC in °C) contoured every 0.2 °C in red, 18 UTC frontogenesis plotted in blue contours every 50 $K$ Day$^{-1}$ 100 km$^{-1}$ and 18 UTC surface wind barbs (full barb 5 $ms^{-1}$, half-barb 2.5 $ms^{-1}$) for Coast Parallel Easterly 5-7 $ms^{-1}$ regime.

The sea breeze begins by 16 UTC under 7-9 $ms^{-1}$ coast parallel flow, one hour earlier than the 5-7 $ms^{-1}$ regime and approximately one hour later than the 3-5 $ms^{-1}$ regime. The timing difference is attributed to the direction of the synoptic scale flow. The direction of the synoptic-scale flow is 91° in the 5-7 $ms^{-1}$ regime, which is coast parallel over the Eglin region. The direction of the synoptic-scale flow in the 3-5 and 7-9 $ms^{-1}$ regimes are from 99° and 94° respectively, both of which contain onshore components. As a result, the sea breeze starts earlier in the 3-5 and 7-9 $ms^{-1}$ regime than the 5-7 $ms^{-1}$ regime. The sea breeze evolves in a similar manner as the other cases with easterly flow across the northern sections of the Eglin Range and southeasterly onshore flow along the coast. The sea breeze front is difficult to detect until 18 UTC. Northern sections of the range that are under easterly flow continue to heat faster than coastal sections of the range that are experiencing onshore flow. Three hour temperatures changes show 2.5 °C rises in air temperature in the northern section of the range while coastal regions increased 1.5 °C. Frontogenesis values of 200 $K$ Day$^{-1}$ 100 km$^{-1}$ 15 km north of the Choctawhatchee Bay and 20 km north of the Gulf of Mexico indicate the intensification of the sea breeze front in that region.

Figure 37 shows that by 21 UTC, air temperatures in the interior of the Eglin Range drop, while the northeastern portion of the Eglin Range that remained under easterly flow continued to warm. The convergence between the southerly onshore flow behind the sea breeze front and northeasterly flow north of the front, coupled with the differential heating of the two air masses, caused the front to intensify as evident by the 350 $K$ Day$^{-1}$ 100 km$^{-1}$ frontogenesis values approximately 20 km inland. As with the other regimes, the sea breeze front strengthens when the temperature perturbation increased while convergence reduces the length scale of the thermal gradient. After 21 UTC, air temperatures decrease across the entire Eglin Range and the sea breeze front weakens rapidly.

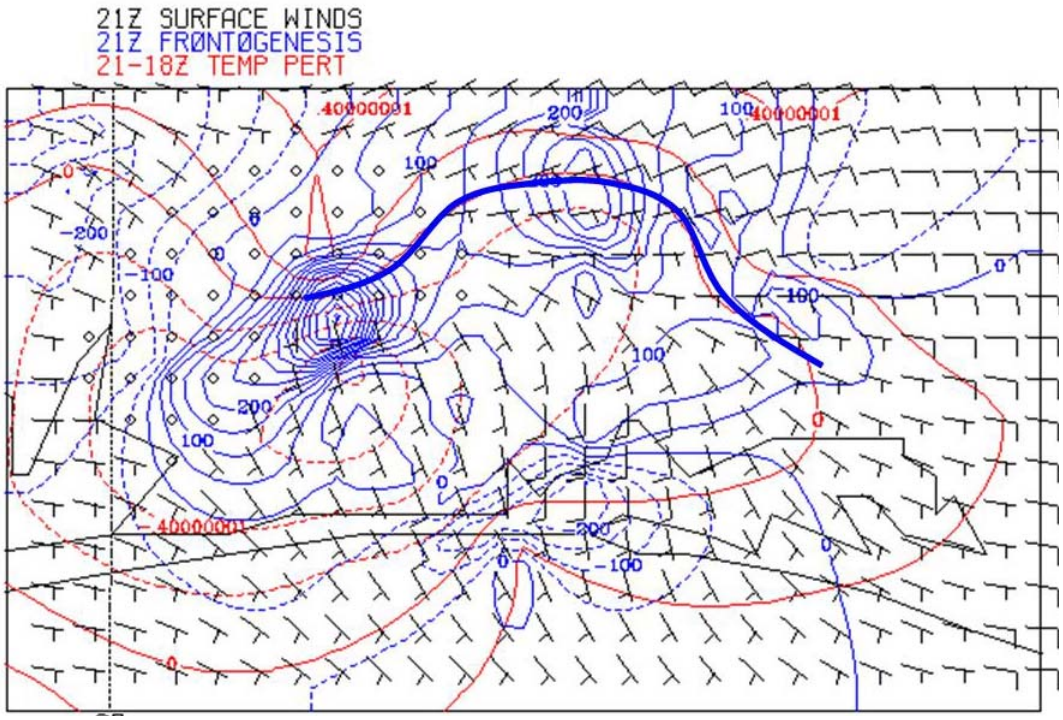


Figure 37. Computed 3-hourly air temperature change (21-18 UTC in °C) contoured every 0.2 °C in red, Frontogenesis plotted in blue contours every 50 $K$ Day$^{-1}$ 100 km$^{-1}$, and wind barbs (full barb 5 $ms^{-1}$, half-barb 2.5 $ms^{-1}$) for Coast Parallel Easterly 7-9 $ms^{-1}$ regime. Solid blue line indicates the location of the sea breeze front based on analysis of temperature, wind and frontogenesis.

Coast Parallel Easterly synoptic-scale flow greater than 9 $ms^{-1}$ suppressed the development of the sea breeze along Eglin's coastline. Winds across the range complex remained east-northeast at 5-10 $ms^{-1}$ through the 23 hour period of the composite. Onshore flow did not develop in this regime, and the absence of cool sea breeze air inland, air temperatures were horizontally uniform over the Eglin Range Complex. The three hour temperature difference between 15 and 18 UTC indicated the largest temperature rise, 2.8 °C, was located offshore of Destin while the rest of the Eglin Range Complex warmed by 2.4 °C. Numerical simulations by Arritt (1993) found that convergence was less effective in strengthening the temperature gradient when offshore flow was strong enough to suppress the sea breeze circulation. In this flow regime, uniform turbulent mixing over land and weak convergence due to lack of onshore flow resulted in the suppression of the sea breeze and supports Arritt's (1993) findings.

A graphical illustration of the position and intensity of the sea breeze front for Coast Parallel Easterly flow is presented in Figure 38. Under coast parallel easterly flow, the sea breeze beings approximately 1 hour earlier than the corresponding offshore flow regimes, except for 7-9 $ms^{-1}$ coast parallel easterly flow. In this regime, the sea begins by 14 UTC while the corresponding offshore flow regime begins by 18 UTC. This difference is attributed to the direction of the synoptic-scale flow. In the coast parallel regime, the synoptic-scale flow is from 94°, which has an onshore component. The synoptic-scale flow in the 7-9 $ms^{-1}$ offshore flow regime is from 355°, which is almost directly offshore. The onshore component of the flow in the coast parallel westerly regime created a sea breeze that is weaker and begins earlier than the offshore regime. Interestingly, the approximate offshore components of the coast parallel regimes are less than 5 $ms^{-1}$ yet the inland propagation of the sea breeze is comparable to the offshore regime. The orientation of the front, however, is parallel to the synoptic-scale flow in the coast parallel easterly regime.

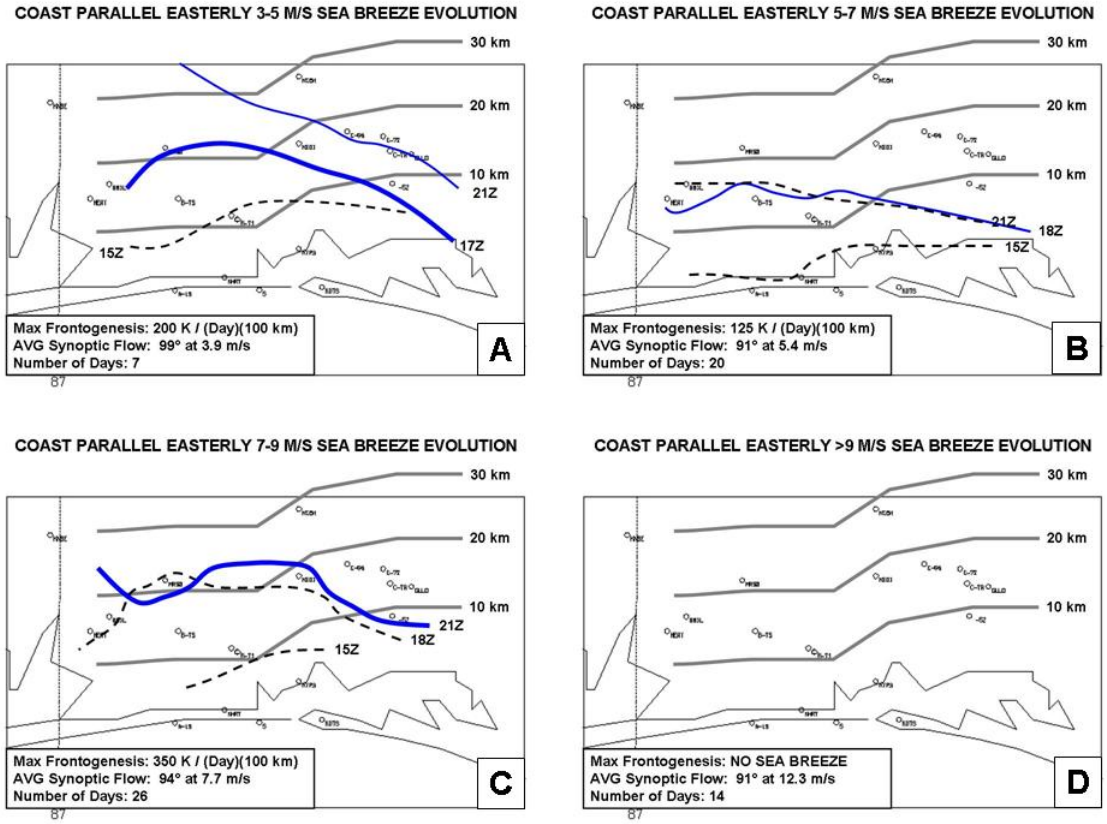


Figure 38. Illustration of the position and intensity of the sea breeze front for (A) 3-5, (B) 5-7, (C) 7-9 and (D) >9 $ms^{-1}$ Coast Parallel Easterly flow in the Eglin Range Complex.

### 5. Coast Parallel Westerly Synoptic-Scale Flow

Synoptic-scale flow with land on the left develops when the large scale pressure pattern has high pressure over water and low pressure over land. Surface friction tends to produce a weak onshore wind component, so a sea breeze that develops in this situation has characteristics of the onshore flow regime (Zhong and Tackle 1993; Nuss 2005). Sea breezes forming under coast parallel onshore flow start later and are more intense than sea breezes forming under the onshore flow regime.

### *a. 14 August 2005 Case Study*

Synoptic-scale flow was from 270° at 3.6 $ms^{-1}$ on 14 August. The 17 UTC surface analyses (Fig. 39) indicated the sea breeze had already begun and the sea breeze front was located 10 km inland from the Gulf of Mexico, but is held close to the coastline of the Choctawhatchee Bay. Westerly synoptic-scale flow was parallel to the coast Gulf Coast at Hulbert Field. It had an offshore component along the northeast-to-southwest oriented coastline near Eglin AFB. As a result, the sea breeze front penetrated farther inland where the flow was coast parallel and remained close to the coastline where the synoptic-scale flow retained an offshore component. Air temperatures are 32 ° C at RAWS site Coupland and 30 °C along the coast at Hulbert Field, indicating a 2 °C temperature gradient associated with the sea breeze front.

By 19 UTC, a thin line was evident on the KEVX base reflectivity product 20 km inland from the Gulf of Mexico and 15 km from the Choctawhatchee Bay (Fig. 40). Reflectivity values of 15 to 20 dBZ associated with the thin line were similar in magnitude to those found along the thin line under offshore flow. The sea breeze front moved to a position 25 km inland by 21 UTC. Thunderstorms formed along the sea breeze front at that time, after which an outflow boundary moved south towards the coastline and disrupted the thermal gradient that forced the sea breeze.

Under the coast parallel westerly flow, the sea breeze began at 1630 UTC and moved 15 and 20 km inland from the coastline by 19 UTC. A thin line was detected by radar on 18 UTC and was indicative of a strong sea breeze front. Under pure onshore flow, the sea breeze began at 15 UTC and no thin line is detected during the life cycle of the sea breeze.

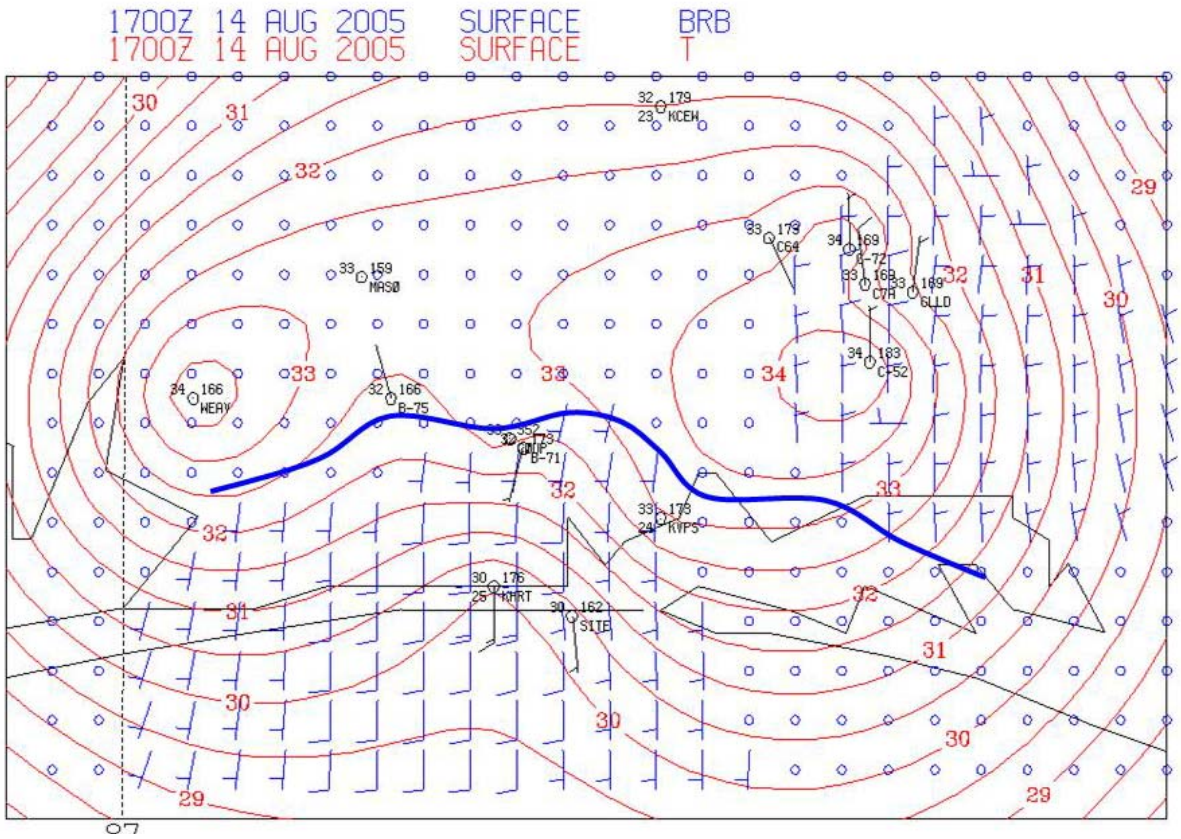


Figure 39. Surface analysis at 17 UTC for 14 August 2005. The location of the sea breeze front is indicated by the solid blue line. The sea breeze front penetrated 10 km inland from the Gulf of Mexico, but remained close to the coastline of the Choctawhatchee Bay. The blue line indicates the location of the sea breeze front.

### *b. Coast Parallel Westerly Composites*

The sea breeze begins at 16 UTC under 0-3 $ms^{-1}$ coast parallel westerly flow and by 17 UTC 2.5 $ms^{-1}$ southerly flow is evident 12 km inland from the Gulf of Mexico and 8 km inland from the Choctawhatchee Bay. The average direction of the synoptic-scale flow for this composite is 270°, which is parallel to the coastline in the Hulbert Field region. This enables the sea breeze to penetrate further inland along this section of coastline while westerly flow has an offshore component along the Choctawhatchee Bay where the sea breeze remains close to the coastline. The temperature perturbation is suppressed under coast parallel westerly flow and a sea breeze front is not present until 19 UTC. By then, the sea breeze front is located 25 km inland. Temperatures in the sea breeze air mass cool while slight warming occurs north

of the sea breeze. This differential heating results in an increase in the temperature gradient between the air masses. The temperature perturbation is 0.6 °C over a 15 km distance and there is no wind convergence at the boundary. The lack of convergence in concert with a weak temperature perturbation over a large length scale results in frontogenesis values of 20 $K$ Day$^{-1}$ 100 km$^{-1}$. By 20 UTC, the sea breeze front moves north of Crestview and out of the Eglin Range Complex.

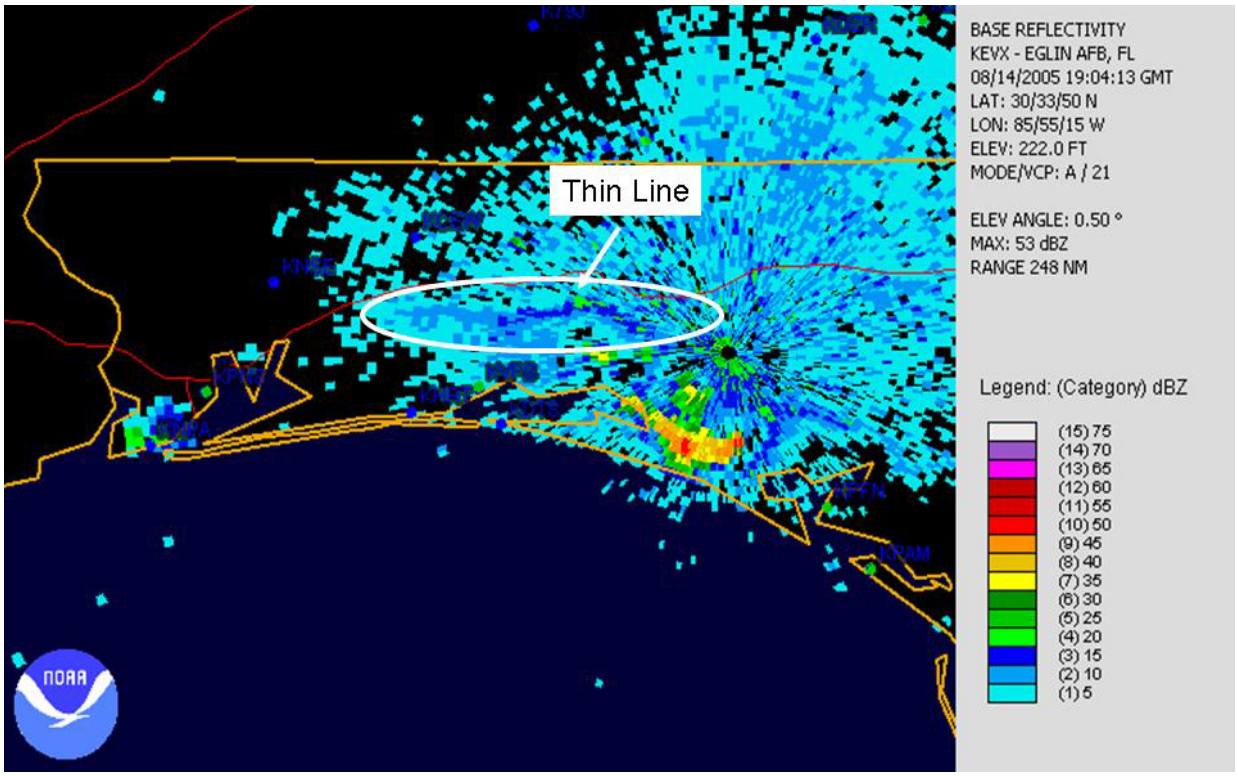


Figure 40. 1900 UTC base reflectivity product from 14 August 2005. (From Ref. National Climatic Data Center, http://www.ncdc.noaa.gov/oa/radar/radardata.html, February 2006).

The most intense sea breeze front forms under 3-5 $ms^{-1}$ coast parallel westerly flow. Unlike the 0-3 $ms^{-1}$ regime, winds are northwesterly at 2.5 $ms^{-1}$ over the Eglin Range Complex as the sea breeze begins at 16 UTC. The presence of offshore flow prior to the onset of the sea breeze is similar to the offshore flow regimes. Southwest winds of 2.5 $ms^{-1}$ are located south of the sea breeze front which penetrated 5 km inland

from the Gulf of Mexico but remained at the coastline of the Choctawhatchee Bay. The northwest flow also restricts the inland penetration of cool sea breeze air and resulted in strong differential heating across the sea breeze front. Air temperatures warmed by 6 °C north of the sea breeze front while locations south of the front warm by 2.5 °C between 13 and 16 UTC. The convergence between the northwest flow over land and the southwesterly sea breeze winds concentrates the thermal gradient in this region and results in a large temperature perturbation over a 12 km distance. The sea breeze front moves north to a position 12 km from the Choctawhatchee Bay and 15 km from the Gulf of Mexico by 18 UTC and intensifies (Fig. 41). Sea breeze winds increase to 5-8 $ms^{-1}$ and cool marine air limits atmospheric heating behind the front. North of the front, temperatures increase by 3 °C between 15 and 18 UTC. The differential heating and convergence at the front results in frontogenesis values of 300 $K$ $Day^{-1}$ 100 $km^{-1}$.

By 19 UTC, the front weakens and moves north to a position 25 km inland. Winds across the entire Eglin Range are southwesterly, decreasing convergence at the sea breeze front. Additionally, differential heating diminishes across the front. This decreases the magnitude of the temperature gradient and increases the length scale associated with the sea breeze front.

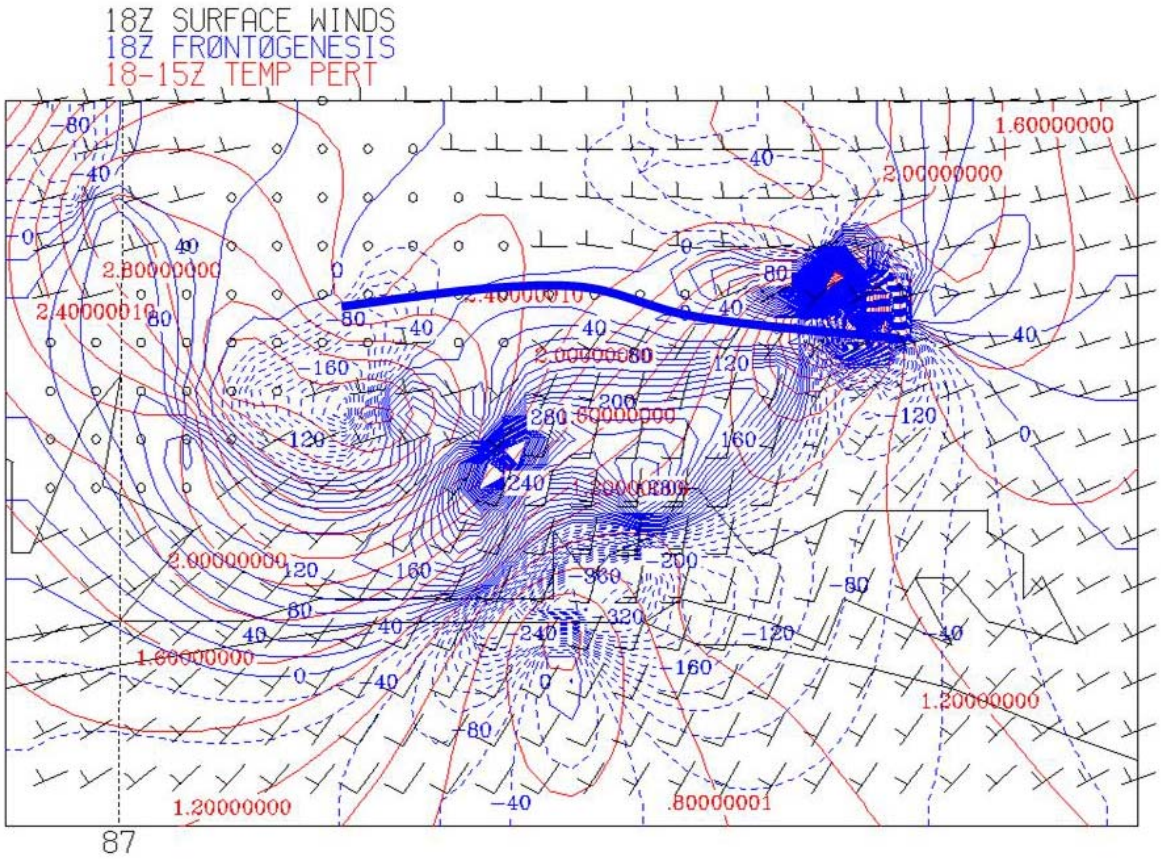


Figure 41. Computed 3-hour air temperature change (18-15 UTC in °C) contoured every 0.2 °C in red, frontogenesis plotted in blue contours every 50 $K$ Day$^{-1}$ 100 km$^{-1}$ at 18 UTC and surface wind barbs (full barb 5 $ms^{-1}$, half-barb 2.5 $ms^{-1}$) at 18 UTC for the Offshore 3-5 $ms^{-1}$ regime. Solid blue line indicates the position of the sea breeze front based on analyses of temperature, wind and frontogenesis.

Increasing the magnitude of the coast parallel westerly flow suppresses the development of a sea breeze front. Prior to the onset of the sea breeze at 15 UTC, the winds are west to northwest across the entire Eglin Range. The increased magnitude of the synoptic scale flow limits heating over land areas and results in little thermal perturbation as the daytime progresses. A wind shift line becomes evident 15 km inland by 17 UTC as winds back from westerly to southwesterly. This wind shift moves north through the Eglin Range Complex by 19 UTC.

Figure 42 illustrates the movement and intensity of the sea breeze front for the three coast parallel westerly synoptic regimes. Coast parallel 0-3 $ms^{-1}$ experiences the largest thermal perturbation but lack of wind convergence limits the frontogenesis until late afternoon, at which time differential heating across the sea breeze front strengthens the thermal gradient and a sea breeze front forms. Coast parallel flow of 3-5 $ms^{-1}$ generates the strongest sea breeze front. A strong thermal perturbation coupled with wind convergence at the leading edge of the sea breeze concentrates the thermal gradient and results in an intense sea breeze front. In addition, the direction of the synoptic scale flow for the composite is slightly north of west and results in a larger offshore wind component along the coast. Frontogenesis values at 19 UTC are of similar magnitude to frontogenesis values associated with offshore flow. Finally, increasing the magnitude of the coast parallel westerly flow results in westerly flow across the entire Eglin Range Complex as daytime heating commences. The stronger winds limit the amount of daytime heating. The lack of a strong thermal perturbation coupled with weak wind convergence suppresses the development of a sea breeze front. A wind shift line is the only evidence of a sea breeze as winds back from westerly to southwesterly. The wind shift line moves through the Eglin Range Complex by 19 UTC.

## 6. Summary of Results

Table 6 summarizes the findings from the composites presented in this chapter. Sea breeze start time, time of maximum frontal intensity, frontogenesis value at the time of maximum intensity, maximum inland penetration and time of maximum inland penetration of the sea breeze front are presented in a tabular format.

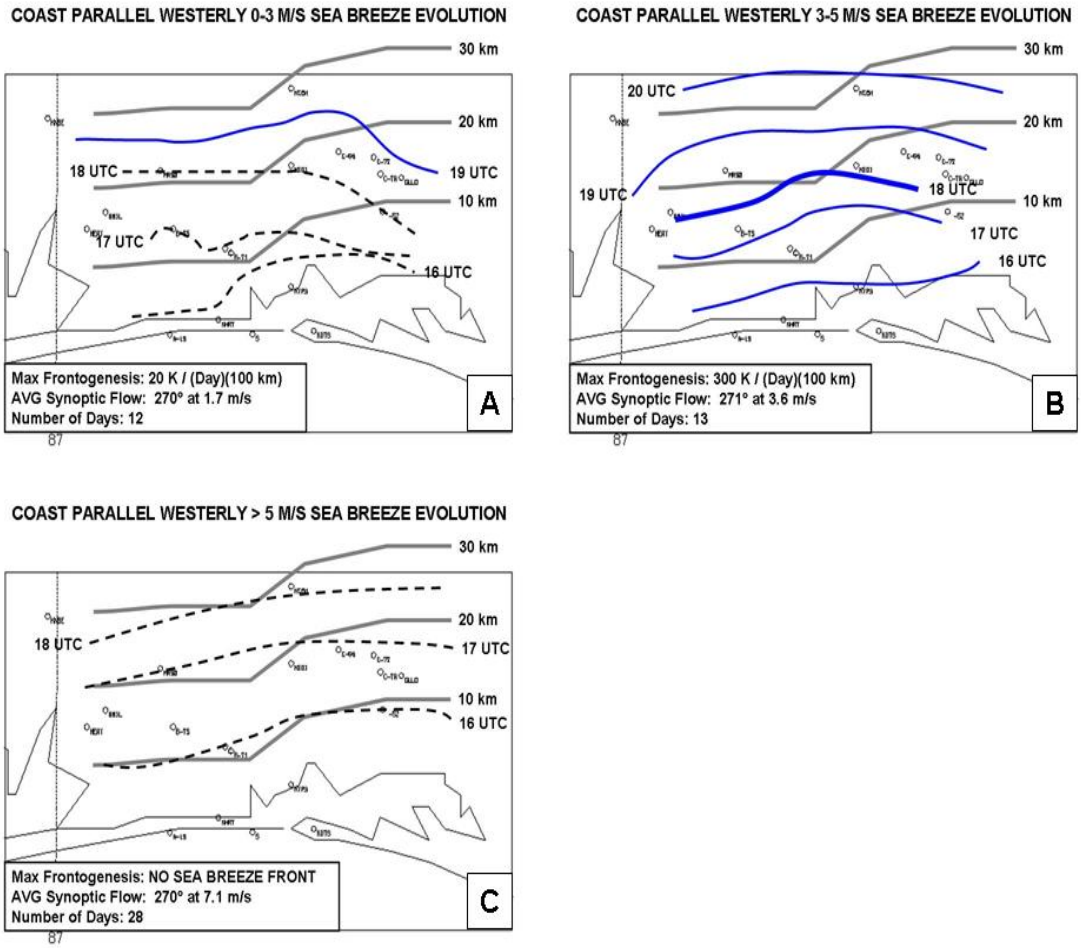


Figure 42. Illustration of the position and intensity of the sea breeze front for Coast Parallel Westerly synoptic-scale flow of (A) 0-3 $ms^{-1}$, (B) 3-5 $ms^{-1}$, and (C) > 5 $ms^{-1}$ in the Eglin Range Complex.

| REGIME | CALM | OFFSHORE | | | | ONSHORE | | |
|---|---|---|---|---|---|---|---|---|
| SPEED BIN | < 3 m/s | 3-5 m/s | 5-7 m/s | 7-9 m/s | > 9 m/s | 0-3 | 3-5 | >5 |
| Sea Breeze Start Time (UTC) | 1530 | 1630 | 1730 | 1800 | N/A | 15 | 1430 | 12 |
| Sea Breeze Front Intensity | | | | | | | | |
| Time (UTC) | 19 | 19 | 16-19 | 19 | N/A | 19 | 19 | 18 |
| Frontogenesis Value (K/Day/100km) | 20 | 325 | 125 | 225 | N/A | 60 | 100 | 40 |
| Maximum Inland Penetration | | | | | | | | |
| Distance (km) | Eglin Range | Eglin Range | 12-15 | 2-10 | N/A | Eglin Range | Eglin Range | Eglin Range |
| Time (UTC) | 21 | 22 | 21 | 21 | N/A | 2030 | 1930 | 1830 |

| REGIME | COAST PARALLEL EASTERLY | | | | COAST PARALLEL WESTERLY | | |
|---|---|---|---|---|---|---|---|
| SPEED BIN | 3-5 m/s | 5-7 m/s | 7-9 m/s | > 9 m/s | 0-3 | 3-5 | >5 |
| Sea Breeze Start Time (UTC) | 1430 | 17 | 16 | N/A | 16 | 16 | 15 |
| Sea Breeze Front Intensity | | | | | | | |
| Time (UTC) | 18 | 18 | 21 | N/A | 19 | 18 | N/A |
| Frontogenesis Value (K/Day/100km) | 150 | 125 | 350 | N/A | 20 | 300 | N/A |
| Maximum Inland Penetration | | | | | | | |
| Distance (km) | Eglin Range | 8-15 | 22 | N/A | Eglin Range | Eglin Range | Eglin Range |
| Time (UTC) | 2130 | 21 | 21 | N/A | 20 | 20 | 1830 |

Table 6. Sea breeze properties by synoptic-scale flow regime. All time in UTC. "Eglin Range" in the Distance column refers to sea breeze fronts that propagated through the Eglin Range Complex.

# V. CONCLUSIONS AND RECOMMENDATIONS

## A. CONCLUSIONS

In this study, the propagation and intensity of the sea breeze front at Eglin AFB was investigated under offshore, onshore, coast parallel easterly and coast parallel westerly synoptic-scale flow regimes. 509 sea breeze days were collected between May and September of 2001 to 2005 and days with similar synoptic-scale flow regimes were composited. Through the use of the frontogenesis equation, the strength and location of the sea breeze front was determined on the Eglin range complex. The major findings of this study are summarized below.

First, the Choctawhatchee Bay disrupts the along-coast temperature contours. Initially, the coastline was considered concave. However, analysis indicated that the northern coastline of the Choctawhatchee Bay is the effective coastline in this region. As a result, under light synoptic-scale flow, the sea breeze at Eglin begins with a southeasterly wind because the coastline in the region is oriented northeast to southwest. Inland penetration distances of the sea breeze were calculated from the northern coast of the Choctawhatchee Bay. The northern coast has numerous bays and headlands that create mesoscale along-front variations in sea breeze location and intensity.

The strength of the sea breeze front is determined by a balance between convergence and turbulent mixing. Under offshore flow, the onset and inland penetration of the sea breeze is delayed by as much as two hours compared to onshore flow. This has important implications regarding sea breeze strength. First, the sea breeze front is held at the coastline keeping cool marine air offshore. This enables radiational heating to continue over land through the day. The turbulent mixing between cool sea breeze air and air warmed by land is minimized as the sea breeze front is held at the coastline. Second, convergence is maximized as onshore sea breeze winds converge with flow off the land, resulting in a concentrated thermal gradient and strong frontogenesis. In addition, the temperature perturbation is largest with offshore flow and the length scale associated with the sea breeze front is smallest, resulting in a strong sea breeze front. Conversely, under onshore synoptic-scale flow, the advection of cool sea breeze air

inland early in the day suppresses the formation of the temperature perturbation. As the sea breeze penetrates inland, turbulent mixing reduces the temperature contrast between the two air masses. This results in weak thermal perturbations at the leading edge of the sea breeze and large length scales associated with the weak thermal gradient. However, sea breeze fronts did form under onshore synoptic-scale flow late in the day between 18 and 19 UTC. At this time, turbulent mixing has decreased and convergence at the sea breeze front has increased which results in the formation of weak sea breeze fronts 20 km inland. These findings are in agreement with past studies (Arritt 1993; Atkins and Wakimoto 1997; Gilliam et al 2004).

Offshore synoptic-scale flow produces strong sea breeze fronts that weaken by afternoon. The average start time for the sea breeze is 1730 UTC. The strongest sea breeze front forms under 3-5 $ms^{-1}$ offshore flow, somewhat in disagreement with past numerical research that found the most intense sea breeze formed under 5-6 $ms^{-1}$ offshore flow. However, this numerical research was conducted using two dimensional models to simulate the sea breeze along straight coastlines and did not account for changes in the magnitude or direction of the synoptic scale flow or important three-dimensional effects of curved coastlines. Results presented in this thesis agree with past research in that increasing the magnitude of the offshore flow suppresses sea breeze front development. Under offshore flow greater than 9 $ms^{-1}$, no sea breeze forms along the Eglin coastline. Offshore synoptic-scale flow of 7-9 $ms^{-1}$ holds the sea breeze front to within 15 km of the coastline. Therefore, thunderstorm development is likely within 15 km of the coast under offshore flow up to 9 $ms^{-1}$.

Onshore flow creates weak sea breeze fronts that strengthened late in the day along the coastline of Eglin AFB. The average start time of the sea breeze under onshore synoptic-scale flow is 1330 UTC, two hours earlier than the offshore case. Initially, the sea breeze front is difficult to detect; however, between 18 and 19 UTC, a weak sea breeze front forms 20 km inland as turbulent mixing of the sea breeze air decreases and convergence at the sea breeze front increases. This is in agreement with studies by Atkins and Wakimoto (1997) and Gilliam et al. (2004). Unlike offshore synoptic-scale flow, sea breeze fronts forming under onshore flow propagate through the Eglin Range

Complex by 19 UTC. The strongest sea breeze front in this regime forms in the presence of 4 $ms^{-1}$ onshore flow while onshore flow greater than 5 $ms^{-1}$ suppressed the development of a sea breeze front. Therefore, convective development along the sea breeze front under onshore flow is likely late in the afternoon in the northern sections of the range complex.

Sea breeze evolution under coast parallel synoptic-scale flow regimes were also investigated in this thesis. The average start time of the sea breeze under coast parallel easterly and westerly flow was 1500 UTC, 2.5 hours earlier than the offshore flow regime and 1.5 hours later than the onshore flow regime. Sea breeze fronts forming under coast parallel easterly flow are weaker than fronts in the offshore regime while sea breeze fronts forming under coast parallel westerly flow are stronger than fronts in the onshore regime, as predicted by theory. Coast parallel easterly flow of 7-9 $ms^{-1}$ produces a strong sea breeze front located 20 km inland while flow greater than 9 $ms^{-1}$ suppresses the development of a sea breeze. Sea breeze fronts forming under coast parallel easterly flow are initially weak, but strengthen by midday in the middle of the Eglin Range Complex. Atkins and Wakimoto (1997) found similar results in their investigation of sea breeze fronts along Cape Canaveral.

One of the strongest sea breeze fronts of this study formed under 3-5 $ms^{-1}$ coast parallel westerly flow. The characteristics of this sea breeze front were similar to sea breeze fronts forming under offshore flow. Initially, this was a surprising result; however, there is evidence that supports the presence of a strong sea breeze front forming on the Eglin Range Complex under coast parallel westerly flow. Camp et al. (1998) found maxima in lightning flash densities along sections of the Florida Panhandle under 2-5 $ms^{-1}$ westerly flow. Sections of coastline that are parallel to the westerly flow exhibited larger flash densities than sections of coastline where the flow was offshore. The region between East Bay and Choctawhatchee Bay was singled out a region of lightning flash maxima. In addition, flash densities under westerly flow exceeded those associated with easterly flow. Coast parallel westerly flow of 0-3 and greater than 5 $ms^{-1}$ suppressed or produced weak sea breeze fronts.

## B. RECOMMENDATIONS

1. This study determined the location and strength of the sea breeze front on the Eglin Range Complex under various synoptic-scale flow regimes. However, the presence of a strong sea breeze front does not equate to thunderstorm formation. Accurately forecasting the location and strength of the sea breeze front is the first step in improving summer thunderstorm forecasting at Eglin AFB. Therefore, this topic should remain on the Air Force Weather Agency Thesis Topic list.

2. It is recognized that the synoptic-scale flow regime can change during the course of the day. However, that was not considered for this study. To get a true sense of the evolution of the sea breeze under the regimes presented, days when the synoptic-scale flow regime changes between 12 and 00 UTC should be filtered from the study. This will require that the period of study be expanded from the five years considered for this study in order to retain a large number of days for compositing. This is especially true for the coast parallel regimes which, in this study, contained approximately 55 days each.

3. In this study, coast parallel westerly flow of 3-5 $ms^{-1}$ produced a strong sea breeze front that was similar in movement and intensity to the offshore regime. Originally, this was a surprising result. However, this finding has some support in the literature. Camp et al. (1998) examined cloud-to-ground lightning strikes over the Florida Panhandle as a function of the prevailing synoptic-scale flow and found lightning flash maxima between East Bay and the Choctawhatchee Bay under 2-5 $ms^{-1}$ westerly flow. The maxima were located where the flow was parallel to the coastline. Regions of the coastline where the westerly flow was offshore, which should create strong sea breeze front, did not show the same lightning maxima. Additionally, their results showed increased lightning activity when the panhandle was under southeast synoptic-scale flow when compared to southwest flow. Therefore, the offshore and onshore synoptic-scale flow regimes presented in this thesis should be subdivided in order to investigate the propagation and intensity of

sea breeze fronts forming under northeast, northwest, southeast and southwest synoptic-scale flow regimes.

4. The method of compositing days by flow regime is not limited to surface meteorological fields. Lack of data at the boundaries of the study domain and poorly sampled wind data within the study area limited the analyses of the sea breeze. However, the KEVX WSR-88D is 60 km to the east of Eglin AFB and provides excellent coverage of the Eglin Range Complex. The case studies presented in this thesis show that the propagation and intensity of the sea breeze front can be monitored at a high temporal and spatial resolution. It is recommended that products such as base reflectivity, velocity, and hourly precipitation be composited by synoptic-scale flow regime to compare the location and strength of the sea breeze front to the composites presented in this thesis. As mentioned above, strong frontogenesis does not necessarily equate to thunderstorms. Composites of WSR-88D products could correlate the timing and location of thunderstorms to the location and intensity of the sea breeze front.

5. The thermodynamic environment is a key component in forecasting summer thunderstorms. Therefore, an investigation into the stability indices that best predict thunderstorm activity over the Eglin Range Complex should be undertaken. In this study, the strongest sea breeze fronts formed under offshore synoptic-scale flow while the weakest fronts formed under onshore flow. However, Camp et al. (1998) found that the atmosphere is thermodynamically stable under offshore flow in the panhandle of Florida and less likely for convection while the third largest number of lightning flashes found on the gulf coast occurred under onshore synoptic-scale flow.

6. A frequency distribution of days by 925 mb wind direction was conducted to determine the most common wind directions for this study (Fig. 43). As expected, southeasterly and southwesterly winds were most common. An unexpected result, however, was the large number of days with westerly 925 mb winds. Further investigation revealed the majority of days with westerly

winds occurred in July of 2001, 2002, and 2004. 2001, 2002, and 2004 had 10, 10, and 12 days respectively with 925 mb westerly winds. Using the NCEP/NCAR reanalysis fields from the Climate Diagnostic Center (CDC), the 10 days with westerly winds in July 2001 were composited and fields were calculated for 925 mb heights, 925 mb winds, and 500 mb heights. The average 500 mb heights for the 10 days in July 2001 revealed a deep trough along the East Coast of North America. This trough caused a southward shift in the mean position of the Azores High across Florida. As a result, 925 mb wind vectors for the 10 days revealed anomalous northwest flow across the Florida Panhandle instead of the normal southwest flow. Interestingly, plots for 2002 and 2004 show the same anomalous trough along the U.S. East Coast creating west to northwest flow across the Florida Panhandle. Gould and Fuelberg (1996), who investigated the role of synoptic-scale flow on thunderstorm activity in the Florida Panhandle, also found an unexpected number of days with westerly to northwesterly winds over the Florida Panhandle during the summer of 1995. Gould and Fuelberg (1996) attributed this anomaly to the large number of continental high pressure systems which affected the region during that summer. According to the CDC's Oceanic Nino Index, 1995, 2002, and 2004 were years where the three month running mean of sea surface temperature anomalies in Nino region 3.4 (5°N-5°N; 120°-170°W) were positive indicating El Nino episodes. 2001 was a transition year between a La Nina episode in 2000 and the El Nino episode in 2001. Results in this study and from Camp et al. (1998) suggests westerly synoptic-scale flow creates a strong sea breeze front with lightning flash maxima located between Choctawhatchee Bay and East Bay. Future research should investigate possible climate impacts due to El Nino episodes on the intensity of the sea breeze front and convective activity in the Florida Panhandle

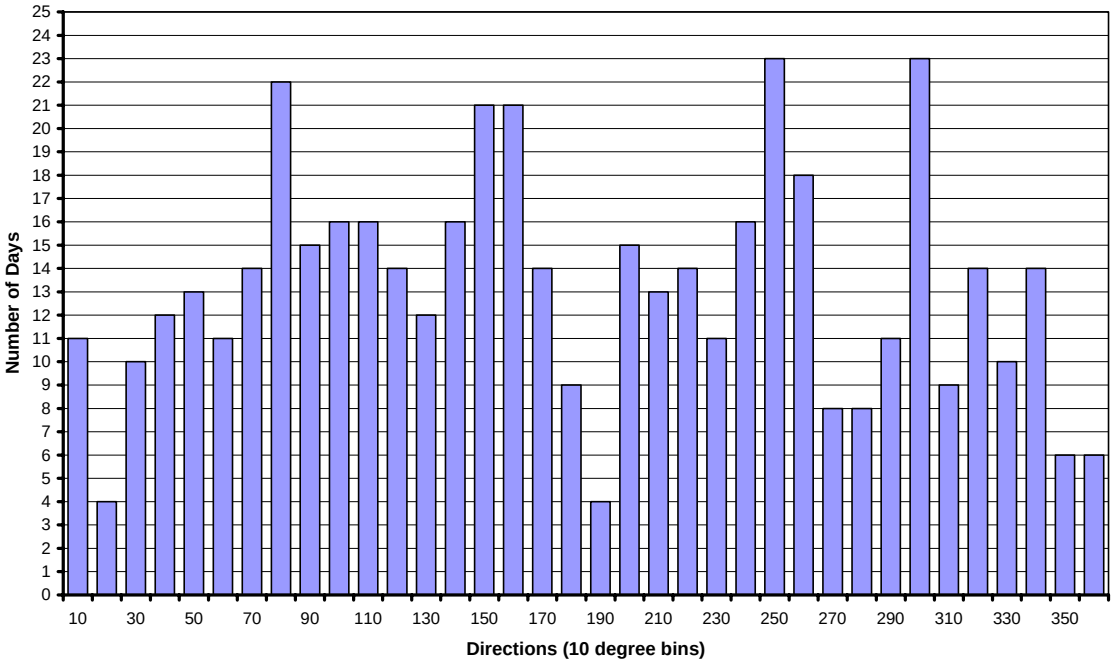


Figure 43. Distribution of days according to their 925 mb wind direction for KTLH from may to September, 2001 to 2005. Directions are grouped in 10° bins.

THIS PAGE INTENTIONALLY LEFT BLANK

# APPENDIX A – CALM COMPOSITE DATES

| CALM | | | |
|---|---|---|---|
| Date | Direction | Kts | m/s |
| 17-Jun-01 | 25 | 4 | 2.06 |
| 20-Jun-01 | 195 | 4 | 2.06 |
| 24-Jun-01 | 360 | 4 | 2.06 |
| 26-Jun-01 | 170 | 2 | 1.03 |
| 7-Jul-01 | 250 | 5 | 2.57 |
| 19-Jul-01 | 205 | 3 | 1.54 |
| 31-Jul-01 | 310 | 2 | 1.03 |
| 4-Aug-01 | 135 | 4 | 2.06 |
| 15-Aug-01 | 340 | 2 | 1.03 |
| 16-Aug-01 | 240 | 4 | 2.06 |
| 22-Aug-01 | 35 | 4 | 2.06 |
| 24-Aug-01 | 270 | 4 | 2.06 |
| 29-Aug-01 | 195 | 6 | 3.09 |
| 6-Sep-01 | 50 | 3 | 1.54 |
| 17-Sep-01 | 260 | 4 | 2.06 |
| 22-Sep-01 | 160 | 5 | 2.57 |
| 11-May-02 | 130 | 4 | 2.06 |
| 1-Jun-02 | 220 | 5 | 2.57 |
| 4-Jun-02 | 45 | 4 | 2.06 |
| 13-Jun-02 | 15 | 2 | 1.03 |
| 16-Jun-02 | 280 | 4 | 2.06 |
| 30-Jun-02 | 50 | 5 | 2.57 |
| 3-Jul-02 | 320 | 4 | 2.06 |
| 4-Jul-02 | 295 | 2 | 1.03 |
| 6-Jul-02 | 40 | 4 | 2.06 |
| 7-Jul-02 | 85 | 4 | 2.06 |
| 12-Jul-02 | 160 | 2 | 1.03 |
| 13-Aug-02 | 150 | 4 | 2.06 |
| 19-Aug-02 | 250 | 5 | 2.57 |
| 21-Aug-02 | 165 | 5 | 2.57 |
| 23-Aug-02 | 270 | 3 | 1.54 |
| 28-Aug-02 | 285 | 4 | 2.06 |
| 29-Aug-02 | 85 | 4 | 2.06 |
| 30-Aug-02 | 130 | 4 | 2.06 |
| 16-Sep-02 | 335 | 2 | 1.03 |
| 17-Sep-02 | 320 | 2 | 1.03 |
| 18-Sep-02 | 180 | 4 | 2.06 |
| 4-May-03 | 300 | 5 | 2.57 |
| 14-May-03 | 145 | 5 | 2.57 |
| 16-May-03 | 220 | 5 | 2.57 |
| 24-May-03 | 55 | 4 | 2.06 |
| 25-May-03 | 260 | 3 | 1.54 |
| 16-Jun-03 | 160 | 5 | 2.57 |
| 22-Jun-03 | 285 | 2 | 1.03 |
| 23-Jun-03 | 95 | 4 | 2.06 |
| 25-Jun-03 | 115 | 4 | 2.06 |
| 8-Jul-03 | 250 | 5 | 2.57 |
| 16-Jul-03 | 355 | 3 | 1.54 |
| 18-Jul-03 | 260 | 1 | 0.51 |
| 26-Jul-03 | 230 | 1 | 0.51 |
| 9-Aug-03 | 112 | 5 | 2.57 |
| 10-Aug-03 | 330 | 3 | 1.54 |
| 16-Aug-03 | 250 | 3 | 1.54 |
| 17-Aug-03 | 230 | 5 | 2.57 |
| 20-Aug-03 | 155 | 1 | 0.51 |
| 24-Aug-03 | 30 | 5 | 2.57 |
| 25-Aug-03 | 90 | 3 | 1.54 |
| 26-Aug-03 | 80 | 1 | 0.51 |
| 27-Aug-03 | 155 | 2 | 1.03 |
| 12-Sep-03 | 344 | 4 | 2.06 |
| 11-May-04 | 165 | 4 | 2.06 |
| 20-May-04 | 20 | 2 | 1.03 |
| 21-May-04 | 275 | 3 | 1.54 |
| 25-May-04 | 265 | 5 | 2.57 |
| 6-Jul-04 | 185 | 4 | 2.06 |
| 8-Jun-04 | 335 | 4 | 2.06 |
| 13-Jun-04 | 330 | 3 | 1.54 |
| 16-Jun-04 | 160 | 5 | 2.57 |
| 11-Jul-04 | 315 | 5 | 2.57 |
| 20-Jul-04 | 295 | 3 | 1.54 |
| 21-Jul-04 | 305 | 5 | 2.57 |
| 22-Jul-04 | 340 | 4 | 2.06 |

| | | | |
|---|---|---|---|
| 23-Jul-04 | 340 | 3 | 1.54 |
| 28-Jul-04 | 302 | 2 | 1.03 |
| 14-Aug-04 | 140 | 4 | 2.06 |
| 24-Aug-04 | 5 | 5 | 2.57 |
| 27-Aug-04 | 150 | 5 | 2.57 |
| 2-Sep-04 | 145 | 4 | 2.06 |
| 9-Sep-04 | 30 | 3 | 1.54 |
| 10-Sep-04 | 60 | 5 | 2.57 |
| 7-May-05 | 45 | 1 | 0.51 |
| 8-May-05 | 235 | 2 | 1.03 |
| 11-May-05 | 65 | 4 | 2.06 |
| 13-May-05 | 80 | 2 | 1.03 |
| 19-May-05 | 165 | 5 | 2.57 |
| 26-May-05 | 80 | 5 | 2.57 |
| 27-May-05 | 335 | 3 | 1.54 |
| 28-May-05 | 255 | 5 | 2.57 |
| 6-Jun-05 | 120 | 2 | 1.03 |
| 7-Jun-05 | 290 | 4 | 2.06 |
| 8-Jun-05 | 30 | 1 | 0.51 |
| 19-Jun-05 | 320 | 3 | 1.54 |
| 22-Jun-05 | 55 | 5 | 2.57 |
| 8-Jul-05 | 150 | 3 | 1.54 |
| 19-Jul-05 | 95 | 2 | 1.03 |
| 21-Jul-05 | 360 | 2 | 1.03 |
| 26-Jul-05 | 325 | 2 | 1.03 |
| 28-Jul-05 | 300 | 2 | 1.03 |
| 16-Aug-05 | 273 | 5 | 2.57 |
| 17-Aug-05 | 225 | 4 | 2.06 |
| 20-Aug-05 | 320 | 2 | 1.03 |
| 21-Aug-05 | 330 | 4 | 2.06 |
| 22-Aug-05 | 290 | 5 | 2.57 |
| 24-Aug-05 | 195 | 2 | 1.03 |
| 16-Sep-05 | 325 | 4 | 2.06 |
| 17-Sep-05 | 260 | 3 | 1.54 |
| 19-Sep-05 | 110 | 3 | 1.54 |
| **# DAYS** | **AVG** | **AVG** | **AVG** |
| 107 | 199 | 3.54 | 1.82 |

# APPENDIX B – OFFSHORE COMPOSITE DATES

| OFFSHORE | | | | | | | | | | | | |
|---|---|---|---|---|---|---|---|---|---|---|---|---|
| 290-074 (3-5 m/s) | | | | | 290-074 (5-7 m/s) | | | | 290-074 (7-9 m/s) | | | |
| Date | Direction | Kts | m/s | | Date | Direction | Kts | m/s | Date | Direction | Kts | m/s |
| 6-May-01 | 70 | 8 | 4.12 | | 14-May-01 | 20 | 12 | 6.18 | 23-May-01 | 10 | 14 | 7.21 |
| 12-May-01 | 320 | 6 | 3.09 | | 13-May-01 | 320 | 10 | 5.15 | 21-May-02 | 45 | 17 | 8.75 |
| 17-May-01 | 300 | 8 | 4.12 | | 16-May-01 | 305 | 10 | 5.15 | 22-May-02 | 70 | 16 | 8.23 |
| 18-May-01 | 300 | 8 | 4.12 | | 26-May-01 | 320 | 10 | 5.15 | 15-Jun-02 | 5 | 17 | 8.75 |
| 25-Jun-01 | 20 | 6 | 3.09 | | 20-Jul-01 | 300 | 10 | 5.15 | 18-Jul-02 | 35 | 16 | 8.23 |
| 14-Jul-01 | 65 | 8 | 4.12 | | 10-Aug-01 | 290 | 12 | 6.18 | 7-Aug-02 | 5 | 14 | 7.21 |
| 25-Aug-01 | 320 | 6 | 3.09 | | 21-Aug-01 | 350 | 10 | 5.15 | 4-Sep-02 | 45 | 15 | 7.72 |
| 26-Aug-01 | 290 | 6 | 3.09 | | 2-May-02 | 318 | 11 | 5.66 | 28-May-03 | 360 | 15 | 7.72 |
| 16-Sep-01 | 10 | 8 | 4.12 | | 20-Jun-02 | 65 | 13 | 6.69 | 29-May-03 | 295 | 14 | 7.21 |
| 21-Sep-01 | 335 | 6 | 3.09 | | 16-Jul-02 | 295 | 12 | 6.18 | 29-Jul-03 | 300 | 17 | 8.75 |
| 27-Sep-01 | 345 | 6 | 3.09 | | 17-Jul-02 | 305 | 11 | 5.66 | 3-May-04 | 295 | 17 | 8.75 |
| 5-May-02 | 320 | 9 | 4.63 | | 20-Aug-02 | 290 | 12 | 6.18 | 12-Jul-04 | 5 | 14 | 7.21 |
| 26-May-02 | 315 | 8 | 4.12 | | 25-Aug-02 | 305 | 13 | 6.69 | 6-Aug-04 | 290 | 14 | 7.21 |
| 3-Jun-02 | 35 | 6 | 3.09 | | 3-Sep-02 | 55 | 10 | 5.15 | 18-Sep-04 | 335 | 15 | 7.72 |
| 29-Jun-02 | 70 | 6 | 3.09 | | 11-Sep-02 | 295 | 10 | 5.15 | 6-May-05 | 25 | 14 | 7.21 |
| 2-Jun-02 | 350 | 8 | 4.12 | | 2-May-03 | 295 | 11 | 5.66 | 10-Sep-05 | 45 | 14 | 7.21 |
| 1-Jul-02 | 40 | 8 | 4.12 | | 13-May-03 | 345 | 11 | 5.66 | 14-Sep-05 | 300 | 14 | 7.21 |
| 2-Jul-02 | 25 | 8 | 4.12 | | 21-Jun-03 | 295 | 13 | 6.69 | | | | |
| 19-Jul-02 | 45 | 9 | 4.63 | | 8-Sep-03 | 10 | 11 | 5.66 | | | | |
| 20-Jul-02 | 295 | 7 | 3.60 | | 28-Sep-03 | 300 | 13 | 6.69 | | | | |
| 2-Aug-02 | 40 | 8 | 4.12 | | 4-May-04 | 335 | 10 | 5.15 | | | | |
| 6-Aug-02 | 325 | 9 | 4.63 | | 13-Jul-04 | 325 | 11 | 5.66 | | | | |
| 2-Sep-02 | 55 | 9 | 4.63 | | 25-Aug-04 | 55 | 10 | 5.15 | | | | |
| 10-Sep-02 | 10 | 9 | 4.63 | | 13-Aug-04 | 350 | 10 | 5.15 | | | | |
| 23-May-03 | 340 | 7 | 3.60 | | 24-May-05 | 330 | 13 | 6.69 | | | | |
| 17-Jul-03 | 305 | 8 | 4.12 | | 15-Jun-05 | 330 | 10 | 5.15 | | | | |
| 7-Sep-03 | 55 | 8 | 4.12 | | 16-Jun-05 | 305 | 13 | 6.69 | | | | |
| 9-Sep-03 | 360 | 6 | 3.09 | | 1-Jul-05 | 290 | 10 | 5.15 | | | | |
| 11-Sep-03 | 50 | 7 | 3.60 | | 22-Jul-05 | 305 | 10 | 5.15 | | | | |
| 18-Sep-03 | 35 | 8 | 4.12 | | 23-Jul-05 | 340 | 13 | 6.69 | | | | |
| 19-Sep-03 | 330 | 9 | 4.63 | | 27-Jul-05 | 300 | 10 | 5.15 | | | | |
| 6-May-04 | 5 | 7 | 3.60 | | 2-Sep-05 | 40 | 10 | 5.15 | | | | |
| 7-May-04 | 10 | 6 | 3.09 | | 3-Sep-05 | 70 | 10 | 5.15 | | | | |
| 8-May-04 | 35 | 9 | 4.63 | | 12-Sep-05 | 335 | 12 | 6.18 | | | | |
| 19-May-04 | 70 | 6 | 3.09 | | | | | | | | | |
| 18-Jun-04 | 315 | 8 | 4.12 | | | | | | | | | |
| 24-Jul-04 | 20 | 9 | 4.63 | | | | | | | | | |
| 19-Jul-04 | 335 | 6 | 3.09 | | | | | | | | | |
| 1-Aug-04 | 315 | 6 | 3.09 | | | | | | | | | |
| 3-Aug-04 | 295 | 9 | 4.63 | | | | | | | | | |
| 4-Aug-04 | 295 | 8 | 4.12 | | | | | | | | | |
| 2-May-05 | 35 | 8 | 4.12 | | | | | | | | | |
| 3-May-05 | 35 | 7 | 3.60 | | | | | | | | | |
| 11-May-05 | 355 | 9 | 4.63 | | | | | | | | | |
| 29-May-05 | 295 | 8 | 4.12 | | | | | | | | | |
| 23-Jun-05 | 55 | 6 | 3.09 | | | | | | | | | |
| 14-Sep-05 | 295 | 7 | 3.60 | | | | | | | | | |
| 17-Jun-05 | 295 | 9 | 4.63 | | | | | | | | | |
| 24-Jul-05 | 70 | 9 | 4.63 | | | | | | | | | |
| 15-Aug-05 | 30 | 8 | 4.12 | | | | | | | | | |
| 15-Sep-05 | 290 | 8 | 4.12 | | | | | | | | | |
| 18-Sep-05 | 10 | 6 | 3.09 | | | | | | | | | |
| # DAYS | AVG | AVG | AVG | | # DAYS | AVG | AVG | AVG | # DAYS | AVG | AVG | AVG |
| 52 | 178 | 7.54 | 3.88 | | 34 | 258 | 11.09 | 5.71 | 17 | 145 | 15.12 | 7.78 |

| 290-074 (>9 m/s) | | | |
|---|---|---|---|
| Date | Direction | Kts | m/s |
| 22-Jul-01 | 70 | 20 | 10.29 |
| 14-Sep-01 | 70 | 33 | 16.98 |
| 15-Sep-01 | 40 | 35 | 18.01 |
| 29-Sep-01 | 70 | 28 | 14.41 |
| 30-Sep-01 | 50 | 26 | 13.38 |
| 19-May-02 | 50 | 29 | 14.93 |
| 20-May-02 | 45 | 23 | 11.84 |
| 3-Aug-02 | 60 | 29 | 14.93 |
| 5-Sep-02 | 65 | 19 | 9.78 |
| 17-Sep-03 | 60 | 20 | 10.29 |
| 29-Sep-03 | 25 | 18 | 9.26 |
| 30-Sep-03 | 50 | 18 | 9.26 |
| 23-Sep-03 | 30 | 16 | 10.29 |
| 5-Sep-04 | 60 | 32 | 16.47 |
| 20-Sep-04 | 70 | 24 | 12.35 |
| 24-Sep-04 | 70 | 19 | 9.78 |
| 1-May-05 | 335 | 18 | 9.26 |
| 7-Sep-05 | 65 | 31 | 15.95 |
| 9-Sep-05 | 30 | 18 | 9.26 |
| # DAYS | AVG | AVG | AVG |
| 19 | 69 | 24.00 | 12.46 |

# APPENDIX C – ONSHORE COMPOSITE DATES

| ONSHORE | | | | | | | | | | | | |
|---|---|---|---|---|---|---|---|---|---|---|---|---|
| 120-255 (0-3 m/s) | | | | 120-255 (3-5 m/s) | | | | 120-255 (> 5 m/s) | | | |
| Date | Direction | Kts | m/s | Date | Direction | Kts | m/s | Date | Direction | Kts | m/s |
| 26-Jun-01 | 170 | 2 | 1.03 | 10-May-01 | 255 | 6 | 3.09 | 21-May-01 | 220 | 14 | 7.21 |
| 20-Jun-01 | 195 | 4 | 2.06 | 24-May-01 | 255 | 8 | 4.12 | 31-May-01 | 250 | 12 | 6.18 |
| 19-Jul-01 | 205 | 3 | 1.54 | 5-Jun-01 | 160 | 8 | 4.12 | 28-Jun-01 | 140 | 12 | 6.18 |
| 7-Jul-01 | 250 | 5 | 2.57 | 19-Jun-01 | 180 | 6 | 3.09 | 29-Jun-01 | 155 | 10 | 5.15 |
| 4-Aug-01 | 135 | 4 | 2.06 | 27-Jun-01 | 120 | 8 | 4.12 | 14-Jun-01 | 255 | 17 | 8.75 |
| 16-Aug-01 | 240 | 4 | 2.06 | 4-Jun-01 | 195 | 8 | 4.12 | 2-Jul-01 | 150 | 11 | 5.66 |
| 29-Aug-01 | 195 | 6 | 3.09 | 21-Jun-01 | 210 | 8 | 4.12 | 18-Jul-01 | 140 | 11 | 5.66 |
| 22-Sep-01 | 160 | 5 | 2.57 | 8-Jul-01 | 255 | 7 | 3.60 | 26-Jul-01 | 150 | 14 | 7.21 |
| 11-May-02 | 130 | 4 | 2.06 | 24-Jul-01 | 225 | 9 | 4.63 | 28-Jul-01 | 175 | 10 | 5.15 |
| 1-Jun-02 | 220 | 5 | 2.57 | 30-Aug-01 | 170 | 8 | 4.12 | 27-Jul-01 | 180 | 15 | 7.72 |
| 12-Jul-02 | 160 | 2 | 1.03 | 31-Aug-01 | 170 | 8 | 4.12 | 29-Jul-01 | 230 | 10 | 5.15 |
| 13-Aug-02 | 150 | 4 | 2.06 | 1-Sep-01 | 180 | 8 | 4.12 | 13-Aug-01 | 215 | 10 | 5.15 |
| 21-Aug-02 | 165 | 5 | 2.57 | 2-Sep-01 | 215 | 9 | 4.63 | 17-Aug-01 | 240 | 10 | 5.15 |
| 30-Aug-02 | 130 | 4 | 2.06 | 6-May-02 | 150 | 7 | 3.60 | 18-Aug-01 | 200 | 14 | 7.21 |
| 19-Aug-02 | 250 | 5 | 2.57 | 24-May-02 | 130 | 9 | 4.63 | 4-Sep-01 | 215 | 11 | 5.66 |
| 18-Sep-02 | 180 | 4 | 2.06 | 27-May-02 | 145 | 6 | 3.09 | 23-Sep-01 | 195 | 10 | 5.15 |
| 14-May-03 | 145 | 5 | 2.57 | 30-May-02 | 135 | 7 | 3.60 | 8-May-02 | 170 | 13 | 6.69 |
| 16-May-03 | 220 | 5 | 2.57 | 31-May-02 | 150 | 6 | 3.09 | 10-May-02 | 160 | 17 | 8.75 |
| 16-Jun-03 | 160 | 5 | 2.57 | 7-May-02 | 195 | 7 | 3.60 | 12-May-02 | 165 | 14 | 7.21 |
| 8-Jul-03 | 250 | 5 | 2.57 | 19-Jun-02 | 150 | 6 | 3.09 | 16-May-02 | 140 | 12 | 6.18 |
| 26-Jul-03 | 230 | 1 | 0.51 | 28-Jun-02 | 175 | 7 | 3.60 | 17-May-02 | 175 | 11 | 5.66 |
| 20-Aug-03 | 155 | 1 | 0.51 | 7-Jun-02 | 215 | 7 | 3.60 | 28-May-02 | 135 | 11 | 5.66 |
| 27-Aug-03 | 155 | 2 | 1.03 | 27-Jun-02 | 245 | 7 | 3.60 | 1-May-02 | 233 | 20 | 10.29 |
| 16-Aug-03 | 250 | 3 | 1.54 | 10-Jul-02 | 145 | 6 | 3.09 | 3-May-02 | 240 | 20 | 10.29 |
| 17-Aug-03 | 230 | 5 | 2.57 | 11-Jul-02 | 145 | 8 | 4.12 | 4-May-02 | 240 | 20 | 10.29 |
| 11-May-04 | 165 | 4 | 2.06 | 5-Jul-02 | 250 | 7 | 3.60 | 9-May-02 | 195 | 15 | 7.72 |
| 16-Jun-04 | 160 | 5 | 2.57 | 24-Jul-02 | 245 | 9 | 4.63 | 8-Jun-02 | 125 | 14 | 7.21 |
| 6-Jul-04 | 185 | 4 | 2.06 | 17-Aug-02 | 140 | 9 | 4.63 | 18-Jun-02 | 160 | 10 | 5.15 |
| 14-Aug-04 | 140 | 4 | 2.06 | 22-Aug-02 | 170 | 9 | 4.63 | 8-Jul-02 | 120 | 10 | 5.15 |
| 27-Aug-04 | 150 | 5 | 2.57 | 29-Sep-02 | 170 | 7 | 3.60 | 9-Jul-02 | 145 | 16 | 8.23 |
| 2-Sep-04 | 145 | 4 | 2.06 | 19-Sep-02 | 180 | 7 | 3.60 | 29-Jul-02 | 230 | 10 | 5.15 |
| 19-May-05 | 165 | 5 | 2.57 | 24-Jun-03 | 130 | 7 | 3.60 | 30-Jul-02 | 220 | 12 | 6.18 |
| 8-May-05 | 235 | 2 | 1.03 | 26-Jun-03 | 160 | 8 | 4.12 | 10-Aug-02 | 120 | 12 | 6.18 |
| 28-May-05 | 255 | 5 | 2.57 | 6-Jul-03 | 125 | 7 | 3.60 | 15-Aug-02 | 160 | 11 | 5.66 |
| 6-Jun-05 | 120 | 2 | 1.03 | 9-Jul-03 | 140 | 7 | 3.60 | 16-Aug-02 | 155 | 12 | 6.18 |
| 8-Jul-05 | 150 | 3 | 1.54 | 7-Jul-03 | 180 | 7 | 3.60 | 14-Aug-02 | 210 | 11 | 5.66 |
| 17-Aug-05 | 225 | 4 | 2.06 | 12-Jul-03 | 250 | 9 | 4.63 | 12-Sep-02 | 160 | 10 | 5.15 |
| 24-Aug-05 | 195 | 2 | 1.03 | 25-Jul-03 | 205 | 10 | 5.15 | 20-Sep-02 | 145 | 17 | 8.75 |
| | | | | 27-Jul-03 | 220 | 9 | 4.63 | 21-Sep-02 | 145 | 13 | 6.69 |
| | | | | 28-Aug-03 | 165 | 6 | 3.09 | 30-Sep-02 | 125 | 12 | 6.18 |
| | | | | 2-Aug-03 | 250 | 6 | 3.09 | 9-May-03 | 205 | 21 | 10.81 |
| | | | | 3-Aug-03 | 235 | 8 | 4.12 | 10-May-03 | 215 | 17 | 8.75 |
| | | | | 8-Aug-03 | 220 | 6 | 3.09 | 17-May-03 | 195 | 11 | 5.66 |
| | | | | 18-Aug-03 | 240 | 9 | 4.63 | 11-Jun-03 | 185 | 14 | 7.21 |
| | | | | 2-Sep-03 | 145 | 9 | 4.63 | 12-Jun-03 | 185 | 14 | 7.21 |
| | | | | 3-Sep-03 | 145 | 6 | 3.09 | 14-Jun-03 | 205 | 15 | 7.72 |
| | | | | 5-Sep-03 | 155 | 9 | 4.63 | 15-Jun-03 | 195 | 11 | 5.66 |
| | | | | 27-Sep-03 | 250 | 9 | 4.63 | 10-Jul-03 | 225 | 12 | 6.18 |
| | | | | 10-May-04 | 145 | 8 | 4.12 | 11-Jul-03 | 240 | 14 | 7.21 |
| | | | | 18-May-04 | 165 | 6 | 3.09 | 13-Jul-03 | 225 | 13 | 6.69 |
| | | | | 22-May-04 | 210 | 7 | 3.60 | 25-Jul-03 | 205 | 10 | 5.15 |
| | | | | 17-Jun-04 | 140 | 6 | 3.09 | 31-Jul-03 | 250 | 12 | 6.18 |
| | | | | 9-Jun-04 | 195 | 7 | 3.60 | 29-Aug-03 | 160 | 17 | 8.75 |
| | | | | 10-Jun-04 | 255 | 6 | 3.09 | 31-Aug-03 | 135 | 15 | 7.72 |
| | | | | 28-Jun-04 | 235 | 7 | 3.60 | 11-Aug-03 | 240 | 13 | 6.69 |
| | | | | 30-Jun-04 | 200 | 8 | 4.12 | 1-Sep-03 | 140 | 15 | 7.72 |
| | | | | 31-Jul-04 | 125 | 7 | 3.60 | 13-Sep-03 | 160 | 12 | 6.18 |
| | | | | 15-Aug-04 | 200 | 6 | 3.09 | 12-May-04 | 145 | 12 | 6.18 |
| | | | | 16-Aug-04 | 230 | 8 | 4.12 | 14-May-04 | 145 | 28 | 14.41 |
| | | | | 20-Aug-04 | 205 | 7 | 3.60 | 17-May-04 | 135 | 12 | 6.18 |
| | | | | 29-Sep-04 | 235 | 7 | 3.60 | 1-May-04 | 195 | 16 | 8.23 |
| | | | | 30-Sep-04 | 210 | 8 | 4.12 | 9-May-04 | 205 | 12 | 6.18 |
| | | | | 14-May-05 | 135 | 11 | 5.66 | 23-May-04 | 220 | 11 | 5.66 |
| | | | | 17-May-05 | 155 | 6 | 3.09 | 24-May-04 | 235 | 11 | 5.66 |
| | | | | 10-May-05 | 250 | 9 | 4.63 | 29-May-04 | 255 | 12 | 6.18 |
| | | | | 9-Jun-05 | 170 | 8 | 4.12 | 6-Jun-04 | 255 | 14 | 7.21 |
| | | | | 5-Jun-05 | 205 | 8 | 4.12 | 11-Jun-04 | 250 | 11 | 5.66 |
| | | | | 17-Jul-05 | 155 | 9 | 4.63 | 21-Jun-04 | 195 | 11 | 5.66 |
| | | | | 18-Jul-05 | 120 | 9 | 4.63 | 24-Jun-04 | 225 | 11 | 5.66 |
| | | | | 20-Jul-05 | 130 | 6 | 3.09 | 25-Jun-04 | 210 | 14 | 7.21 |
| | | | | 25-Jul-05 | 120 | 7 | 3.60 | 26-Jun-04 | 255 | 14 | 7.21 |

| | | | | | | | | | | | | | |
|---|---|---|---|---|---|---|---|---|---|---|---|---|---|
| | | | | | 12-Jul-05 | 210 | 9 | 4.63 | | 27-Jun-04 | 245 | 12 | 6.18 |
| | | | | | 14-Jul-05 | 240 | 8 | 4.12 | | 30-Jul-04 | 140 | 12 | 6.18 |
| | | | | | 8-Aug-05 | 185 | 8 | 4.12 | | 1-Jul-04 | 245 | 10 | 5.15 |
| | | | | | 11-Aug-05 | 255 | 9 | 4.63 | | 3-Jul-04 | 225 | 11 | 5.66 |
| | | | | | 12-Aug-05 | 250 | 9 | 4.63 | | 4-Jul-04 | 250 | 13 | 6.69 |
| | | | | | 18-Aug-05 | 240 | 6 | 3.09 | | 5-Jul-04 | 245 | 12 | 6.18 |
| | | | | | 19-Aug-05 | 255 | 6 | 3.09 | | 9-Jul-04 | 220 | 11 | 5.66 |
| | | | | | 30-Sep-05 | 155 | 8 | 4.12 | | 18-Aug-04 | 245 | 13 | 6.69 |
| | | | | | 29-Sep-05 | 215 | 7 | 3.60 | | 13-Sep-04 | 125 | 14 | 7.21 |
| | | | | | | | | | | 17-Sep-04 | 255 | 30 | 15.44 |
| | | | | | | | | | | 12-May-05 | 125 | 14 | 7.21 |
| | | | | | | | | | | 14-May-05 | 135 | 11 | 5.66 |
| | | | | | | | | | | 18-May-05 | 160 | 10 | 5.15 |
| | | | | | | | | | | 23-May-05 | 250 | 12 | 6.18 |
| | | | | | | | | | | 27-Jun-05 | 120 | 10 | 5.15 |
| | | | | | | | | | | 9-Jul-05 | 135 | 13 | 6.69 |
| | | | | | | | | | | 16-Jul-05 | 165 | 15 | 7.72 |
| | | | | | | | | | | 3-Jul-05 | 250 | 18 | 9.26 |
| | | | | | | | | | | 4-Jul-05 | 240 | 11 | 5.66 |
| | | | | | | | | | | 13-Jul-05 | 250 | 10 | 5.15 |
| | | | | | | | | | | 28-Aug-05 | 130 | 24 | 12.35 |
| **# DAYS** | **AVG** | **AVG** | **AVG** | | **# DAYS** | **AVG** | **AVG** | **AVG** | | **# DAYS** | **AVG** | **AVG** | **AVG** |
| 38 | 185 | 3.87 | 1.99 | | 80 | 189 | 7.56 | 3.89 | | 92 | 192 | 13.32 | 6.85 |

# APPENDIX D – COAST PARALLEL EASTERLY COMPOSITE DATES

| COAST PARALLEL EASTERLY | | | | | | | |
|---|---|---|---|---|---|---|---|
| 75-119 (3-5 m/s) | | | | 75-119(5-7 m/s) | | | |
| Date | Direction | Kts | m/s | Date | Direction | Kts | m/s |
| 15-May-05 | 90 | 6 | 3.09 | 2-May-01 | 105 | 10 | 5.15 |
| 19-Sep-01 | 115 | 6 | 3.09 | 5-May-01 | 95 | 10 | 5.15 |
| 12-Jun-02 | 85 | 9 | 4.63 | 23-Aug-01 | 105 | 10 | 5.15 |
| 12-Aug-02 | 100 | 8 | 4.12 | 28-Sep-01 | 75 | 11 | 5.66 |
| 29-Jul-04 | 95 | 7 | 3.60 | 25-May-02 | 80 | 10 | 5.15 |
| 22-May-05 | 110 | 9 | 4.63 | 29-May-02 | 80 | 11 | 5.66 |
| 24-Jun-05 | 100 | 9 | 4.63 | 23-May-02 | 105 | 12 | 6.18 |
| | | | | 5-Jun-02 | 110 | 10 | 5.15 |
| | | | | 31-Aug-02 | 115 | 13 | 6.69 |
| | | | | 10-Sep-03 | 75 | 10 | 5.15 |
| | | | | 16-Sep-03 | 80 | 11 | 5.66 |
| | | | | 20-Sep-03 | 110 | 11 | 5.66 |
| | | | | 26-Aug-04 | 85 | 11 | 5.66 |
| | | | | 3-Sep-04 | 80 | 11 | 5.66 |
| | | | | 4-May-05 | 110 | 10 | 5.15 |
| | | | | 21-Jun-05 | 100 | 10 | 5.15 |
| | | | | 25-Aug-05 | 80 | 10 | 5.15 |
| | | | | 11-Sep-05 | 75 | 10 | 5.15 |
| | | | | 12-Sep-05 | 85 | 10 | 5.15 |
| | | | | 20-Sep-05 | 75 | 12 | 6.18 |
| | | | | | | | |
| # DAYS | AVG | AVG | AVG | # DAYS | AVG | AVG | AVG |
| 7 | 99 | 7.71 | 3.97 | 20 | 91 | 10.65 | 5.48 |

| 75-119(7-9 m/s) | | | | 75-119(>12 m/s) | | | |
|---|---|---|---|---|---|---|---|
| Date | Direction | Kts | m/s | Date | Direction | Kts | m/s |
| 1-May-01 | 95 | 17 | 8.75 | 13-Sep-01 | 90 | 27 | 13.90 |
| 3-May-01 | 115 | 16 | 8.23 | 6-Sep-02 | 115 | 24 | 12.35 |
| 4-May-01 | 90 | 14 | 7.21 | 7-Sep-02 | 105 | 22 | 11.32 |
| 7-May-01 | 105 | 14 | 7.21 | 8-Sep-02 | 95 | 26 | 13.38 |
| 8-May-01 | 110 | 17 | 8.75 | 14-Aug-03 | 75 | 26 | 13.38 |
| 9-May-01 | 105 | 14 | 7.21 | 7-Aug-04 | 90 | 27 | 13.90 |
| 18-Jun-01 | 80 | 16 | 8.23 | 19-Sep-04 | 90 | 19 | 9.78 |
| 16-Jul-01 | 75 | 14 | 7.21 | 21-Sep-04 | 80 | 31 | 15.95 |
| 15-Jul-01 | 95 | 14 | 7.21 | 22-Sep-04 | 100 | 30 | 15.44 |
| 2-Aug-01 | 115 | 17 | 8.75 | 23-Sep-04 | 110 | 22 | 11.32 |
| 15-May-02 | 80 | 14 | 7.21 | 25-Jun-05 | 75 | 19 | 9.78 |
| 10-Jun-02 | 85 | 15 | 7.72 | 26-Aug-05 | 90 | 23 | 11.84 |
| 9-Jun-02 | 105 | 14 | 7.21 | 5-Sep-05 | 80 | 24 | 12.35 |
| 11-Jun-02 | 105 | 17 | 8.75 | | | | |
| 8-Aug-02 | 75 | 14 | 7.21 | | | | |
| 9-Aug-02 | 80 | 16 | 8.23 | | | | |
| 4-Aug-02 | 95 | 14 | 7.21 | | | | |
| 11-Aug-02 | 105 | 14 | 7.21 | | | | |
| 9-Sep-02 | 90 | 14 | 7.21 | | | | |
| 15-Aug-03 | 95 | 16 | 8.23 | | | | |
| 24-Sep-03 | 100 | 16 | 8.23 | | | | |
| 12-Sep-04 | 95 | 15 | 7.72 | | | | |
| 20-Jun-05 | 85 | 16 | 8.23 | | | | |
| 25-Aug-05 | 80 | 10 | 5.15 | | | | |
| 4-Sep-05 | 80 | 17 | 8.75 | | | | |
| 21-Sep-05 | 100 | 17 | 8.75 | | | | |
| # DAYS | AVG | AVG | AVG | # DAYS | AVG | AVG | AVG |
| 26 | 94 | 15.08 | 7.76 | 13 | 92 | 24.62 | 12.67 |

THIS PAGE INTENTIONALLY LEFT BLANK

# APPENDIX E – COAST PARALLEL WESTERLY COMPOSITE DATES

| COAST PARALLEL WESTERLY | | | | | | | | | | | | |
|---|---|---|---|---|---|---|---|---|---|---|---|---|
| 256-289 (0-3 m/s) | | | | | 256-289 (3-5 m/s) | | | | 256-289 (> 5 m/s) | | | |
| Date | Direction | Kts | m/s | | Date | Direction | Kts | m/s | Date | Direction | Kts | m/s |
| 24-Aug-01 | 270 | 4 | 2.06 | | 22-Jul-02 | 265 | 7 | 3.60 | 2-Jun-01 | 270 | 19 | 9.78 |
| 17-Sep-01 | 260 | 4 | 2.06 | | 23-Jul-02 | 280 | 7 | 3.60 | 15-Jun-01 | 275 | 12 | 6.18 |
| 16-Jun-02 | 280 | 4 | 2.06 | | 9-Jun-03 | 260 | 9 | 4.63 | 6-Jul-01 | 270 | 11 | 5.66 |
| 23-Aug-02 | 270 | 3 | 1.54 | | 27-Jun-03 | 270 | 7 | 3.60 | 11-Aug-01 | 270 | 12 | 6.18 |
| 28-Aug-02 | 285 | 4 | 2.06 | | 28-Jul-03 | 275 | 7 | 3.60 | 15-Jul-02 | 280 | 16 | 8.23 |
| 25-May-03 | 260 | 3 | 1.54 | | 5-May-04 | 265 | 6 | 3.09 | 31-Jul-02 | 285 | 13 | 6.69 |
| 22-Jun-03 | 285 | 2 | 1.03 | | 4-Jun-04 | 280 | 8 | 4.12 | 24-Aug-02 | 260 | 11 | 5.66 |
| 18-Jul-03 | 260 | 1 | 0.51 | | 12-Jun-04 | 265 | 8 | 4.12 | 28-Sep-02 | 270 | 11 | 5.66 |
| 25-May-04 | 265 | 5 | 2.57 | | 19-Jun-04 | 285 | 6 | 3.09 | 12-May-03 | 280 | 13 | 6.69 |
| 21-May-04 | 275 | 3 | 1.54 | | 29-Aug-04 | 260 | 7 | 3.60 | 30-May-03 | 275 | 11 | 5.66 |
| 16-Aug-05 | 273 | 5 | 2.57 | | 17-Aug-04 | 279 | 6 | 3.09 | 19-Jun-03 | 260 | 13 | 6.69 |
| 17-Sep-05 | 260 | 3 | 1.54 | | 10-Aug-05 | 275 | 8 | 4.12 | 21-Jul-03 | 260 | 11 | 5.66 |
| | | | | | 14-Aug-05 | 270 | 7 | 3.60 | 22-Jul-03 | 260 | 18 | 9.26 |
| | | | | | | | | | 30-Jul-03 | 265 | 14 | 7.21 |
| | | | | | | | | | 20-Jul-03 | 285 | 12 | 6.18 |
| | | | | | | | | | 19-Aug-03 | 265 | 10 | 5.15 |
| | | | | | | | | | 5-Aug-03 | 275 | 16 | 8.23 |
| | | | | | | | | | 26-May-04 | 265 | 18 | 9.26 |
| | | | | | | | | | 27-May-04 | 265 | 18 | 9.26 |
| | | | | | | | | | 28-May-04 | 260 | 24 | 12.35 |
| | | | | | | | | | 16-Jul-04 | 260 | 14 | 7.21 |
| | | | | | | | | | 7-Jul-04 | 270 | 10 | 5.15 |
| | | | | | | | | | 22-Aug-04 | 265 | 12 | 6.18 |
| | | | | | | | | | 5-Aug-04 | 270 | 14 | 7.21 |
| | | | | | | | | | 19-Aug-04 | 280 | 12 | 6.18 |
| | | | | | | | | | 31-Aug-05 | 260 | 15 | 7.72 |
| | | | | | | | | | 13-Aug-05 | 280 | 11 | 5.66 |
| | | | | | | | | | 1-Sep-05 | 270 | 14 | 7.21 |
| # DAYS | AVG | AVG | AVG | | # DAYS | AVG | AVG | AVG | # DAYS | AVG | AVG | AVG |
| 12 | 270 | 3.42 | 1.76 | | 13 | 271 | 7.15 | 3.68 | 28 | 270 | 13.75 | 7.08 |

THIS PAGE INTENTIONALLY LEFT BLANK

# LIST OF REFERENCES


Arritt, R. W, 1993: Effects of large scale flow on characteristic features of the sea breeze. *J. Appl. Meteor.* **32**, 116–125.

Atkins, N. T, and R. M. Wakimoto, 1997: Influence of the synoptic-scale flow on sea breezes observed during CaPE. *Mon. Wea. Rev.*, **125**, 2112–2130.

Baker, R. D., B. H. Lynn, A. Boone, W. Tao, and J. Simpson, 2001: Influence of soil moisture, coastline curvature, and land-breeze circulations on sea-breeze-initiated precipitation. *J. Hydrometeor.*, **2**, 193–211.

Bechtold, P. J., P. Pinty, and P. Mascart, 1991: A numerical investigation of the influence of large-scale winds on sea-breeze and inland-breeze type circulations. *J. Appl. Meteor.*, **30**, 1268–1279.

Biggar, David G., 1992: A mesoscale study of sea breeze enhanced summer thunderstorms in the Florida Panhandle. M.S. Thesis, Department of Meteorology, Florida State University, 59 pp.

Blanchard, D. O. and R. E. Lopez, 1985: Spatial patterns of convection in south Florida. *Mon.Wea. Rev.* **113**, 1282–1299.

Borne, K., D. Chen, M. Munez, 1998: A method for finding sea breeze days under stable synoptic conditions and its application to the Swedish west coast. *Int. J. Climatol.*, **18,** 901-914.

Boybeyi, Z., and S. Raman, 1992: A three-dimensional numerical sensitivity study of convection over the Florida peninsula. *Bound.-Layer Meteor.*, **60,** 325-359.

Burpee, R.W., 1979: Peninsula scale convergence in the south Florida sea breeze. *Mon. Wea. Rev.*, **107,** 852–860.

-------, and N. L. Lahiff, 1984: Area-average rainfall variations on sea-breeze days in south Florida. *Mon. Wea. Rev.*, **112,** 520–534.

Byers, H. R., and H. R. Rodebush, 1948: Causes of thunderstorms on the Florida peninsula. *J. Meteor.*, **5**, 275-280.

Camp, J. P., A. I. Watson, and H. E. Fuelberg, 1998: The diurnal distribution of lightning over North Florida and its relation to the prevailing low-level flow. *Wea. Forecasting*, **13**, 729-739.

Carlson, Toby N., 1991: *Mid-Latitude Weather Systems.* HarperCollins, 435 pp.

Cetola, Jeffrey D., 1997: A climatology of the sea breeze at Cape Canaveral, Florida. M.S. Thesis, Department of Meteorology, Florida State University, 56 pp.

Cooperative Program for Operational Meteorology, Education and Training (COMET), University Corporation for Atmospheric Research, cited Nov 2003: COMET Computer-based Training Module: Thermally-forced Circulation 1: Sea Breezes. [Available online at http://meted.ucar.edu/mesoprim/seabreeze/]

Estoque, M. A., 1962: The sea breeze as a function of the prevailing synoptic situation. *J. Atmos. Sci.*, **19**, 244–250.

Frank, N. L., P. L. Moore, and G. E. Fisher, 1997: Summer shower distribution over the Florida peninsula as deduced from digitized radar data. *J. Appl. Meteor.*, **6,** 309-316.

Gilliam, R. C., S. Raman, and D. D. S. Niyogi, 2004: Observations and numerical study on the influence of large-scale flow direction and coastline shape on sea-breeze evolution. *Bound.-Layer Meteor.,* **111,** 275-300.

Gould, K. J., and H. E. Fuelburg, 1996: The use of GOES-8 imagery and RAMSDIS to develop a sea breeze climatology over the Florida panhandle. Preprints, 8th Conf. on Satellite and Oceanography, Atlanta, GA, Amer. Meteor. Soc., 100-104.

Hodanish, S., D. Sharp, W. Collins, C. Paxton, and R. E. Orville, 1997: A 10-year monthly lightning climatology of Florida: 1986-95. *Wea. Forecasting*, **12,** 439-448.

Hsu, S. A., 1970: Coastal air-circulations system: observations and empirical model. *Mon. Wea. Rev.*, **98**, 487-509.

Kalnay, E., M. Kanamitsu, R. Kistler, W. Collins, D. Deaven, L. Gandin, M. Iredell, S. Saha, J. Woollen, Y. Zhu, M. Chelliah, W. Ebisuzaki, W. Higgins, J. Janowiak, K. C. Mo, C. Ropelewski, J. Wang, A. Leetmaa, R. Reynolds, R. Jenne, and D Joseph, 1996: The NCEP/NCAR 40-year reanalysis project. *Bull. Am. Meteorol. Soc.*, **77**, 437-471.

Kingsmill, D E., 1995: Convection initiation associated with a sea-breeze front, a gust front and their collision. *Mon. Wea. Rev.,* **123**, 2913-2933.

Laird, N. F., D. A. R. Kristovich, R. M. Rauber, H. T. Ochs III, and L. J. Miller, 1995: The Cape Canaveral sea and river breezes: Kinematic structure and convective initiation. *Mon. Wea. Rev.*, **123,** 2942-2956.

Lopez, R.E., and R. L. Holle, 1987: The distribution of summertime lightning as a function of low-level wind flow in central Florida. NOAA Tech. Memo ERL ESG-28, National Sever Storms Laboratory, Norman, OK, 43 pp.

Mackey, J. B., 2005: Personal Communication.

Marshall, C. H., R. A. Pielke, L. T. Steyaert, and D. A. Willard, 2004: The impact of anthropogenic land-cover change on the Florida peninsula sea breezes and warm season sensible weather. *Mon. Wea. Rev.*, **132,** 28-52.

Nicholls, M. E., R. A. Pielke, and W. R. Cotton, 1991: A two-dimensional numerical investigation of the interaction between sea breezes and deep convection over the Florida Peninsula. *Mon. Wea. Rev.*, **119,** 298-323.

Nuss, W. A., 2005: *Coastal Meteorology:* Course Notes for MR4240. Department of Meteorology, Naval Postgraduate School, Monterey, California, 68 pp.

-------, and S. Drake, 1995: *VISUAL Meteorological Diagnostic and Display Program*. Department of Meteorology, Naval Postgraduate School, Monterey, California, 51 pp.

-------, and D. W. Titley, 1994: Use of multquadric interpolation for meteorological objective analysis. *Mon. Wea. Rev.*, **122**, 1612-1631.

Pielke, R. A., 1974: A Three-dimensional numerical model of the sea breezes over South Florida. *Mon. Wea. Rev.*, **102**, 115–139.

Rao, P. A., H. E. Fuelberg, and K. K. Droegemeier, 1999: An investigation of convection behind the Cape Canaveral sea breeze front. *Mon. Wea. Rev.*, **128**, 3437-3458.

Stroupe, J. S., H. E. Fuelberg, and A. I. Watson, 2004: Warm season lightning distribution over the northern Gulf of Mexico coast and their relation to synoptic scale and mesoscale environments. *Wea. Forecasting*, **12,** 439- 448.

Walsh, J. E., 1974: Sea-breeze theory and applications. *J. Atmos. Sci.*, **31**, 2012-2026.

Wakimoto, R. M., 2001: Convectively driven high wind events. *Severe Convective Storms, Meteor. Mono.*, No. 50, Amer. Meteor. Soc., 255-298.

Wilson, J. W., 1996: Thunderstorm initiation, organization, and lifetime associated with Florida boundary layer convergence lines. *Mon. Wea. Rev.*, **125**, 1507-1525.

Zhong, S. and E. S. Takle, 1993: The effects of large-scale winds on the sea-land-breeze circulations in an area of complex coastal heating. *J. Appl. Meteorol.* **32**, 1181–1195.

THIS PAGE INTENTIONALLY LEFT BLANK

# INITIAL DISTRIBUTION LIST

1. Defense Technical Information Center
   Ft. Belvoir, Virginia

2. Dudley Knox Library
   Naval Postgraduate School
   Monterey, California

3. Dr. Wendell A. Nuss
   Naval Postgraduate School
   Monterey, California

4. Dr. Haflidi H. Jonsson
   Naval Postgraduate School
   Monterey, California

5. Dr. Philip A. Durkee
   Naval Postgraduate School
   Monterey, California

6. J. Bryan Mackey, Maj, USAF
   Eglin AFB, Fl

7. Air Force Weather Technical Library
   Asheville, NC